Development of algorithms of statistical signal processing for the detection and pattern recognition in time series. Application to the diagnosis of electrical machines and to the features extraction in actigraphy signals.

A thesis submitted for the degree of Doctor in Mathematics at

Universitat Politècnica de València (UPV)

Author: Miguel Enrique Iglesias Martínez

Directors: Pedro José Fernández de Córdoba Castellá,

José Alberto Conejero Casares

José Alfonso Antonino Daviu

Valencia, Marzo 2020

Dr. Pedro José Fernández de Córdoba Castellá,

Dr. José Alberto Conejero Casares

Dr. José Alfonso Antonino Daviu

CERTIFICAN que la presente memoria" Development of algorithms of statistical signal processing for the detection and pattern recognition in time series. Application to the diagnosis of electrical machines and to the features extraction in Actigraphy signals" resume el trabajo de investigación realizado, bajo su dirección, por D. Miguel enrique Iglesias Martínez y constituye su Tesis para optar al título de Doctor.

Y para que conste, en cumplimiento de la legislación vigente, firman el presente certificado en Valencia

Fdo.: Dr. Pedro José Fernández de Córdoba Castellá

Fdo.: Dr. José Alberto Conejero Casares

Fdo.: Dr. José Alfonso Antonino Daviu

Para Mami , Papi y mi Pequeño Diego

***Hay hombres** que luchan un día y son **buenos**. **Hay** otros que luchan un año y son mejores. **Hay** quienes luchan muchos años, y son muy **buenos**. Pero **hay** los que luchan toda la vida: esos son los imprescindibles».*

Bertolt Brecht

Agradecimientos

A mis directores de Tesis Pedro José Fernández de Córdoba Castellá, José Alberto Conejero Casares y José Alfonso Antonino Daviu por confiar en mi desde el principio, gracias de Corazón!!!. Para mi son una familia.

A Dagoberto Acosta Iglesias por abrir el camino, gracias Dago!!!

A Juanka y Esperanza por su constante apoyo!!!

Al profesor Sarira Sahu por confiar en mi y por su enseñanza!!!

A Juan Miguel García-Gomez y Carlos Sáez Silvestre por su apoyo!!!

A Carlos Fortin por su apoyo!!!

A Victor Milián-Sánchez por su sabiduría!!!!

A Eduardo Balvis por su amistad y apoyo!!!

A los padres de Pedro Fernández de Córdoba Castellá, por acogerme como hijo y por disfrutar de mi cocina!!!

A todos los que ayudaron en algún momento, gracias infinitas!!!, y a los que no, también gracias, ellos me han hecho más fuerte!!!

Resumen

En la actualidad, el desarrollo y aplicación de algoritmos para el reconocimiento de patrones que mejoren los niveles de rendimiento, detección y procesamiento de datos en diferentes áreas del conocimiento resulta un tema de gran interés.

En este contexto, y específicamente en relación con la aplicación de estos algoritmos en el monitoreo y diagnóstico de máquinas eléctricas, el uso de señales de flujo es una alternativa muy interesante para detectar las diferentes fallas.

Asimismo, y en relación con el uso de señales biomédicas, es de gran interés extraer características relevantes en las señales de actigrafía para la identificación de patrones que pueden estar asociados con una patología específica.

En esta tesis, se han desarrollado y aplicado algoritmos basados en el procesamiento estadístico y espectral de señales, para la detección y diagnóstico de fallas en máquinas eléctricas, así como su aplicación al tratamiento de señales de actigrafía.

Con el desarrollo de los algoritmos propuestos, se pretende tener un sistema dinámico de indicación e identificación para detectar la falla o la patología asociada que no depende de parámetros o información externa que pueda condicionar los resultados, sólo de la información primaria que inicialmente presenta la señal a tratar (como la periodicidad, amplitud, frecuencia y fase de la muestra).

A partir del uso de los algoritmos desarrollados para la detección y diagnóstico de fallas en máquinas eléctricas, basados en el procesamiento estadístico y espectral de señales, se pretende avanzar, en relación con los modelos actualmente existentes, en la identificación de fallas mediante el uso de señales de flujo.

Además, y por otro lado, mediante el uso de estadísticas de orden superior, para la extracción de anomalías en las señales de actigrafía, se han encontrado parámetros alternativos para la identificación de procesos que pueden estar relacionados con patologías específicas.

Resum

En l'actualitat, el desenvolupament i aplicació d'algoritmes per al reconeixement de patrons que milloren els nivells de rendiment, detecció i processament de dades en diferents àrees del coneixement és un tema de gran interés.

En aquest context, i específicament en relació amb l'aplicació d'aquests algoritmes a la monitorització i diagnòstic de màquines elèctriques, l'ús de senyals de flux és una alternativa molt interessant per tal de detectar les diferents avaries.

Així mateix, i en relació amb l'ús de senyals biomèdics, és de gran interés extraure característiques rellevants en els senyals d'actigrafia per a la identificació de patrons que poden estar associats amb una patologia específica.

En aquesta tesi, s'han desenvolupat i aplicat algoritmes basats en el processament estadístic i espectral de senyals per a la detecció i diagnòstic d'avaries en màquines elèctriques, així com la seua aplicació al tractament de senyals d'actigrafia.

Amb el desenvolupament dels algoritmes proposats, es pretén obtindre un sistema dinàmic d'indicació i identificació per a detectar l'avaria o la patologia associada, el qual no depenga de paràmetres o informació externa que puga condicionar els resultats, només de la informació primària que inicialment presenta el senyal a tractar (com la periodicitat, amplitud, freqüència i fase de la mostra).

A partir de l'ús dels algoritmes desenvolupats per a la detecció i diagnòstic d'avaries en màquines elèctriques, basats en el processament estadístic i espectral de senyals, es pretén avançar, en relació amb els models actualment existents, en la identificació de avaries mitjançant l'ús de senyals de flux.

A més, i d'altra banda, mitjançant l'ús d'estadístics d'ordre superior, per a l'extracció d'anomalies en els senyals d'actigrafía, s'han trobat paràmetres alternatius per a la identificació de processos que poden estar relacionats amb patologies específiques.

Abstract

Nowadays, the development and application of algorithms for pattern recognition that improve the levels of performance, detection and data processing in different areas of knowledge is a topic of great interest.

In this context, and specifically in relation to the application of these algorithms to the monitoring and diagnosis of electrical machines, the use of stray flux signals is a very interesting alternative to detect the different faults.

Likewise, and in relation to the use of biomedical signals, it is of great interest to extract relevant features in actigraphy signals for the identification of patterns that may be associated with a specific pathology.

In this thesis, algorithms based on statistical and spectral signal processing have been developed and applied to the detection and diagnosis of failures in electrical machines, as well as to the treatment of actigraphy signals.

With the development of the proposed algorithms, it is intended to have a dynamic indication and identification system for detecting the failure or associated pathology that does not depend on parameters or external information that may condition the results, but only rely on the primary information that initially presents the signal to be treated (such as the periodicity, amplitude, frequency and phase of the sample).

From the use of the algorithms developed for the detection and diagnosis of failures in electrical machines, based on the statistical and spectral signal processing, it is intended to advance, in relation to the models currently existing, in the identification of failures through the use of stray flux signals.

In addition, and on the other hand, through the use of higher order statistics for the extraction of anomalies in actigraphy signals, alternative parameters have been found for the identification of processes that may be related to specific pathologies.

General Index

Chapter 1

General Introduction

In any fields of the science, the implications of occassional interferences that pollute the useful information contained in measured signals can be very serious: false readings of the information obtained by the sensors, activation of false alarms, lack of communication between communication systems, etc… Many of these interferences are, from a practical point of view, impossible to eliminate, although it is possible to establish methods and techniques that tend to diminish their effect on useful signals.

The previous statements confirm the interest of solving the problems that the disturbing signals produce, due to the consequences that such physical manifestations may provoke with their influence.

Numerous methods have been developed in order to seek for the extraction of disturbing signal and to enable the identification of faults or patterns immersed in interference. These methods can be classified according to various criteria. However, from the point of view of the number of signals available to perform the task in question, they can be classified into methods that use two or more input signals and methods that use a single input signal.

Regarding the methods that use a single signal input, they generally have the advantage of requiring less information for processing. This can be very useful for different applications in which only the input signal to be processed is available.

In the field of electric machines, the analysis of the noise emitted by the motor is an interesting and very useful option due to the low cost of implementation for processing [1,2,3]. The idea that underlies the noise analysis is the interpretation of the acoustic waves produced by the mechanical vibrations of the motor that, according to their features and characteristics, can give rise to patterns identifying certain failures in electric machines. Likewise, the use of stray flux signals has brought considerable interest because this type of methodology is completely non-invasive and, from the analysis of this type of signals, characteristics and patterns that can identify the nature and severity of the fault can be extracted [4 -10].

With regards to the methods of statistical signal processing, it can be argued that these allow the extraction of characteristics along the entire effective working spectral band (infinite, for the case of continuous signals; from 0 Hz to the half of the sampling frequency, in the case of sampled signals).

However, its traditional application is based on the assumption of linearity and stationarity, limited to the estimation of second-order characteristics, which does not take advantage of the benefits that, for example, higher order statistical analysis could represent for its use in electrical and electrical signals of other nature [11-16].

The most significant peculiarity of the methods that are based on higher order statistical processing (calculation of cumulants) is that if the noise is Gaussian in nature; it is completely

canceled from its theoretical foundation. For this reason, this research is focused on the work with higher order statistical analysis techniques and their combination with second-order classical techniques.

On the other hand, regarding the use of signal processing and pattern recognition in biomedical signals, actigraphy represents an increasingly used and appreciated exploration in sleep laboratories. Its greatest advantage is its easy use, low cost and the fact that it allows prolonged registrations in time and assessment of the patient in ambulatory conditions without interference on normal activity. It is considered a very useful tool for the control and monitoring of circadian alterations and insomnia, as well as to avoid false positives in the assessment of daytime sleepiness explorations such as the multiple sleep latency test and wakefulness maintenance test [17,18].

This research has used extensive applications of higher-order statistical analysis and their combination with second-order processes such as convolution and covariance, to obtain some reliable pattern recognition in time series of different types. Several theoretically developed and experimentally tested algorithms with real signals of different kinds are proposed, providing satisfactory results in each case.

In turn, the results have been applied to experimental physics, and to psychology through the analysis of response times of individuals to visual stimuli; likewise, an extension of the obtained results in this research has been performed for its application to electrical machines. with wound rotor [19-27].

1.1 Objectives of the Research

General Objectives

The general objective of the research is to develop algorithms based on statistical signal processing for pattern recognition, diagnosis, detection and identification of characteristic features in actigraphy signals and electrical machines, based only on the initial amplitude, frequency and phase information of the signal to be treated

To achieve this general objective, the following process has been followed:

- Review of the state of the art of the field to be treated.
- Theoretical development of the algorithms to be evaluated based on the use of higher order statistics and their combination with second order processes.
- Preparation and description of the data.
- Application of algorithms that allow analyzing available data through different methods.
- Validation and other possible uses of the described methods.

1.2 Thesis Structure

Firstly, it should be noted that this is a Ph. D. thesis based on the compilation of scientific articles resulting from the developed research.In this regard, it fulfils the rules established by Universitat

Politecnica de Valencia concerning the development of a Ph. D. thesis based on scientific papers compilation. Each of the papers can be read autonomously by having the aspects necessary for its understanding (theoretical framework, objectives, results and conclusions), but it is important to emphasize that the union of all of them constitutes a single work with a clear plot thread.

The Thesis document is structured in 5 chapters:

1. General Introduction

   1.1 Objectives of the Research.
   1.2 Thesis Structure.

2. Publications.
   - Higher Order Spectra Analysis of Stray Flux Signals for Faults Detection in Induction Motors
   - Detection of adjacent and non-adjacent bar breakages in induction motors via convolutional analysis of sound signals
   - Detection of Bar Breakages in Induction Motor via Spectral Subtraction of Stray Flux Signals
   - Detection of Nonadjacent Rotor Faults in Induction Motors via Spectral Subtraction and Autocorrelation of Stray Flux Signals
   - Rotor Fault Detection in Induction Motors Based on Time-Frequency Analysis Using the Bispectrum and the Autocovariance of Stray Flux Signals
   - Feature Extraction and Similarity of Movement Detection during Sleep, Based on Higher Order Spectra and Entropy of the Actigraphy Signal: Results of the Hispanic Community Health Study/Study of Latinos

3. General Discussion of the Results.

4. Conclusions.

   4.2 Main contributions
   4.3 Future Research Lines

5. Bibliography

Chapter 1 defines the framework in which the Thesis is developed. In addition, the objectives pursued are presented and then the structure of the Thesis is detailed. The plot line that the articles follow, as well as their respective impact on the achievement of the objectives are also described.

Chapter 2 includes the six articles published in congress and scientific journals indexed in JCR. This chapter constitutes the main body of the Thesis. The first article is entitled: **Higher Order Spectra Analysis of Stray Flux Signals for Faults Detection in Induction Motors** and it is

accepted for publication in Applied Mathematics and Nonlinear Sciences from the editorial https://www.sciendo.com, Indexed in: Mathematical Reviews .
The work gathers the experience of working with higher order statistics and its use in stray flux signals, both the theoretical and practical foundations of the work and the obtained results are described as well as the references to the uses of higher order statistical analysis in the detection of failures. in electric machines.

The second work is entitled: **Detection of adjacent and non-adjacent bar breakages in induction motors via convolutional analysis of sound signals** and has been sent for publication in a special issue of Applied Sciences journal of the MDPI editorial.
The work is an approach to the detection of failures in induction motors, specifically the adjacent and non-adjacent bars breakage, using acoustic noise. The work is based on an algorithm that uses the convolutional analysis of the noisy signal to obtain a unique spectral pattern of bar breakage. Furthermore a noise reduction algorithm that uses the cumulant of the contaminated signal is also proposed. The obtained results from the theoretical and practical point of view are shown.

The third work is entitled: **Detection of Bar Breakages in Induction Motor via Spectral Subtraction of Stray Flux Signals** and it is a first approach the detection of bar break using the dispersion flow signals, the work was presented at the ICEM IEEE Congress and was published and indexed IEEE Xplore as part of the congress reports.

The fourth work is entitled: **Detection of Nonadjacent Rotor Faults in Induction Motors via Spectral Subtraction and Autocorrelation of Stray Flux Signals** and is a generalization of the previous work presented in the ICEM conference, which also incorporates a new method of indication of the healthy-damaged state based on the autocovariance of the flux signal. The work was published in the journal IEEE TRANSACTIONS ON INDUSTRY APPLICATIONS.

The fifth work is entitled: **Rotor Fault Detection in Induction Motors Based on Time-Frequency Analysis Using the Bispectrum and the Autocovariance of Stray Flux Signals**, and it is an analysis on the detection of the condition of the healthy-damaged state of the induction motor using two types of indicators, the first based on the median of the quadratic value of the covariance function and the second using the bispectrum of the flux signal. The work was published in Energies journal of the MDPI editorial.

Finally, the sixth work is entitled: **Feature Extraction and Similarity of Movement Detection during Sleep, Based on Higher Order Spectra and Entropy of the Actigraphy Signal: Results of the Hispanic Community Health Study / Study of Latinos**, and it is an analysis of the extraction of characteristics in actigraphy signals, for patterns recognition and the clinical diagnosis of possible pathologies associated with movement during sleep. The work was published in the Sensors journal of the MDPI editorial.

Chapter 3 explains the main results obtained from the research carried out during the doctoral period. In Chapter 4, as a conclusion, the level of compliance with the objectives set at the beginning of the doctoral research is analyzed, as well as the research lines that will be carried out to extend the results to other branches of knowledge. Finally, the bibliography used in the main introduction is added.

Chapter 2
Publications

sciendo Applied Mathematics and Nonlinear Sciences

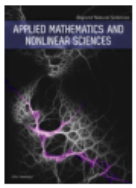

Applied Mathematics and Nonlinear Sciences

https://www.sciendo.com

Higher Order Spectra Analysis of Stray Flux Signals for Faults Detection in Induction Motors

Miguel E. Iglesias Martínez[1;2], Jose A. Antonino-Daviu[3], Pedro Fernández de Córdoba[2], Alberto Conejero[2]

[1]Departamento de Telecomunicaciones, Universidad de Pinar del Río, Pinar del Río, Martí 270, CP 20100,Cuba, migueliglesias2010@gmail.com

[2]Instituto Universitario de Matemática Pura y Aplicada, Universitat Politècnica de València, E46022 València,Spain

[3]Instituto de Tecnología Eléctrica, Universitat Politècnica de València, E46022 València,Spain

Applied Mathematics and Nonlinear Sciences (Accepted for publication)
https://www.sciendo.com,, **Indexed**: Mathematical Reviews.

Abstract

This work is a review of current trends in the stray flux signal processing techniques applied to the diagnosis of electrical machines. Initially, a review of the most commonly used standard methods is performed in the diagnosis of failures in induction machines and using stray flux; and then specifically it is treated and performed the algorithms based on statistical analysis using cumulants and polyspectra. In addition, the theoretical foundations of the analyzed algorithms and examples applications are shown from the practical point of view where the benefits that processing can have using HOSA and its relationship with stray flux signal analysis, are illustrated. Keywords: Cumulants; Higher Order Spectra; Stray Flux; Faults Diagnosis.

Keywords: Cumulants; Higher Order Spectra; Stray Flux; Faults Diagnosis.

1. Introduction

The monitoring and diagnosis of rotary electric machines have taken great importance in current applications of industry, aeronautics, and telecommunications, among other branches of science and technology. They has fostered the development of numerous methods to monitor and diagnose different types of failures in electric machines. These techniques have been designed to increase machines efficiency, safety, and performance, from the reliability and energy point of view [16,28].

In principle, each one of these techniques is based on processing different signals that can be captured by sensors that measure parameters such as mechanical vibrations, stator current,

acoustic signal, and stray flux. They let us monitor the condition of electric machines and detect numerous failures such as design and manufacture defects, improper ambient conditions, overload and over-speed, fatigue, stator insulation failure, bearing fault, broken rotor bar/end-ring detection, and air gap eccentricity [16].

One of the most commonly used techniques is vibration analysis [9,11,53] and motor-current analysis or motor current signature analysis (MCSA) [31,59,60] These techniques are based on the spectrum analysis using the Fourier transform for the detection of specific faults since the frequency spectrum shows numerous harmonics including the fundamental and the faults adjacent frequencies, that differ between faulty and healthy motors, because different electrical and mechanical faults generate different signatures [10,12,15].

On the other hand, there are other techniques based on the acoustic signal processing that emanates from the rotor noise [1, 11,18] Their goal is to identify and extract features of signals that correspond to faults [17]. For this purpose, techniques like the Fourier transform has been used to analyze the noise [39]. However, it presents the fundamental disadvantage hat the power spectrum is not immune to noise. Other techniques applied to this identification are based on high-resolution spectral analysis, wavelet transforms [2, 32,50] and empirical modes decomposition [11].

Relating to artificial intelligence-based methods for diagnosing failures [34], there are several works for failure classifications and pattern recognition. These works are differentiated in dissimilar methods of artificial intelligence such as artificial neural networks [5,24,37,43,44,51], genetic algorithms[49,64] support vector machines [4,19,35,52,54,63], Bayesian classifiers [38,40,65]

In general, these methods are based on the initial information available to the system, in addition to learning the process that can be supervised or unsupervised, and extracting characteristics based on logical knowledge,using the stator current, vibration signals and sounds of the motor.
Furthermore, failure detection methods based on higher-order statistical analysis have been applied to vibration signals, by considering the information provided by cumulants and moments of orders greater than or equal to two, as well as the spatial information that extracted from the analysis of higher-order spectra such as the bispectrum [29,30,45,58,6] . In addition to statistical estimators such as variance, kurtosis and skewness derived from the cumulants of second, third, and fourth orders respectively are performed.

At present, the treatment of failures in electric induction machines has taken a high boom in relation to the analysis of the stray flux signals for the detection of failures, see the recent review of Jiang et al. [28]. However, it is not considered based on the use of statistical analysis of cumulants nor High-Order Spectra Analysis (HOSA). Since HOSA-based techniques are immune to Gaussian probabilistic density function noise, the spectral properties of the signal are preserved. So as to, HOSA-based analysis of stray flux signals can be potentially used for fault detection.

We focus on providing an update of the statistical analysis techniques based on cumulants and higher-order spectra applied to the diagnosis of failures using stray flux signals. The work is organized as follows: In Section II, we review existing fault diagnosis methods from stray flux signals. In Section III, we show the theoretical foundations of a statistical analysis based on high-order cumulants and polyspectra. The use of HOSA on stray flux signals for fault detection is shown in Section IV. Finally, we provide some conclusions and prospective lines for future work in this line.

2. Faults Detection Based on Stray Flux Analysis

The magnetic flux is measured by circular search coils and hall sensors, that are concentric with the shaft inside the machine. They generate a voltage proportional to the magnetic field generated by the flux. In addition to these sensors, other types of sensors based on optical fiber and radiofrequency have been already used [62]. Recently, a smart sensor has been proposed to detect winding insulation failures based on reconfigurable FPGA technology and using artificial neural networks [62].

2.1 Stator Insulation Monitoring And Failure Detection

Stray flux has been proved to detect the stator winding insulation failure. The main difference for fault detection respect to the use of flow signals consists of the type of sensor to be used and the position where the measurement is taken. One way to detect this type of failure is by applying a load and not load test, that provides significant similarities, even if the stator current gives interesting diagnostic information only when the motor is loaded.

Considering power supply harmonics, it is possible to easily detect the stator winding faults in the low frequency range of the flux spectrum. One of the most used methods to detect this type of failure is the timefrequency analysis based on the signal spectrogram since this analysis generates important amplitude components in specific harmonics [28].

2.2 Bearing Fault Detection

It is estimated that approximately 35-55 percent of all cases of failures in electrical machines are Bearing Fault Detection, so this type of failure is investigated very frequently in the monitoring and diagnosis of electrical machines. Approximately 40 percent of these are caused by inappropriate use of lubricants. Some indicators that reveals that the nature of this type of failure lies in the increase in temperature and mechanical vibrations and the increase in the acoustic noise level generated by the machine [13, 22,27].Some experimental measurements were carried out by means of a current probe and by means of different flux probes, positioned in different positions [13,21], The comparison is conducted to find the main advantages which are th,e simplicity and the flexibility of the custom flux probe with its amplification and filtering stage depend on the relative position used for the experiments [42].

2.3 Air Gap Eccentricity Detection

Motor eccentricity failures are permissible up to 10 percent, and they do not have a significant influence on the characteristics of the motor and its useful life. However, a high level of eccentricity can cause a magnetic imbalance and therefore an increase in noise and vibrations [66]. Experimental results have revealed the potential of a simple search coil for the detection and the distinction of the accurate eccentricity nature even in the presence of similar mechanical faults [48]. Dynamic eccentricity produces low-frequency air gap flux components.
However, they can be observed in stator current only under mixed eccentricity. Moreover, detection of dynamic eccentricity in stator current around the principal slot harmonic (PSH) is only useful for some combination of pole pairs and rotor slots [48, 56,57]

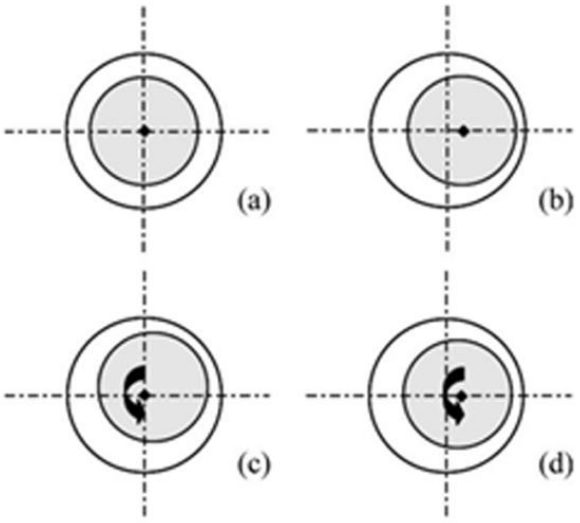

Fig. 1 Examples of Eccentricity: a) Without eccentricity (b) Static eccentricity (c) Dynamic eccentricity (d) Mixed eccentricity. [42].

Under mixed eccentricity conditions, the stator currents contain the following frequencies [42]:

$$f_{ecc} = f \pm k(1-s)/pf \quad (1)$$

where s is the machine slip. Since the frequencies related to the eccentricity and to the load torque overlap on the current sidebands, the frequencies provided by (1) are no longer enough for the diagnosis.

2.4 Broken Bars Detection

Induction motors are widely extended in industry, and among the defects which may appear, broken rotor bars represent 10 percent to 20 percent of the whole faults. This kind of failure does

not cause an immediate breakdown, but it deteriorates the machine operation, decreasing its performance [7,41], For the detection of this type of failure, different algorithms based on the stray flux signal time-frequency analysis of the Fourier and wavelets transforms have been used. Each technique presents its particular advantages and drawbacks. When a bar breakage occurs, a backward rotating magnetic field is generated due to the open-circuited bar. This creates an asymmetry in the rotor cage that is clearly reflected in the motors harmonic content [7,14].

The lower sideband harmonic leads to a torque (and speed) oscillation, which provokes the appearance of s, another harmonic in the stator current spectrum: the upper (or right) sideband harmonic given by $1 \pm 2sf$. Moreover, the frequency modulation on the rotational frequency f , provoked by the speed oscillation, also leads to sideband harmonics in the vibration (and, accordingly, in the noise) spectrum:

$$f_{bb} = f_{rr} \pm 2ksf \tag{2}$$

3. Higher Order Statistical Analysis: Theoretical Foundations

Higher-order spectral analysis, also known as polyspectra, is defined in terms of higher-order statistics (cumulants, in particular). Among the specific cases of the higher-order spectra, we find the third-order spectrum, also called bispectrum or Fourier Transform of the third-order temporal cumulant, and the trispectrum or Fourier Transform of the fourth-order temporal cumulant Figure 2 illustrates the classification of the higher-order spectra of a signal. Although the higher-order statistical characteristics and the spectrum of a signal can be defined in terms of moments and cumulants, moments and their spectra can be very useful in the analysis of deterministic signals (transient and periodic), while cumulants and their spectra are of great importance in the analysis of stochastic signals [36].

There are several motivations behind the use of higher-order spectra in signal processing, which can be used to: (1) eliminate Gaussian additive colored noise from an unknown power spectrum; (2) extract information due to process deviations whose probabilistic distribution function is Gaussian, and (3) detect and characterize the nonlinear properties in the signals, as well as identify nonlinear systems. The first motivation is based on the property that for stationary signals with Gaussian probabilistic distribution function, higher-order cumulants are equal to zero. If a non-Gaussian signal is received together with additive Gaussian noise, a calculation of the higher-order cumulant of the signal sample plus noise will eliminate the noise. Therefore, in these signal processing environments, there will be certain advantages for the detection and/or estimation of signal parameters through the cumulant of the observed data [36].

3.1 Higher-Order Statistics. Definition and Properties

In this section, the definitions, properties, and the way of calculating higher-order statistics are introduced. Let be $X = \{X(k)\}, k = 0, \pm 1, \pm 2, \ldots$ be a stationary random vector and its higher order moments exist, then:

$$m_n^X(\tau_1, \tau_2, \ldots, \tau_{n-1}) = E\{X(k)X(k+\tau_1) \ldots X(k+\tau_{n-1})\} \tag{3}$$

Where E denotes the expected value operator [6, 33,36] represents the n-th order moment of X, which depends only on the different temporary displacements $\tau_1, \tau_2, \dots, \tau_{n-1}$ with $\tau_i = 0, \pm 1, \dots$ It can be seen that the second order moment $m_2^X(\tau_1)$ is the autocorrelation function of X, likewise $m_3^X(\tau_1)$ And $m_4^X(\tau_1)$ represent the third and fourth order moments, respectively. The cumulants are similar to the moments, the difference is that the moments of a random process are derived from the characteristic function of the random variable, while the cumulant generating function is defined as the logarithm of the characteristic function of the random variable.

The n-th order cumulant of X can be written as, see [33]:

$$c_n^X(\tau_{1,\dots,}\tau_{n-1}) = m_n^X(\tau_{1,\dots,}\tau_{n-1}) - m_n^G(\tau_{1,\dots,}\tau_{n-1}), \quad n = 3,4 \tag{4}$$

Where $m_n^G(\tau_{1,\dots,}\tau_{n-1})$ is the n-order moment of a process with equivalent Gaussian distribution. with the same average value and autocorrelation function as X, the stationary random vector. From (4) it is evident that for a process following a Gaussian distribution, the cumulants of order greater or equal than 2 are null, since $m_n^X(\tau_{1,\dots,}\tau_{n-1})$ and $m_n^G(\tau_{1,\dots,}\tau_{n-1})$ are null too [23].

Although fourth-order cumulants imply a considerable increase in calculation complexity, they are especially necessary when third-order cumulants are canceled in the case of symmetrically distributed processes, such as uniform distributed processes from $[-a, a]$, with a $a \in \Re$, such as Laplace and Gaussian processes. Third order cumulants are not canceled for processes whose probabilistic density function is not symmetric, such as exponential or Rayleigh processes, but can take extremely small values compared to the values presented by their fourth-order cumulants [55].

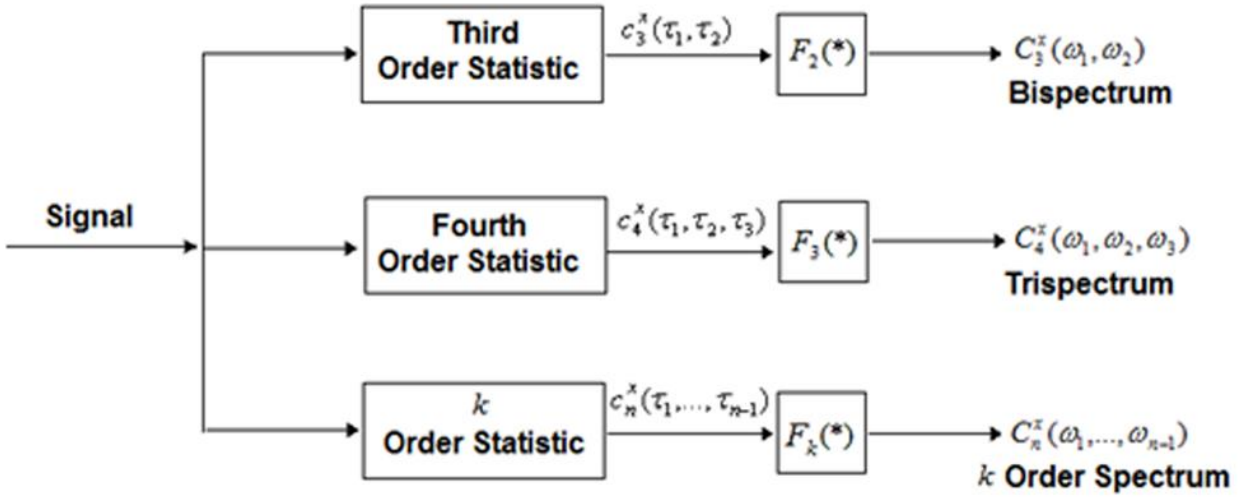

Fig. 2 Higher-Order Spectral classification. Here, $F_k(*)$ denote the k-dimensional Fourier Transform, see [36].

3.2 Higher-Order Spectrum

The n-th order spectrum of a stationary random vector $X = \{X(k)\}, k = 0, \pm1, \pm2, ...$ is defined as the multidimensional Fourier Transform $F_k(*)$ of order $n-1$ on the higher order statistical characteristics (moments and cumulants). The spectrum of the n-moment is defined as [23,55].

$$M_n^X(\omega_1, \dots, \omega_{n-1}) = F_n[m_n^X(\tau_{1,\dots,}\tau_{n-1})] \tag{5}$$

and, similarly, the spectrum of the n-cumulant is defined as:

$$C_n^X(\omega_1, \dots, \omega_{n-1}) = F_n[c_n^X(\tau_{1,\dots,}\tau_{n-1})] \tag{6}$$

Note that the spectrum of the n-th order cumulant is also periodic with period 2π, that is:

$$C_n^X(\omega_1, \dots, \omega_{n-1}) = C_n^X(\omega_1 + 2\pi, \dots, \omega_{n-1} + 2\pi) \tag{7}$$

Equation expression also reads as:

$$C_n^X(\omega_1, \dots, \omega_{n-1}) = \frac{1}{(2\pi)^{n-1}} \sum_{\tau_1=-\infty}^{\infty} \dots \sum_{\tau_{n-1}=-\infty}^{\infty} c_n^X(\tau_1, \dots, \tau_{n-1}) e^{j(\omega_1\tau_1 + \dots + \omega_{n-1}\tau_{n-1})} \tag{8}$$

In particular, for $n = 2$ in (8), we have the power spectrum:

$$C_2^X(\omega) = \frac{1}{2\pi} \sum_{\tau=-\infty}^{\infty} c_2^x(\tau) e^{-j\omega\tau} \tag{9}$$

where $|\omega| \leq \pi$ and c_2^x represents the process covariance sequence, see [23,55]

For $n = 3$ in (8), we have the bispectrum:

$$C_3^X(\omega_1, \omega_2) = \frac{1}{(2\pi)^2} \sum_{\tau_1=-\infty}^{\infty} \sum_{\tau_2=-\infty}^{\infty} c_3^X(\tau_1, \tau_2) e^{j(\omega_1\tau_1 + \omega_2\tau_2)} \tag{10}$$

where $|\omega_1| \leq \pi$, $|\omega_2| \leq \pi$ and $c_3^X(\tau_1, \tau_2)$ represents the the sequence of third order cumulants of $X(k)$. The expression of the cumulant complies with the following symmetric relationships [55]:

$$c_3^X(\tau_1, \tau_2) = c_3^X(\tau_2, \tau_1) = c_3^X(-\tau_2, \tau_1 - \tau_2) = c_3^X(\tau_2 - \tau_1, -\tau_1) =$$

$$= c_3^X(\tau_1 - \tau_2, -\tau_2) = c_3^X(-\tau_1, \tau_2 - \tau_1) \tag{11}$$

From these relationships, we can get a division of the plane (τ_1, τ_2) in six regions and, consequently, upon wing the third-order cumulant in any of these six regions (see Figure 3), we can reconstruct the complete sequence corresponding to the third-order cumulants. Note that each one of these regions contains its border. Thus, for example, sector I is an infinite region

characterized by $0 \leq \tau_1 \leq \tau_2$.For non-stationary processes, these regions of symmetry disappear. From these relationships and the definition of the spectrum of third-order cumulants, the following relationships in the two-dimensional frequency domain can be obtained [6, 23,33].

$$C_3^X(\omega_1, \omega_2) = C_3^X(\omega_2, \omega_1) = C_3^X(-\omega_2, -\omega_1) = C_3^X(-\omega_1 - \omega_2, \omega_2) \quad (13)$$

$$= C_3^X(\omega_1, -\omega_1 - \omega_2) = C_3^X(-\omega_1 - \omega_2, \omega_1) = C_3^X(\omega_2, \omega_1 - \omega_2) \quad (14)$$

Figure 3(b) shows the 12 symmetry regions of the bispectrum when real stochastic processes are considered and, similar to the temporal domain, the knowledge of the bispectrum in the triangular region It is enough for a total reconstruction of the bispectrum. Note that, in the frequency domain, the symmetry regions have a finite area and in general, the bispectrum takes complex values and, consequently, the phase information is preserved [55].

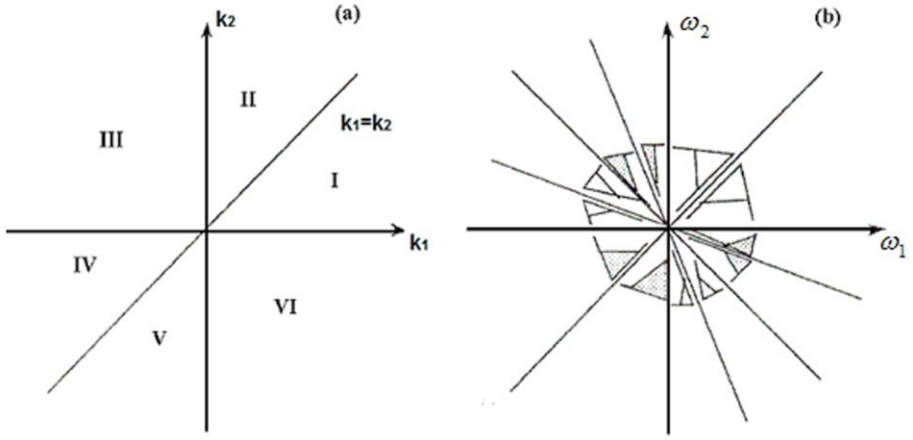

Fig. 3 Symmetry regions for (a) the third-order cumulant and for (b) the bispectrum.

In the case $n = 4$, we get the trispectrum:

$$C_4^X(\omega_1, \omega_2, \omega_3) = \frac{1}{(2\pi)^3} \sum_{\tau_1=-\infty}^{\infty} \sum_{\tau_2=-\infty}^{\infty} \sum_{\tau_3=-\infty}^{\infty} c_4^X(\tau_1, \tau_2, \tau_3) e^{j(\omega_1\tau_1 + \omega_2\tau_2 + \omega_3\tau_3)} \quad (15)$$

where $|\omega_1| \leq \pi$, $|\omega_2| \leq \pi$, $|\omega_3| \leq \pi$ and $|\omega_1 + \omega_2 + \omega_3| \leq \pi$ whre $c_4^X(\tau_1, \tau_2, \tau_3)$represents the the sequence of fourth order cumulants. By combining the definition of the trispectrum and the fourth-order cumulants, 96 regions of symmetry appear associated with a real process. From the spectra of higher-order cumulants, the expressions of their respective cumulants in the temporal domain can be retrieved, by applying the n-order inverse Fourier transform [55].

3.3 Examples of calculation of the Higher Order Spectra

To illustrate in more detail the calculation of the higher-order spectra, we show several examples with periodic signals.

3.3.1 Cosine signal

First, let us consider the cosine signal:

$$X = A_k \cos(2\pi f_k + \vartheta_k) \tag{16}$$

with amplitude $A_k = 1$, frequency $f_k = 50\ Hz$, and phase $\vartheta_k = \pi/4$, discretely generated from a sampling frequency $f_s = 1000$ and a duration of 1024 samples. Then the bispectrum for a 1024 sample data window is equivalent to discretely performing the Fourier transform of the third order cumulant of the signal. In figures 4 (a) and (b) respectively shows the cosine signal and its frequency spectrum using the onedimensional Fourier Transform (FT). Likewise, as a comparison mode, the bispectrum of the 50 Hz cosine signal (0.05 normalized to 1) it is shown in Figure 5, to illustrate that the fundamental frequency of the signal prevails; and also showing other frequency components that by means of the one-dimensional spectrum using Fourier, they do not appear, which gives the bispectrum a higher resolution from the spectral point of view, which can be useful for dissimilar applications to find linear combinations or not, of existing relations between frequencies, for the development of identifying spectral patterns.

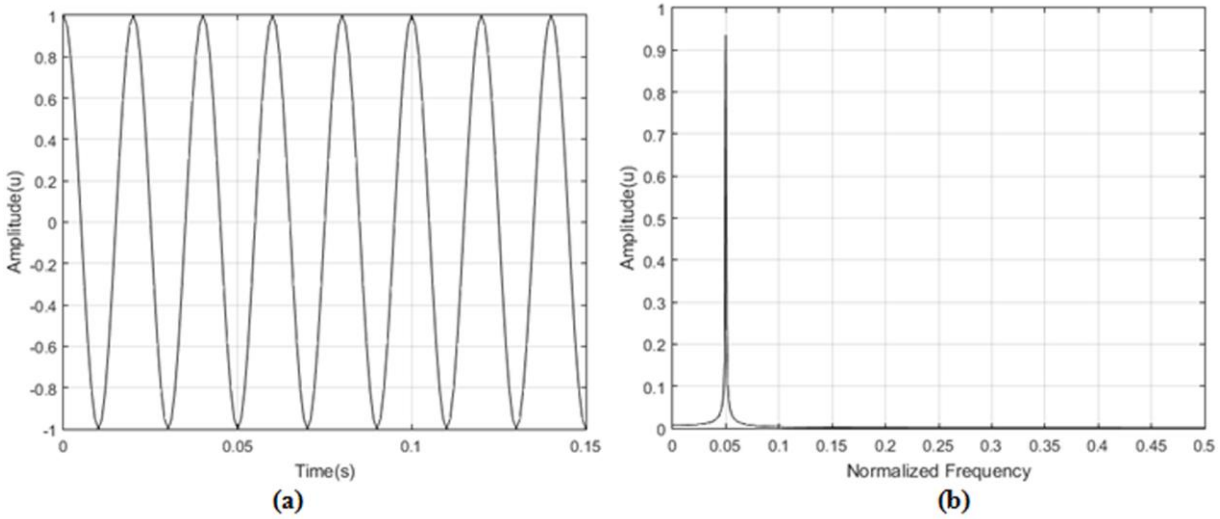

Fig. 4 (a) A cosine signal of 50Hz (0.05 normalized frequency) and (b) its spectrum

Apart from the fundamental frequency component 0.05 (50Hz) normalized to 1, there are other components as results of linear combinations of the fundamental frequency (16), since the

calculation of bispectrum results in a two-dimensional frequency and a phase matrix, see Figure 5.

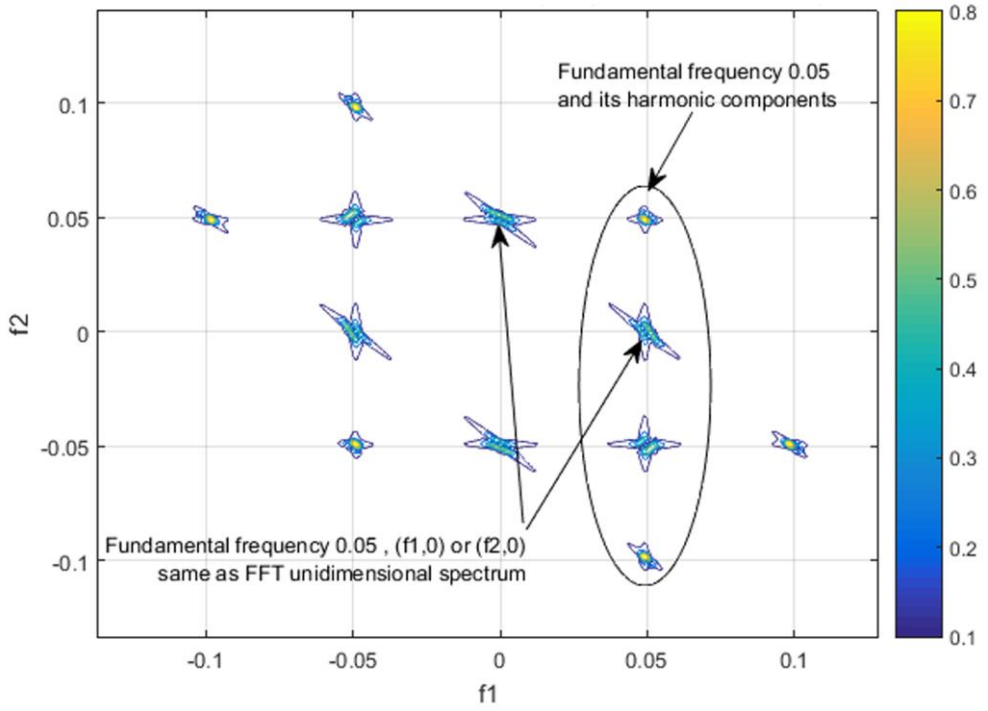

Fig. 5 Contour plot of the bispectrum of the 50 Hz (0.05) cosine signal.

On the other hand, although less used, the phase spectrum of the cosine signal of (16) is also shown. The phase spectrum contains an arrangement with the amplitude in degrees of the phase of the signal, that is taken as $\vartheta_k = \pi/4$ in (16). Its corresponding phase spectrum is shown below in Figure 6 . We also show the phase bispectrum, see Figure 7, where the linear phase of the cosine signal is resalted in the bispectrum phase matrix. The bispectrum preserves the phase information of every spectral component, that is the phase of the original signaland it can be otained from the original signal as:

$$\vartheta_{C_3^X}(\omega_1, \omega_2) = \vartheta_X(\omega_1) + \vartheta_X(\omega_2) + \vartheta_X(\omega_1 + \omega_2) \tag{17}$$

where $\vartheta_{C_3^X}(\omega_1, \omega_2)$ represents the phases matrix of every spectral component. This relation also permits to retrieve the original phase of the signal.

3.3.2 Harmonic signal

Secondly, we have also experimented by calculating the bispectrum of a harmonic signal of the form:

$$X = A_k \cos(2\pi f_k + \vartheta_k) + 2A_k \cos(2\pi \cdot 3 f_k + \vartheta_k) \tag{18}$$

In figure 8 (a and (b) we show the harmonic signal in time and its frequency spectrum using the onedimensional Fourier Transform (FT). In figure (9) the bispectrum of the harmonic signal is shown. We notice that the calculation of the bispectrum preserves the fundamental frequencies of each signal in the sum of harmonics, analogous to the calculation of the one-dimensional FT. We also observe that since the bispectrum is absolutely summable, multiple frequency components appear as a result of the linear combinations of the bispectrum of both cosine signals individually.

We also show the phase bispectrum of the harmonic signal in figure (10) It is more complex than the one of the cosine signal because the bispectrum is absolutely additive and the phase of the 50Hz and 150Hz components are totally mixed.

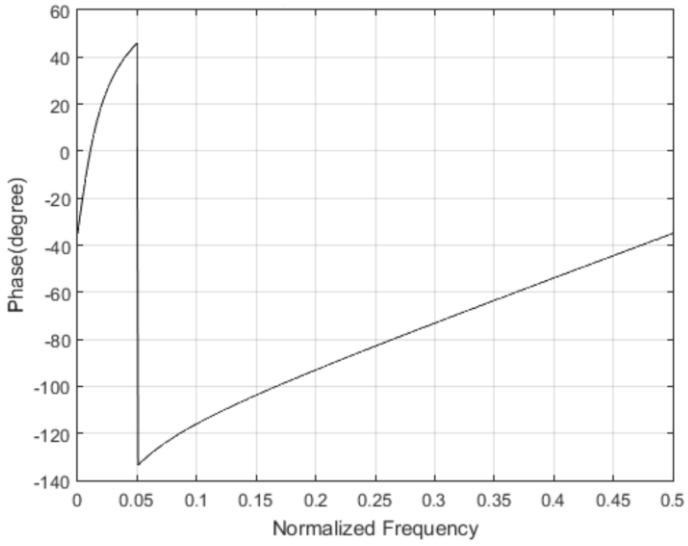

Fig. 6 A phase spectrum of a cosine signal of 50Hz (0.05 normalized frequency)

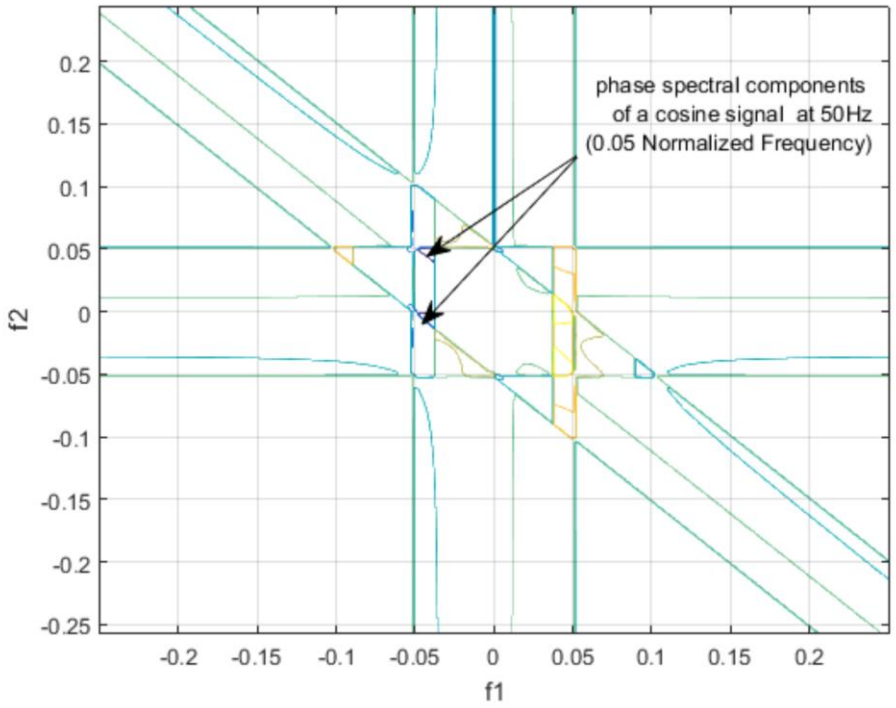

Fig. 7 Contour plot of the phase bispectrum of a cosine signal of 50Hz (0.05 normalized frequency)

4. Using second and higher-order statistics with stray flux signals for faults detection

Although the analysis based on higher-order spectra in relation to the processing using the classical analysis based on the power spectrum can be advantageous, and the use of the stray flux signals is a non-invasive method, few works are linking HOSA (Higher Order Statistic Analysis) and stray flux signals. This may be because computational complexity increases when using higher-order statistics in comparison to second-order statistics based on the Fourier one-dimensional transform. Most of the works based on the use of HOSA for diganosing electric machines are based on the processing of vibration signals [3,8,20,46,47].

However, we have recently exposed the advantages of HOSA of stray flux signals [25], where an algorithm for the detection of the healthy-damaged state condition is proposed using temporary indicators in the frequency domain based on the bispectrum. Likewise, in [26], a second-order statistical analysis based on the autocorrelation function is linked with stray flux signals for the detection of non-adjacent bar breaks.

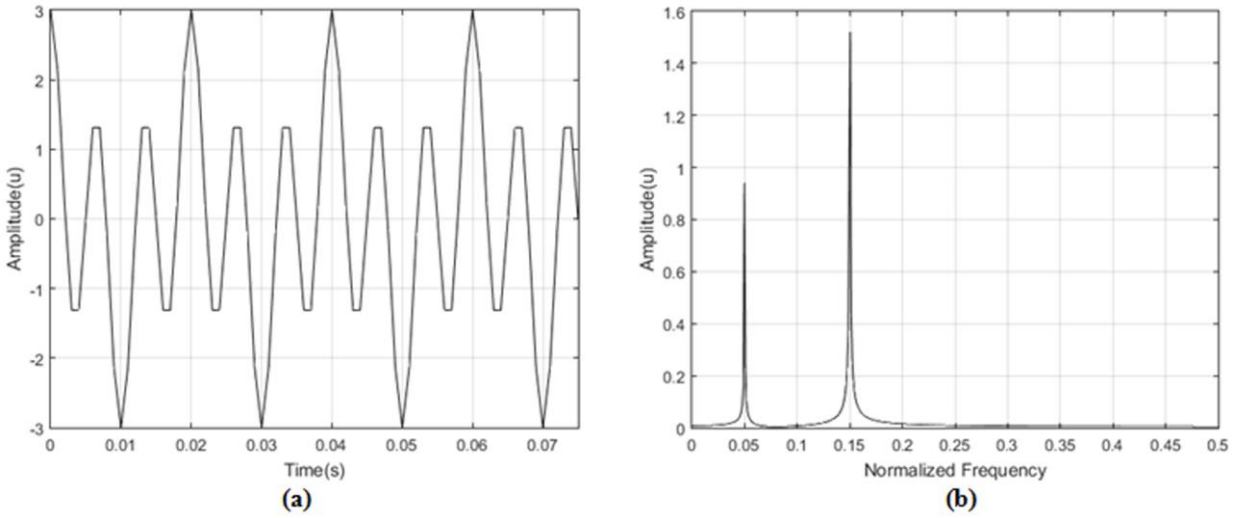

Fig. 8 Ilustration of : a) Harmonic Signal b) Harmonic Signal Spectrum

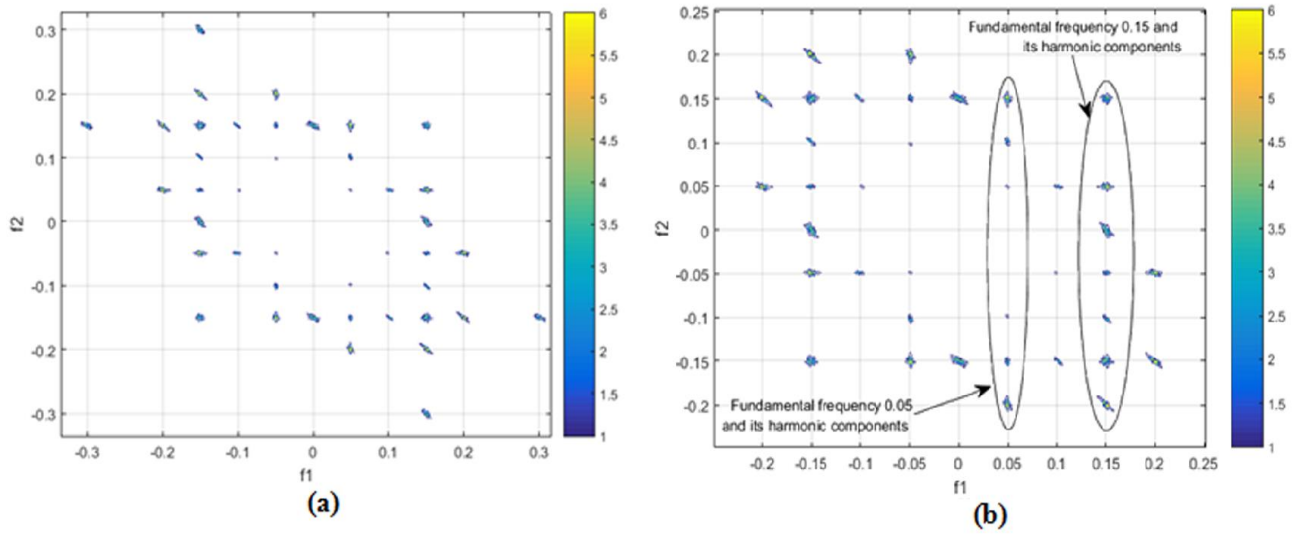

Fig. 9 Contour Plot of: a) Bispectrum of the Harmonic Signal described in (14) and b) an expanded version of it.

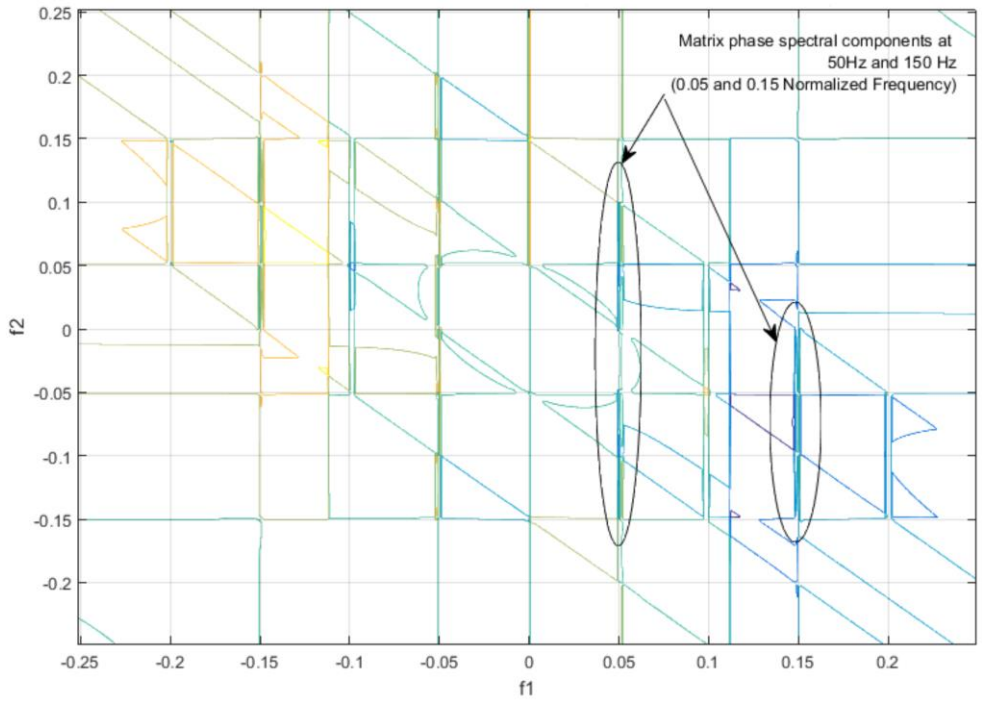

Fig. 10 Contour plot of the phase bispectrum of a harmonic signal described in (14).

5. Conclusions

This work has shown a review of the techniques of processing and diagnosing of failures in electric induction machines. In particular, we have reported how to use them with flux signals. The theoretical foundations and with practical examples of the High-order statistical analysis (HOSA) and its potential for detecting failures in electrical machines have also been shown. On the other hand, validated results are also shown in references, of their use, using stray flux signals, which demonstrates that the linking of high-order statistical analysis techniques with the detection of failures in electric machines can be a very useful tool.

6. References

1. H. Akçay and E. Germen. Subspace-based identification of acoustic noise spectra in induction motors. IEEE Transactions on Energy Conversion, 30(1):32–40, 2015.
2. J. Antonino-Daviu, M. Riera-Guasp, J. Roger-Folch, F. Martínez-Giménez, and A. Peris. Application and optimization of the discrete wavelet transform for the detection of broken rotor bars in induction machines. Applied and Computa- tional Harmonic Analysis, 21(2):268–279, 2006.
3. N. Arthur and J. Penman. Induction machine condition monitoring with higher order spectra. IEEE Transactions on Industrial Electronics, 47(5):1031–1041, 2000.
4. T. P. Banerjee and S. Das. Multi-sensor data fusion using support vector machine for motor fault detection. Information Sciences, 217:96–107, 2012.

5. G. Bin, J. Gao, X. Li, and B. Dhillon. Early fault diagnosis of rotating machinery based on wavelet packets—empirical mode decomposition feature extraction and neural network. Mechanical Systems and Signal Processing, 27:696–711, 2012.
6. B. Boashash, E. J. Powers, and A. M. Zoubir. Higher-order statistical signal processing. Longman Cheshire, 1995.
7. A. Ceban, R. Pusca, and R. Romary. Eccentricity and broken rotor bars faults-effects on the external axial field. In The XIX International Conference on Electrical Machines-ICEM 2010, pages 1–6. IEEE, 2010.
8. T. Chow and G. Fei. Three phase induction machines asymmetrical faults identification using bispectrum. IEEE Transactions on Energy Conversion, 10(4):688–693, 1995.
9. X. Dai and Z. Gao. From model, signal to knowledge: A data-driven perspective of fault detection and diagnosis. IEEE Transactions on Industrial Informatics, 9(4):2226–2238, 2013.
10. J. de Jesus Rangel-Magdaleno, H. Peregrina-Barreto, J. M. Ramirez-Cortes, P. Gomez-Gil, and R. Morales-Caporal. Fpga-based broken bars detection on induction motors under different load using motor current signature analysis and mathematical morphology. IEEE Transactions on Instrumentation and Measurement, 63(5):1032–1040, 2013.
11. P. A. Delgado-Arredondo, D. Morinigo-Sotelo, R. A. Osornio-Rios, J. G. Avina-Cervantes, H. Rostro-Gonzalez, and R. de Jesus Romero-Troncoso. Methodology for fault detection in induction motors via sound and vibration signals. Mechanical Systems and Signal Processing, 83:568–589, 2017.
12. M. Drif and A. J. M. Cardoso. Stator fault diagnostics in squirrel cage three-phase induction motor drives using the instantaneous active and reactive power signature analyses. IEEE Transactions on Industrial Informatics, 10(2):1348–1360, 2014.
13. L. Frosini, C. Harlişca, and L. Szabó. Induction machine bearing fault detection by means of statistical processing of the stray flux measurement. IEEE Transactions on Industrial Electronics, 62(3):1846–1854, 2014.
14. Z. Gao, C. Cecati, and S. X. Ding. A survey of fault diagnosis and fault-tolerant techniques—part i: Fault diagnosis with model-based and signal-based approaches. IEEE Transactions on Industrial Electronics, 62(6):3757–3767, 2015.
15. M. Geethanjali and H. Ramadoss. Fault diagnosis of induction motors using motor current signature analysis: A review. In Advanced Condition Monitoring and Fault Diagnosis of Electric Machines, pages 1–37. IGI Global, 2019.
16. T. Ghanbari and A. Farjah. A magnetic leakage flux-based approach for fault diagnosis in electrical machines. IEEE Sensors Journal, 14(9):2981–2988, 2014.
17. A. Glowacz. Acoustic based fault diagnosis of three-phase induction motor. Applied Acoustics, 137:82–89, 2018.
18. A. Glowacz, W. Glowacz, Z. Glowacz, and J. Kozik. Early fault diagnosis of bearing and stator faults of the single-phase induction motor using acoustic signals. Measurement, 113:1–9, 2018.
19. K. C. Gryllias and I. A. Antoniadis. A support vector machine approach based on physical model training for rolling ele ment bearing fault detection in industrial environments. Engineering Applications of Artificial Intelligence, 25(2):326– 344, 2012.
20. F. Gu, Y. Shao, N. Hu, A. Naid, and A. Ball. Electrical motor current signal analysis using a modified bispectrum for fault diagnosis of downstream mechanical equipment. Mechanical Systems and Signal Processing, 25(1):360–372, 2011.
21. C. Harlişca, L. Szabó, L. Frosini, and A. Albini. Diagnosis of rolling bearings faults in electric machines through stray magnetic flux monitoring. In 2013 8TH International Symposium on Advanced Topics in Electrical Engineering (Atee), pages 1–6. IEEE, 2013.
22. R. Hoppler and R. A. Errath. Motor bearings, not must a piece of metal. In 2007 IEEE Cement Industry Technical Conference Record, pages 214–233. IEEE, 2007.
23. R. M. Howard. Principles of random signal analysis and low noise design: The power spectral density and its appli- cations. John Wiley & Sons, 2004.
24. J.-N. Hwang and Y. H. Hu. Handbook of neural network signal processing. CRC press, 2001.

25. M. E. Iglesias-Martínez, J. A. Antonino-Daviu, P. Fernández de Córdoba, and J. A. Conejero. Rotor fault detection in induction motors based on time-frequency analysis using the bispectrum and the autocovariance of stray flux signals. Energies, 12(4):597, 2019.
26. M. E. Iglesias-Martinez, P. F. de Cordoba, J. Antonino-Daviu, and J. A. Conejero. Detection of nonadjacent rotor faults in induction motors via spectral subtraction and autocorrelation of stray flux signals. IEEE Transactions on Industry Applications, 2019.
27. F. Immovilli, A. Bellini, R. Rubini, and C. Tassoni. Diagnosis of bearing faults in induction machines by vibration or current signals: A critical comparison. IEEE Transactions on Industry Applications, 46(4):1350–1359, 2010.
28. C. Jiang, S. Li, and T. G. Habetler. A review of condition monitoring of induction motors based on stray flux. In 2017 IEEE Energy Conversion Congress and Exposition (ECCE), pages 5424–5430. IEEE, 2017.
29. L. Jiang, Y. Liu, X. Li, and S. Tang. Using bispectral distribution as a feature for rotating machinery fault diagnosis. Measurement, 44(7):1284–1292, 2011.
30. Q. Jiang and F. Chang. A novel rolling-element bearing faults classification method combines lower-order moment spectra and support vector machine. Journal of Mechanical Science and Technology, 33(4):1535–1543, 2019.
31. X. Jin and T. W. Chow. Anomaly detection of cooling fan and fault classification of induction motor using mahalanobis–taguchi system. Expert Systems with Applications, 40(15):5787–5795, 2013.
32. J. Józwik. Identification and monitoring of noise sources of CNC machine tools by acoustic holography methods. Advances in Science and Technology Research Journal, 10(30), 2016.
33. S. M. Kay. Fundamentals of statistical signal processing. Prentice Hall PTR, 1993.
34. R. Liu, B. Yang, E. Zio, and X. Chen. Artificial intelligence for fault diagnosis of rotating machinery: A review.Mechanical Systems and Signal Processing, 108:33–47, 2018.
35. Z. Liu, H. Cao, X. Chen, Z. He, and Z. Shen. Multi-fault classification based on wavelet svm with pso algorithm to analyze vibration signals from rolling element bearings. Neurocomputing, 99:399–410, 2013.
36. J. M. Mendel. Tutorial on higher-order statistics (spectra) in signal processing and system theory: Theoretical results and some applications. Proceedings of the IEEE, 79(3):278–305, 1991.
37. M. Mrugalski, M. Witczak, and J. Korbicz. Confidence estimation of the multi-layer perceptron and its application in fault detection systems. Engineering Applications of Artificial Intelligence, 21(6):895–906, 2008.
38. V. Muralidharan and V. Sugumaran. A comparative study of naïve bayes classifier and bayes net classifier for fault diagnosis of monoblock centrifugal pump using wavelet analysis. Applied Soft Computing, 12(8):2023–2029, 2012.
39. Y. Ono, Y. Onishi, T. Koshinaka, S. Takata, and O. Hoshuyama. Anomaly detection of motors with feature emphasis using only normal sounds. In Acoustics, Speech and Signal Processing (ICASSP), 2013 IEEE International Conference on, pages 2800–2804. IEEE, 2013.
40. R. H. C. Palácios, I. N. da Silva, A. Goedtel, and W. F. Godoy. A comprehensive evaluation of intelligent classifiers for fault identification in three-phase induction motors. Electric Power Systems Research, 127:249–258, 2015.
41. P. A. Panagiotou, I. Arvanitakis, N. Lophitis, J. Antonino-Daviu, and K. N. Gyftakis. A new approach for broken rotor bar detection in induction motors using frequency extraction in stray flux signals. IEEE Transactions on Industry Applications, 2019.
42. K. Pandey, P. Zope, and S. Suralkar. Review on fault diagnosis in three-phase induction motor. MEDHA–2012, Proceedings published by International Journal of Computer Applications (IJCA), 2012.
43. J. Rafiee, F. Arvani, A. Harifi, and M. Sadeghi. Intelligent condition monitoring of a gearbox using artificial neural network. Mechanical systems and signal processing, 21(4):1746–1754, 2007.
44. A. Sadeghian, Z. Ye, and B. Wu. Online detection of broken rotor bars in induction motors by wavelet packet decom- position and artificial neural networks. IEEE

Transactions on Instrumentation and Measurement, 58(7):2253–2263, 2009.
45. L. Saidi, J. B. Ali, and F. Fnaiech. Application of higher order spectral features and support vector machines for bearing faults classification. ISA transactions, 54:193–206, 2015.
46. L. Saidi, F. Fnaiech, G. Capolino, and H. Henao. Stator current bi-spectrum patterns for induction machines multiple- faults detection. In IECON 2012-38th Annual Conference on IEEE Industrial Electronics Society, pages 5132–5137. IEEE, 2012.
47. L. Saidi, F. Fnaiech, H. Henao, G. Capolino, and G. Cirrincione. Diagnosis of broken-bars fault in induction machines using higher order spectral analysis. ISA Transactions, 52(1):140–148, 2013.
48. M. Salah, K. Bacha, and A. Chaari. An improved spectral analysis of the stray flux component for the detection of air-gap irregularities in squirrel cage motors. ISA transactions, 53(3):816–826, 2014.
49. B. Samanta. Gear fault detection using artificial neural networks and support vector machines with genetic algorithms. Mechanical systems and signal processing, 18(3):625–644, 2004.
50. P. Sangeetha and S. Hemamalini. Dyadic wavelet transform-based acoustic signal analysis for torque prediction of a three-phase induction motor. IET Signal Processing, 11(5):604–612, 2017.
51. J. Sanz, R. Perera, and C. Huerta. Gear dynamics monitoring using discrete wavelet transformation and multi-layer perceptron neural networks. Applied Soft Computing, 12(9):2867–2878, 2012.
52. Z. Shen, X. Chen, X. Zhang, and Z. He. A novel intelligent gear fault diagnosis model based on emd and multi-class tsvm. Measurement, 45(1):30–40, 2012.
53. A. Singhal and M. A. Khandekar. Bearing fault detection in induction motor using fast fourier transform. In IEEE Int. Conf. on Advanced Research in Engineering & Technology, 2013.
54. A. Soualhi, K. Medjaher, and N. Zerhouni. Bearing health monitoring based on hilbert–huang transform, support vector machine, and regression. IEEE Transactions on Instrumentation and Measurement, 64(1):52–62, 2014.
55. A. Swami, G. B. Giannakis, and G. Zhou. Bibliography on higher-order statistics. Signal processing, 60(1):65–126, 1997.
56. O. Vitek, M. Janda, and V. Hajek. Effects of eccentricity on external magnetic field of induction machine. In Melecon, 2010-2010 15th IEEE Mediterranean Electrotechnical Conference, pages 939–943. IEEE, 2010.
57. H. Wang, X. Bao, C. Di, and Z. Cheng. Detection of eccentricity fault using slot leakage flux monitoring. In 2015 9th International Conference on Power Electronics and ECCE Asia (ICPE-ECCE Asia), pages 2188–2193. IEEE, 2015.
58. Y. Wang, J. Xiang, R. Markert, and M. Liang. Spectral kurtosis for fault detection, diagnosis and prognostics of rotating machines: A review with applications. Mechanical Systems and Signal Processing, 66:679–698, 2016.
59. Z. Wang and C. Chang. Online fault detection of induction motors using frequency domain independent components analysis. In 2011 IEEE International Symposium on Industrial Electronics, pages 2132–2137. IEEE, 2011.
60. Z. Wang, C. Chang, and Y. Zhang. A feature based frequency domain analysis algorithm for fault detection of induction motors. In 2011 6th IEEE Conference on Industrial Electronics and Applications, pages 27–32. IEEE, 2011.
61. W. Wenbing and X. Jinquan. The application of coupled three order cumulants' differential feature in fault diagnosis. In 2017 International Conference on Virtual Reality and Visualization (ICVRV), pages 374–375. IEEE, 2017.

62. I. Zamudio-Ramirez, R. A. Osornio-Rios, M. Trejo-Hernandez, R. d. J. Romero-Troncoso, and J. A. Antonino-Daviu. Smart-sensors to estimate insulation health in induction motors via analysis of stray flux. Energies, 12(9):1658, 2019.
63. X. Zhang and J. Zhou. Multi-fault diagnosis for rolling element bearings based on ensemble empirical mode decom- position and optimized support vector machines. Mechanical Systems and Signal Processing, 41(1-2):127–140, 2013.
64. W. Zhao, T. Tao, and E. Zio. System reliability prediction by support vector regression with analytic selection and genetic algorithm parameters selection. Applied Soft Computing, 30:792–802, 2015.
65. W. Zhao, Y. Zhang, and Y. Zhu. Diagnosis for transformer faults based on combinatorial Bayes Network. In 2009 2nd International Congress on Image and Signal Processing, pages 1–3. IEEE, 2009.
66. F. Zidat, J.-P. Lecointe, F. Morganti, J.-F. Brudny, T. Jacq, and F. Streiff. Non invasive sensors for monitoring the efficiency of ac electrical rotating machines. Sensors, 10(8):7874–7895, 2010.

applied sciences

MDPI

Article

Detection of adjacent and non-adjacent bar breakages in induction motors via convolutional analysis of sound signals

Miguel Enrique Iglesias Martínez[1], Pedro Fernández de Córdoba[2], Jose Alfonso Antonino-Daviu[3,*] and J. Alberto Conejero[1]

[1,2] Departamento de Telecomunicaciones, Universidad de Pinar del Río, Pinar del Río, Martí #270, CP 20100, Cuba; migueliglesias2010@gmail.com (M.E.I.M)

[2] Instituto Universitario de Matemática Pura y Aplicada, Universitat Politècnica de València (UPV), Camino de Vera s/n, 46022 Valencia, Spain; pfernandez@mat.upv.es (P.F.d.C.); aconejero@upv.es (J.A.C.)

[3] Instituto Tecnológico de la Energía, Universitat Politècnica de València (UPV), Camino de Vera s/n,46022 Valencia, Spain

* Correspondence: joanda@die.upv.es; (J.A.A.D), Tel.: +34-963877592

Featured Application: The investigation can give as an application that can be useful for the detection of adjacent and non-adjacent bars breakage, which can be developed in a portable device. It is not invasive and only depends on processing the acoustic noise emitted by the electric machine, to emit a result.

Abstract: We apply second-order statistical signal processing techniques to the acoustic signal of an induction motor for detecting adjacent and non-adjacent bar breakages. We obtain a unique identifier pattern when the signal has either one or several broken bars, inde- pendently of the relative position of the bar breakages. Our proposal provides good results for fault detectability compared to several state-of-art works. Moreover, we also present the identification of the faults and the signal to noise ratio obtained during the preprocessing stage.

Keywords: Induction machines; fault diagnosis; rotor bar breakages; autocovariance.

1. INTRODUCTION

Nowadays, the monitoring of acoustic signals has found different applications in medicine, in- dustry, telecommunications, and other branches of science. In the field of electric motors condition monitoring, the analysis of acoustic noise is an interesting option, at least to complement other diagnostic measures [3, 7, 11, 26]. For instance, a common problem in these machines is the detec- tion of rotor damages such as broken bars. These faults may even lead to catastrophic failures and forced motor outages, that can imply significant losses for the industries using them. In particular, it is especially relevant in the case of large high voltage motors. Figure 1 shows a picture of the rotor of an industrial induction motor with broken bars.

The underlying idea of noise analysis is to interpret the acoustic waves produced by mechanical vibrations of breaking bars [8]. Such analysis has been applied not only to detect rotor damages but also to consider the case of adjacent broken rotor bars. To the best of our knowledge, the case of acoustic noise-based detection of non-adjacent bar breakages has not yet been investigated; despite being a serious issue that other well-known techniques (such as

current or vibration analysis) have not correctly solved. Indeed, the current analysis of these cases may lead to false-negative indications for certain relative positions between the broken bars [26].

Figure 1. Rotor of a real industrial motor (2000 H.P) with broken rotor bars.

Noise-based detection of different failures based on the use of the Fast Fourier Transform (FFT) and high-resolution spectral analysis was considered in the following works [2, 10, 13, 17, 18, 23, 29] However, the FFT has the main disadvantage that it is not immune to noise since the spectrum of a measured signal also contains the spectrum of the noise. To overcome this overlapping, some authors have used high-resolution spectral analysis methods, with the disadvantage of not knowing a priori the number of subspaces allocated to the noise [2, 10]. Some of the last works in this line have considered related methods such as the design of an active resonant filter based on the Win- dowed Fourier Transform (WFT) analysis [21], the method of selection of amplitudes of frequency - multiexpanded [12], or a spectral estimation algorithm on vector subspaces such as MUSIC and ESPRIT[30]. Alternative approaches have been proposed based on wavelet methods [1, 5, 6, 9, 19, 24, 32] or on Empirical Mode Decomposition (EMD) methods [8]. The application of higher-order statistics analysis to the information contained in the bispectrum, or only in its diagonal, has been considered for condition monitoring in [4, 16, 27, 28]. Furthermore, the use of all the information contained in the bispectrum involves a two-dimensional function whose phase recovery process may involve a high computational cost.

Apart from the analysis of sound signals, other approaches permit to identify the number of broken bars and to diagnose their faults, such as pattern recognition algorithms [15, 22, 33], termal images [14], genetic algorithms [20], and chaos theory [25].

However, none of them have been proven to be valid enough for the reliable detection of the failures considered in this work. Hence, we propose an algorithm that uses second-order statistics, convolution, and spectral analysis for fault diagnosis in induction motors, which also uses the acoustic noise as a means of detection. This algorithm is applied not only to detect adjacent bar breakages, but also to investigate the possibility of detecting non-adjacent broken bars, improving the performance of classical techniques. Our results show the

potential of this approach, that provides us valuable information to detect rotor damages or, at least, to complement the information provided by other quantities.

In Section 2, we outline the case of broken rotor bars considered in this work. Then, we process the acoustic signal of the motor for reducing the noise. This is obtained by convolving the input signal with its autocovariance, as it is described in Section 3. In Section 4, we show the experimental results and the proposed pattern recognition method. Finally, conclusions are outlined in Section 5.

2. MATERIALS AND METHODS

2.1. Description of the treated fault: Broken Rotor Bars (BRB)

Previous studies have shown that a broken bar in an induction motor leads to a distortion in the air gap magnetic field, known as a fault field). This fault field induces some harmonics in the stator current spectrum. The most relevant one is the lower sideband harmonic or left sideband harmonic, with the frequency given by $(1-2s)f$. Here, f is the power supply frequency, s is the slip, which is defined by (1), where n_s represent the synchronous speed of the machine (in r.p.m., calculated by $60f/p$, p is the number of poles), and n is the actual motor speed.

$$s = \frac{n_s - n}{n_s}, \tag{1}$$

The lower sideband harmonic leads to a torque (and speed) oscillation, which provokes the appearance of another harmonic in the stator current spectrum: the upper (or right) sideband harmonic given by $(1-2s)f$ Moreover, the frequency modulation on the rotational frequency of f_R, provoked by the speed oscillation, also leads to sideband harmonics in the vibration (and, accordingly, in the noise) spectrum, according to (2). For further information, see [8].

$$F_{BB=}F_R \pm 2ksf\ , k\ \in\ \mathbb{N}_0 \tag{2}$$

2.2. Proposed method for noise reduction

We propose a method for noise reduction that permits to identify and separate the spectral components in the acoustic signal that do not provide useful information on the broken bars. We consider these components as interferences from external sources or the environment. We can consider them as random processes modeled as white noise. We first try to eliminate them. However, if it is not possible, we will reduce them in order only to process the useful information provided by the spectrum of the acoustic noise from the motor.

The method goes as follows:

1. We first convolute the input signal with its autocovariance, working as a matched filter. At the end of this section, we provide further details on the convolution of a signal with its covariance.
2. The output of the convolution process is adjusted in amplitude via spectral analysis using the Fourier Transform, by means of the nonlinear factor derived from equation (3)

$$A'_k = 4[A_k)^{1/3}] \;\; k \in \mathbb{N}_0 \tag{3}$$

where A'_k is the signal amplitude at the output of the convolution process and A_k is the original ignal amplitude.

3. An envelope detector is applied to the result of the inverse Fourier transform of the second step output. This enables us to demodulate the signal because of the signal spectrum symmetry. loss due to multiplication by a nonlinear factor when the phase and amplitude are combined.

4. Finally, we divide the resulting signal of the last step into the signal obtained from the inverse Fourier Transform in order to recover the original signal.

To sum up, we show the block diagram of the algorithm in Figure 2, where the input signal is the noisy signal or the acoustic signal from the induction motor.

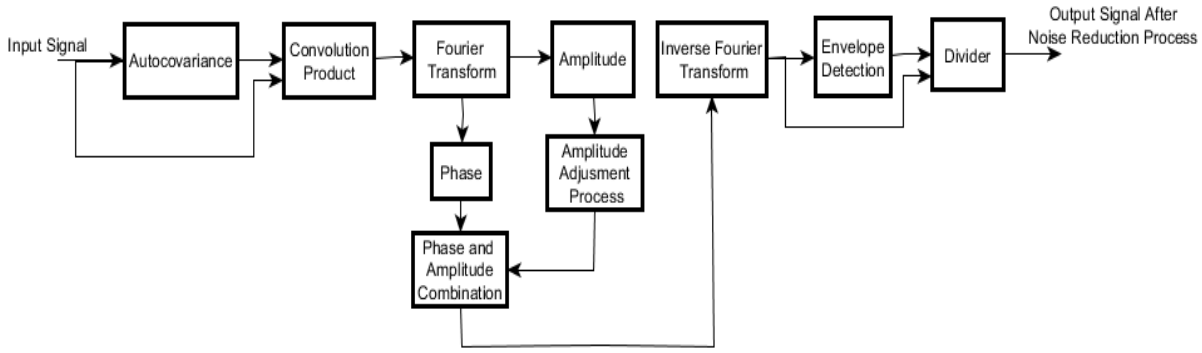

Figure 2. Block diagram of the proposed method for noise reduction

In the rest of the section, we use second-order statistics to explain what is the effect of convolving a signal with its autocovariance.

We recall that the autocovariance function of a stochastic process $y = \{y(t)\}_{t\geq 0}$ is a measure of the dispersion of the process about the mean value, and can be defined in term of its joint moments, see for instance [31].

$$\begin{aligned} C_2^y(t_1,t_2) &= E\left[(y(t_1)-u_y(t_1))(y(t_2)-u_y(t_2))\right] \\ &= R_2^y(t_1,t_2) - u_y(t_1)u_y(t_2) \end{aligned} \tag{3}$$

where $u_y(t)$ is the mean of the variable $y(t)$ and R_2^y is the autocorrelation function. For a zero-mean process, the autocorrelation and the autocovariance functions are identical. For a

stationary process, we consider $u_y(t)$ to be constant for all $t \geq 0$. If we denote this amount by $u_y(t)$, we have that the autocovariance function of (3) becomes:

$$C_2^y(t_1,t_2) = R_2^y(t_1,t_2) - u_y(t)^2 \tag{4}$$

2.3 Convolution of a signal with its autocovariance

For real value periodic signals, the observed data can be described as follows:

$$a(t) = x(t) + n(t) = \sum_{k=1}^{N} A_k \cos(w_k t + \phi_k) + n(t) \tag{5}$$

Where $x(t)$ is the signal to be detected and $n(t)$ is an additive zero mean stationary noise. Besides, A_k, f_k, and ϕ_k for $k = 1,...N$ stand for the amplitude, frequency and phase, respectively, of the harmonic signals. Then, applying second order statistics to (5) we get:

$$\begin{aligned} C_2^a(\tau) &= C_2^x(\tau) + C_2^n(\tau) \\ &= E\{x(t)\cdot x(t+\tau)\} + \cdot E\{n(t)\cdot n(t+\tau)\} \end{aligned} \tag{6}$$

The autocorrelation function of a continuous-time zero-mean white noise process $n(t)$ with variance ${\sigma_n}^2$ is a Dirac delta function $\delta_0(t)$. For a harmonic signal, the autocorrelation is a zero-phase harmonic signal. Then, from (3), we get that the autocovariance $C_2^a(t), t \geq 0$ is given by:

$$C_2^a(t) = \sum_{k=1}^{N} \frac{{A_k}^2}{2} \cos(w_k t) + \sigma_n^2 \delta_0(t) \tag{7}$$

It is clear from (7) that it does not preserve the waveform of the original signal. This is due to the loss of phase information of the original signal in the noise cancellation process. However, convolving $a(t) * C_2^a(t)$, we can see that we recover the phase information:

$$\begin{aligned} a * C_2^a(\tau) &= \lim_{T\to\infty} \int_{-T/2}^{T/2} a(t)\cdot C_2^a(\tau - t)dt \\ &= \lim_{T\to\infty} \int_{-T/2}^{T/2} \left[\sum_{k=1}^{N} A_k \cos(w_k t + \phi_k) + n(t)\right] \cdot \left[\sum_{k=1}^{N} \frac{{A_k}^2}{2} \cos(w_k(\tau - t)) + \sigma_n^2 \delta_0(\tau - t)\right] dt \\ &= \lim_{T\to\infty} \int_{-T/2}^{T/2} \left[\begin{array}{l} \sum_{k=1}^{N} A_k \cos(w_k t + \phi_k) \cdot \sum_{k=1}^{N} \frac{{A_k}^2}{2} \cos(w_k(\tau - t)) + n(t)\sum_{k=1}^{N} \frac{{A_k}^2}{2} \cos(w_k(\tau - t)) + \\ + \sum_{k=1}^{N} A_k \cos(w_k t + \phi_k) \cdot \sigma_n^2 \delta_0(\tau - t) + n(t) \cdot \sigma_n^2 \delta_0(\tau - t) \end{array}\right] dt \cdot \end{aligned}$$

When the number of samples tends to infinity, $a * C_2^a(\tau)$ can be reduced to:

$$a(t) * C_2^a(\tau) = \sum_{k=1}^{N} \frac{A_k^3}{4} \cos(w_k \tau + \phi_k) \quad (9)$$

In this way, we have obtained an equivalent signal to the original periodic one but preserving the phase information.

3. RESULTS

3.1. Detection of failure

To detect the different cases of broken bar failures, we consider five real samples of acousticnoise of a 1.1 kW motor at full load (100%). The motor was a 4 pole machine coupled to a D.C. machine acting as a load. We show a picture of the test-bench in figure 3.

Figure 3. Picture of the laboratory test bench.

We consider the following conditions:

1. Healthy rotor.
2. Rotor with one broken bar.100
3. Rotor with two broken bars (relative positions 1-2).
4. Rotor with two broken bars (relative positions 1-3)
5. Rotor with two broken bars (relative positions 1-5)

The total number of rotor bars in the experiments was 28, and the sampling rate used was 16 kHz.

Firstly, all digitized samples were processed to remove all unwanted spectral components, starting with the healthy rotor signal. In Figure 4, it is shown the signal spectrum of the healthy rotor after the digitization process and the representation of the characteristic harmonics peaks.

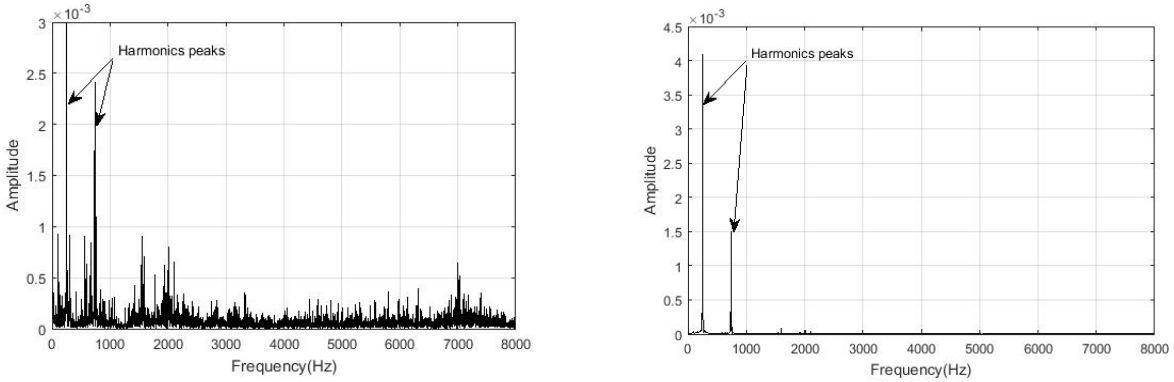

Figure 4. A) Healthy rotor spectrum after the digitization process and before processing with the proposed algorithm for noise reduction and B) healthy rotor spectrum after processing with the noise reduction.

After obtaining the results for the healthy rotor signal, we process the digitized signal of the motor sound with one broken bar. We show our results in Figure 5.It is important to note that in Figure 5c (Signal motor spectrum with one broken bar) a third harmonic is present respect to the healthy motor, see Figure 4b. This harmonic may correspond to a fault identifier. To consolidate the hypothesis of a third harmonic present in the signals of rotors with one broken bar, the remaining signal samples relative to two broken bars in different relative positions were processed (bars 1-2, bars 1-3, and bars 1-5, respectively). Firstly, the signal with two broken bars in relative position 1-2 was processed. We show the obtained results in Figure 6a.

As can be seen, four harmonics peaks are present, transferred in frequency respect to the spec-trum of the signal with the healthy motor. In this case, the greatest harmonic amplitude is twice that amplitude in the healthy rotor signal and also in the one broken bar signals. Furthermore, the signal of two broken bars in relative position 1-3, were processed. We notice in Figure 6b that there are two characteristic harmonics of higher amplitude. This is very significant since there is no repetition of the pattern of four characteristic harmonics shown in Figure 6a. Finally, the simple corresponding to the signal with two broken bars in the relative position 1-5 was processed. We show the results in Figure 6c, where we notice the presence of four characteristic harmonics of greater amplitude.

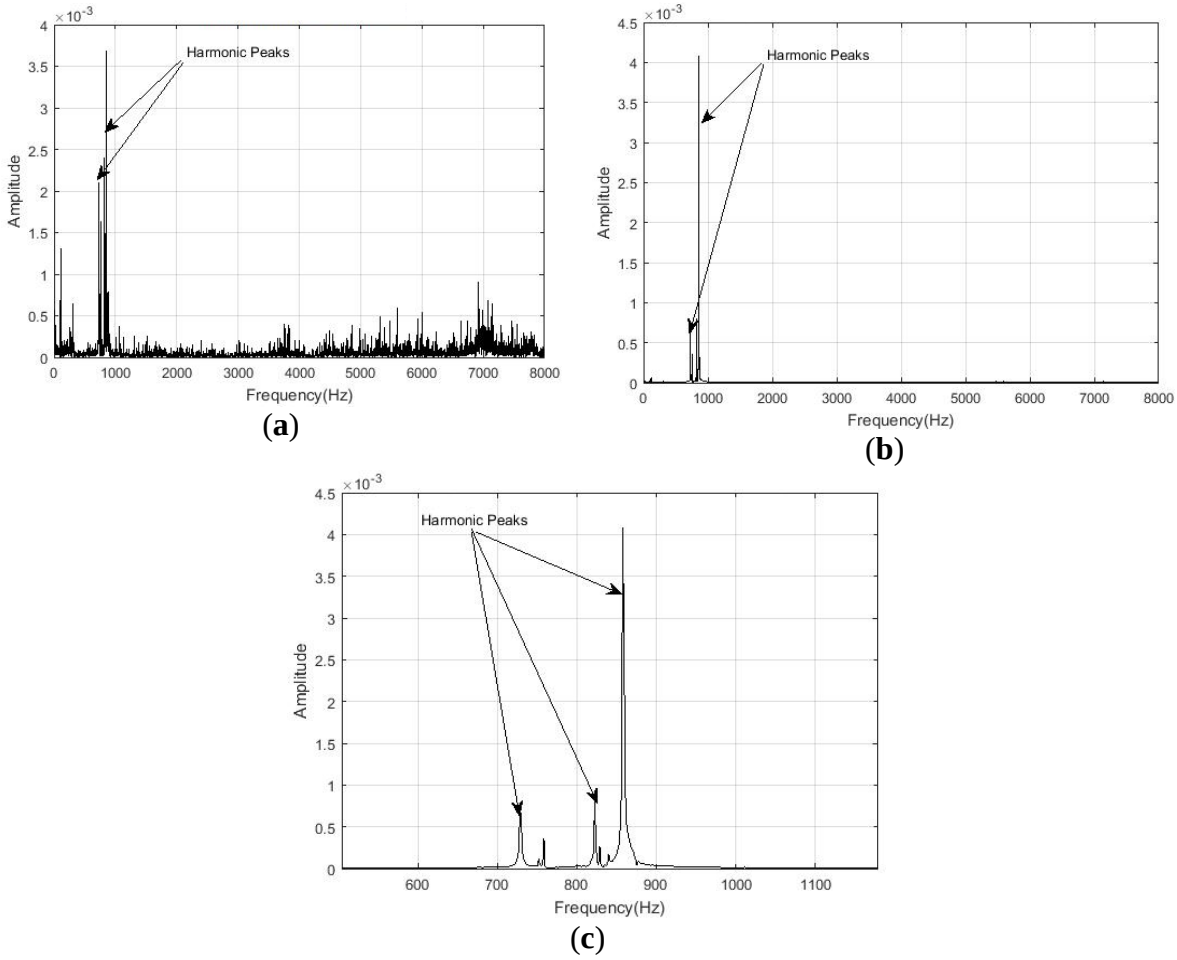

Figure 5. A) Signal spectrum with one broken bar after the digitization process and before processing with the proposed algorithm for noise reduction. B) Signal spectrum with one broken bar, after processing with the noise reduction algorithm. C) Signal spectrum with one broken bar, after processing with the noise reduction algorithm, with zoom in the range of 500-1200 Hz..

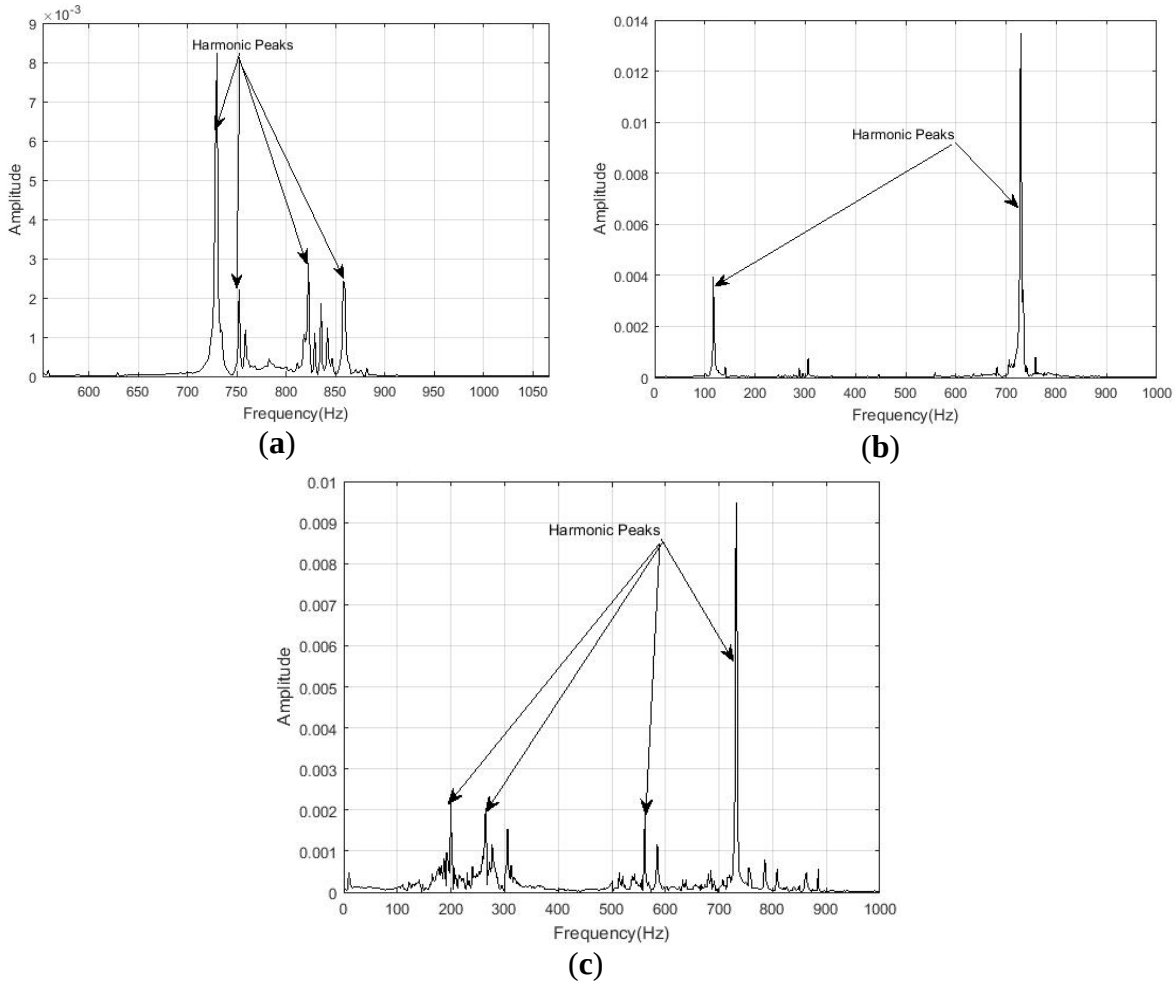

Figure 6. A) Signal spectrum with two broken bar (relative position 1-2), after processing with the noise reduction algorithm. B) Signal motor spectrum with two broken bar (relative position 1-3), after processing with the noise reduction algorithm. C) Signal motor spectrum with two broken bar (relative position 1-3), after processing with the noise reduction algorithm.

It is important to note that, in all processed signals, a characteristic harmonic is present, that is oscillating on 750Hz frequency. It is significant that the differences only appear in the processed signal spectra. To further illustrate the results mentioned above, we show in Figure 7 a comparison of all signals spectrum, processed with the proposed noise reduction algorithm. Here the characteristics of all harmonics peaks are shown together. At the light of these results, it is necessary to find a pattern which permits us to conclude if we are in the presence of a motor with one or two broken bars.

The noise reduction process is used to eliminate the noise in the typical band of frequencies. We recall that what we process is the noise itself as a signal and only useful information is wanted, that is, the deterministic component of the acoustic signal described in Section 2.1 about noise reduction process using second-order statistic and convolution. Figures 5 and 6, respectively, show the peaks of frequencies that appear in the spectrum before and after the processing to reduce the noise. This does not imply that the harmonics shown were those corresponding to the fault; they were only the harmonics with peaks of highest amplitudes. The

novelty of the proposed algorithm is that it does not require to know the frequency component of the fault. It is only based on the processing of the statistical characteristics and the stationary or cycle stationary nature of the acoustic signal. The bar recognition patterns obtained permit us to distinguish between the sound of a healthy motor and a faulty one.

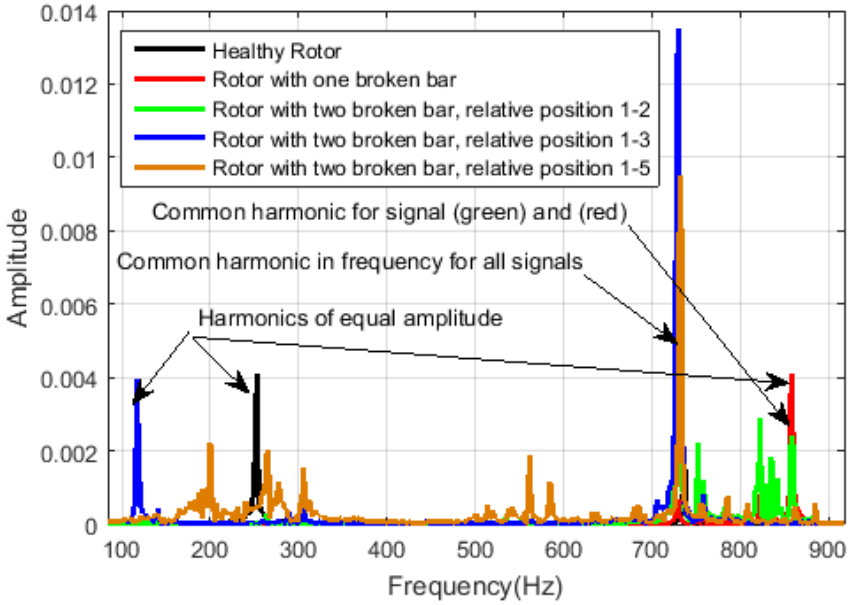

Figure 7. Comparison of all signals spectrum, processed with the proposed noise reduction algorithm.

3.2 Proposed pattern recognition method

To set some recognition criteria that permit us to classify damages, we applied a method based on the descending order spectrum to the signal obtained after preprocessing (output signal after noise reduction). Later, we perform a spectral subtraction respect to the healthy motor signal. Finally, a moving average block is used as a smoothing filter to eliminate impulsive components of the spectral subtraction. The resulting algorithm given by this process is described in Figure 8. The pattern recognition algorithm requires the use, as a basic pattern, of the healthy motor signal. The real samples of faults obtained can be compared with the healthy one, analogously to the schemes of adaptive systems.

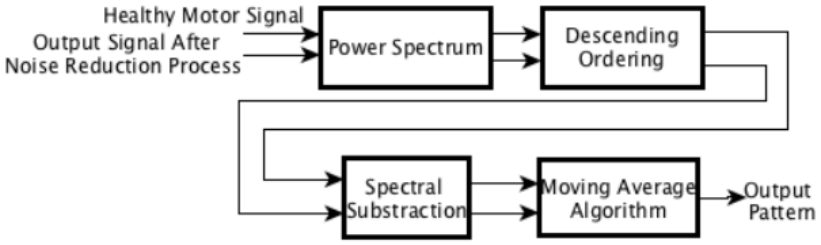

Figure 8. The proposed algorithm for identifying broken bars .

4. DISCUSSION

Then, we search for patterns looking at the differences in the spectrum of both signals. What is obtained at the output, and in each represented pattern, is a spectral pattern that identifies the number of broken bars present in the motor. We show the results in Figure 9, where we notice that there is a similar pattern when the signal has two broken bars independently of the relative position of the broken bars. Besides, there is an identification pattern when the signal has only one broken bar.

To confirm that a pattern appears when the motor has two broken bars, we compute the Pearson correlation coefficients of the vectors (red, green, blue) derived from the output of the algorithm shown in Figure 8.

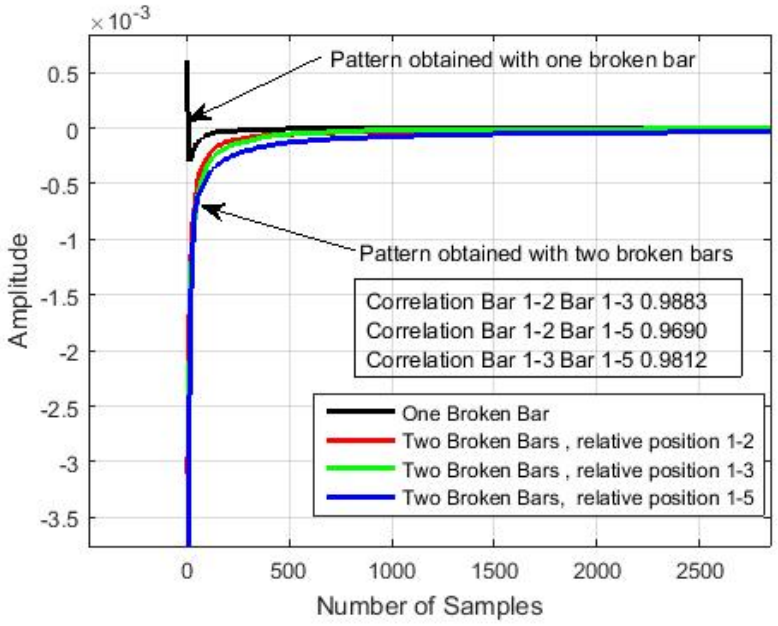

Figure 9. Resulting pattern to identify the broken bars.

We show the results in Table I, demonstrating that there is a similar pattern when we are in the presence of two broken bars independently of the relative position where the breakages take place.

Table 1. Correlation between output signals of signals with two broken bars.

Signal	Correlation
Bar 1-2 vs. Bar 1-3	0.9883
Bar 1-2 vs. Bar 1-5	0.9690
Bar 1-2 vs. Bar 1-5	0.9812

5. CONCLUSIONS

We have shown that there are common characteristics in the amplitudes and frequencies of signals corresponding to different types of motors with broken bars. The noise and interferences of the digitized signals were reduced using an algorithm that combines statistical analysis, a convolution process, and an amplitude adjustment process. This adjustment is positive when processing only the relevant information concerning the broken bars. It was possible to obtain a unique identifier pattern when the signal has only one broken bar. Furthermore, we have obtained common patterns when we are in the presence of two broken bars, independently of their relative position. The patterns can be obtained by applying an algorithm that combines reordering vectors, the spectral subtraction, and a moving average filter. Results reveal high effectiveness, given by the significant signal-to-noise rate enhancement achieved and the identification pattern obtained for the broken bars.

Author Contributions: Conceptualization, M.E.I.-M., J.A.A.-D., P.F.d.C., and J.A.C.; Methodology, M.E.I.-M.; Software,M.E.I.-M.;Validation,M.E.I.-M.,J.A.A.-D.,P.F.d.C.,andJ.A.C.;FormalAnalysis,M.E.I.-M.; Investigation, M.E.I.-M., J.A.A.-D., P.F.d.C., and J.A.C.; Resources, M.E.I.-M., J.A.A.-D., P.F.d.C. and J.A.C.; Data Curation, M.E.I.-M. and J.A.A.-D.; Writing—Original Draft Preparation, M.E.I.-M., J.A.A.-D., P.F.d.C., and J.A.C.; Writing—Review & Editing, M.E.I.-M., J.A.A.-D., P.F.d.C., and J.A.C.; Visualization, M.E.I.-M.; Supervision, J.A.A.-D., J.A.C.

Funding: This research was funded by MEC, grant number MTM 2016-7963-P.

Acknowledgments:

Conflicts of Interest: The authors declare no conflict of interest. The funders had no role in the design of the study; in the collection, analyses, or interpretation of data; in the writing of the manuscript, or in the decision to publish the results.

REFERENCES

1. H. Akcay and E. Germen. Identification of acoustic spectra for fault detection in induction motors. In AFRICON, 2013, pages 1–5. IEEE, **2013**.
2. H. Akçay and E. Germen. Subspace-based identification of acoustic noise spectra in induction motors. IEEE Transactions on Energy Conversion, 30(1):32–40, **2015**.
3. M. A. Alsaedi. Fault diagnosis of three-phase induction motor: A review. Optics. Special Issue: Applied Optics and Signal Processing, 4(1):1–8, **2015**.
4. A. Alwodai. Motor fault diagnosis using higher order statistical analysis of motor power supply parameters. PhD thesis, University of Huddersfield, **2015**.
5. J. Antonino-Daviu, M. Riera-Guasp, J. Roger-Folch, F. Martínez-Giménez, and A. Peris. Application and optimization of the discrete wavelet transform for the detection of broken rotor bars in induction machines. Applied and Computational Harmonic Analysis, 21(2):268–279, **2006**.
6. V.A. Bazhenov and O.S. Pogorelova and T.G. Postnikova. Intermittent transition to chaos in vibro impact system, Applied Mathematics and Nonlinear Sciences, 3(2): 475–486, **2018**
7. J. Cusidó, L. Romeral, J. A. Ortega, A. Garcia, and J. Riba. Signal injection as a fault detection technique. Sensors, 11(3):3356–3380, **2011**.
8. P. A. Delgado-Arredondo, D. Morinigo-Sotelo, R. A. Osornio-Rios, J. G. Avina-Cervantes, H. Rostro-Gonzalez, and R. de Jesus Romero-Troncoso. Methodology for fault detection in induction motors via sound and vibration signals. Mechanical Systems and Signal Processing, 83:568–589, **2017**.

9. K. S. Gaeid, H. W. Ping, M. Khalid, and A. Masaoud. Sensor and sensorless fault tolerant control for induction motors using a wavelet index. Sensors, 12(4):4031–4050, **2012**.
10. A. Garcia-Perez, R. J. Romero-Troncoso, E. Cabal-Yepez, R. A. Osornio-Rios, and J. A. Lucio Martinez. Application of high-resolution spectral analysis for identifying faults in induction motors by means of sound. Journal of Vibration and Control, 18(11):1585–1594, **2012**.
11. V. Ghorbanian and J. Faiz. A survey on time and frequency characteristics of induction motors with broken rotor bars in line-start and inverter-fed modes. Mechanical Systems and Signal
12. A. Glowacz, W. Glowacz, Z. Glowacz, and J. Kozik. Early fault diagnosis of bearing and stator faults of the single-phase induction motor using acoustic signals. Measurement, 113:1–9, **2018**.
13. A. Glowacz, W. Glowacz, Z. Glowacz, J. Kozik, M. Gutten, D. Korenciak, Z. Khan, M. Irfan, and E. Carletti. Fault diagnosis of three phase induction motor using current signal, MSAFRatio15 and selected classifiers. Archives of Metallurgy and Materials, 62(4):2413–2419, **2017**.
14. A. Glowacz and Z. Glowacz. Diagnosis of the three-phase induction motor using termal imaging. Infrared Physics & Technology, 81:7–16, **2017**.
15. A. Glowacz and Z. Glowacz. Recognition of rotor damages in a dc motor using acoustic signals. Bulletin of the Polish Academy of Sciences Technical Sciences, 65(2):187–194, **2017**.
16. F. Gu, T. Wang, A. Alwodai, X. Tian, Y. Shao, and A. Ball. A new method of accurate broken rotor bar diagnosis based on modulation signal bispectrum analysis of motor current signals. Mechanical Systems and Signal Processing, 50:400–413, **2015**.
17. S. GüÇlü, A. Ünsal, and M. A. Ebeoglu. Vibration analysis of induction motors with unbalanced loads. Environment, 2:3, **2017**.
18. A. Guezmil, H. Berriri, R. Pusca, A. Sakly, R. Romary, and M. F. Mimouni. Detecting interturn short-circuit fault in induction machine using high-order sliding mode observer: Simulation and experimental verification. Journal of Control, Automation and Electrical Systems, pages 1–9, **2017**.
19. J. C. Hernández, J. Antonino-Daviu, F. Martínez-Giménez, and A. Peris. Comparison of different wavelet families for broken bar detection in induction motors. In IEEE International Conference on Industrial Technology (ICIT), 2015, pages 3220–3225. IEEE, **2015**.
20. A. M. Júnior, V. V. Silva, L. M. Baccarini, and L. F. Mendes. The design of multiple linear regression models using a genetic algorithm to diagnose initial short-circuit faults in 3-phase induction motors. Applied Soft Computing, 63:50–58, **2018**.
21. H. Khang, R. Puche-Panadero, J. L. Senanayaka, and K. Robbersmyr. Bearing fault detection of gear-box drive train using active filters. In 19th International Conference on Electrical Machines and Systems (ICEMS), 2016 , pages 1–6. IEEE, **2016**.
22. O. Ondel, E. Boutleux, and G. Clerc. A method to detect broken bars in induction machine using pattern recognition techniques. IEEE Transactions on Industry Applications, 42(4):916–923, **2006**.
23. Y. Ono, Y. Onishi, T. Koshinaka, S. Takata, and O. Hoshuyama. Anomaly detection of motors with feature emphasis using only normal sounds. In IEEE International

Conference on Acoustics, Speech and Signal Processing (ICASSP), 2013, pages 2800–2804. IEEE, **2013**.

24. P. S. Panigrahy, P. Konar, and P. Chattopadhyay. Broken bar fault detection using fused dwt-fft in fpga platform. In International Conference on Power, Control and Embedded Systems (ICPCES), 2014, pages 1–6. IEEE, **2014**.
25. C. A. Perez-Ramirez, J. P. Amezquita-Sanchez, M. Valtierra-Rodriguez, A. DominguezGonzalez, D. Camarena-Martinez, and R. J. Romero-Troncoso. Fractal dimension theory-based approach for bearing fault detection in induction motors. In IEEE International Autumn Meeting on Power, Electronics and Computing (ROPEC), 2016, pages 1–6. IEEE, **2016**.
26. M. Riera-Guasp, M. F. Cabanas, J. A. Antonino-Daviu, M. Pineda-Sánchez, and C. H. R. García. Influence of nonconsecutive bar breakages in motor current signature analysis for the diagnosis of rotor faults in induction motors. IEEE Transactions on Energy Conversion, 25(1):80–89, **2010**.
27. L. Saidi, F. Fnaiech, G. Capolino, and H. Henao. Stator current bi-spectrum patterns for induction machines multiple-faults detection. In 38th Annual Conference on IEEE Industrial Electronics Society, IECON 2012, pages 5132–5137. IEEE, **2012**.
28. L. Saidi, F. Fnaiech, H. Henao, G. Capolino, and G. Cirrincione. Diagnosis of broken-bars fault in induction machines using higher order spectral analysis. ISA transactions, 52(1):140–148, **2013**.
29. F. Salazar-Villanueva and O. G. Ibarra-Manzano. Spectral analysis for identifying faults in induction motors by means of sound. In International Conference on Electronics, Communications and Computing (CONIELECOMP), 2013 , pages 149–153. IEEE, **2013**.
30. A. K. Samanta, A. Naha, A. Routray, and A. K. Deb. Fast and accurate spectral estimation for online detection of partial broken bar in induction motors. Mechanical Systems and Signal Processing, 98:63–77, **2018**.
31. S. V. Vaseghi. Advanced digital signal processing and noise reduction. John Wiley & Sons, **2008**.

32. K. Yahia, A. Cardoso, A. Ghoggal, and S. Zouzou. Induction motors airgap-eccentricity detection through the discrete wavelet transform of the apparent power signal under non-stationary operating conditions. ISA Transactions, 53(2):603–611, **2014**.
33. J.-H. Zhong, P. K. Wong, and Z.-X. Yang. Simultaneous-fault diagnosis of gearboxes using probabilistic committee machine. Sensors, 16(2):185, **2016**.

Detection of Bar Breakages in Induction Motor via Spectral Subtraction of Stray Flux Signals

M.E. Iglesias Martínez, Universidad de Pinar del Río Hermanos Saíz Montes de Oca, Departamento de Telecomunicaciones, Martí # 270,Pinar del Río, Cuba, E-mail: migueliglesias2010@gmail.com. Instituto Universitario de Matemática Pura y Aplicada, Universitat Politècnica de València, E-46022 Valencia, Spain

Pedro Fernández de Córdoba, Instituto Universitario de Matemática Pura y Aplicada, Universitat Politècnica de València, E-46022 Valencia, Spain, E-mail: pfernandez@mat.upv.es

Jose A. Antonino-Daviu, Instituto Tecnológico de la Energía, Universitat Politècnica de València, E-46022 Valencia, Spain, E-mail: joanda@die.upv.es

J. Alberto Conejero, Instituto Universitario de Matemática Pura y Aplicada, Universitat Politècnica de València, E-46022 Valencia, Spain
E-mail address: aconejero@upv.es

IEEE. 2018 XIII International Conference on Electrical Machines (ICEM), 3-6 Sept. 2018, Alexandroupoli, Greece , pp:1796-1802, DOI: 10.1109/ICELMACH.2018.8507078, **ISSN:** 2381-4802, https://ieeexplore.ieee.org/document/8507078

***Abstract* – In this paper, statistical signal processing techniques are applied to electromotive force signals captured in external coil sensors for broken bars detection in induction motors. An algorithm based spectral subtraction analysis is applied for broken bar identification, independent of the relative position of the bar breakages. Moreover, power spectrum analyses enable the discrimination between healthy and faulty conditions.**

The results obtained with experimental data prove that the proposed approach provides good results for fault detectability. Moreover the identification of the faults, and the signal correlation indicator to prove the results, are also presented for different positions of the flux sensor.

***Index Terms*-- Fault Diagnosis, Induction Motors, Flux, Signals, Spectral Analysis.**

1. INTRODUCTION

A recent trend in the electric motor condition monitoring area relies on combining the information obtained from the analyses of different machine quantities (currents, vibrations, temperatures, etc…) to reach a more reliable conclusion about its health. This is due to the fact that it has been proven that the analysis of a single quantity enables to diagnose specific faults or anomalies but it is not enough to determine the health of the whole motor. In this context, the analysis of classical quantities that are well-known in the industry, such as currents or vibrations, has shown certain problems or drawbacks for the diagnosis of certain faults [1].

With regards to the condition of the rotor, neither current nor vibration analysis have proven to be valid in all the cases that may rise in industry; it has been reported, for instance, the occasional occurrence of false indications when these techniques are used [2-5]. One of the cases where these techniques have not shown good results when detecting rotor damages is under the presence of non-adjacent bar breakages in the rotor cage.

Under such situation, the effects of one bar breakage can be partially compensated by those of other breakage, for certain relative positions, making difficult the identification of the fault components in the resulting spectra [6-8]. This may result in incorrect indications.

Due to these problems, other technologies are being explored by many researchers worldwide. One of these technologies relies on studying the external magnetic field in the vicinity of the motor [9-23]. Specifically in relation to rotor faults[24],eccentricity [25] and stator faults[26], It has been proven that, when certain faults are present, specific harmonics are amplified in the Fourier spectra of the electromotive force (emf) signals induced in external coil sensors installed at different positions [9,16]. More specifically, some authors have characterized the components amplified by rotor faults, eccentricities or even stator failures and have proven the potential of this technique for the detection of such faults. The simplicity, low cost and easy implementation of the technique makes it a very interesting option to complement the information obtained with other well-known technologies, especially considering the progressive reduction in price of the available flux sensors that comes together with an increase of their features [21].

Though most of the works related to flux monitoring have explored the applicability of the technique under stationary conditions [9,20], some recent works have also studied the viability of the method under transient operation, obtaining very promising results [23,27,28].
In this work, a new algorithm to detect rotor damages in induction motors based on the analysis of stray flux signals is proposed. It uses a spectral pattern recognition method based on the spectral subtraction of the power spectrum. In relation to the uses of pattern recognition [29] and spectral subtraction [30,31] techniques , some works has been made, applying different points of view, to detect de specifics fault. The proposed algorithm is applied not only to detect adjacent bar breakages, but also non-consecutive broken bars.
The results show the potential of this approach, that provides valuable information to detect rotor damages or, at least, to complement the information provided by other quantities, enhancing the performance of classical techniques.
Section II describes the considered fault as well as its related harmonics. The proposed pattern recognition method and the experimental results are shown in Section III and IV respectively. Finally, conclusions are outlined in Section V.

2. ROTOR BAR BREAKAGE DETECTION VIA ANALYSIS OF FLUX SIGNALS

Different authors have proven that the presence of certain faults in the motor amplifies some components in the stray flux spectrum [9-16]. Former works in [15-20] proposed the use of external coil sensors for the capture of the necessary signals and the subsequent Fourier analysis of these signals to detect the components amplified by the rotor damages and other faults. With regards to the detection of bar damages, in [32] it is suggested the study of the sideband components appearing at $f\cdot(1\pm2\cdot s\cdot f)$ (with s=slip and f=supply frequency) around the main frequency component in the FFT spectrum of the captured emf signals. More recent works in [33] and [9,11-12] proposed the study of other components in the low frequency region of the FFT spectrum of the emf induced in external coil sensors; according to these authors, when rotor faults are present, the components located at $s\cdot f$ and $3\cdot s\cdot f$ are amplified in that FFT spectrum. Therefore, the study of the amplitudes of these harmonics may become a reliable indicator of the presence of the fault.

Although most of the works developed in the literature are focused on the analysis of the emf signals induced in external coil sensors at steady-state operation of the motor, some recent papers have explored the viability of the analysis of these signals under the startup, obtaining very promising results [23]. These works have proven that, during transient operation, these components follow particular trajectories that can be used as evidences of the presence of the fault.

The present work focuses on the flux-based detection of rotor faults but considering the case of non-adjacent broken bars, an issue that has been barely considered in past works.

3. THE PROPOSED ALGORITHM

To try to achieve some recognition criteria to classify the damages, a method based on spectrum descending order was applied to the signal obtained after preprocessing (output signal after noise reduction). Later, a spectral subtraction operation with respect to the signal with the healthy motor was also performed. Finally, a moving average block is used as a smoothing filter to eliminate impulsive components of the spectral subtraction. The resulting algorithm given by these processes is described in Fig. 1.

The pattern recognition algorithm is based on the use as a basic pattern of the signal of the healthy motor. This is not a serious restriction under a practical point of view, since that signal could be obtained after motor commissioning or after motor inspection, once the rotor is guaranteed to be healthy. In the method, once the actual samples have been captured, they can be compared with the healthy ones. The proposed method is based on searching for patterns, by looking at the differences in the spectrum of both signals (actual sample vs. healthy one). The use of the signal of the healthy motor as a signal reference is analogous to the schemes of adaptive systems. What is obtained at the output and in each represented pattern is a spectral pattern that identifies the number of broken bars present in the motor.

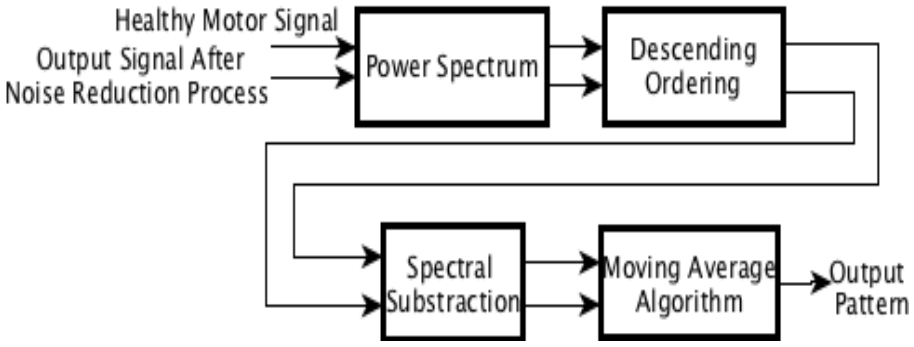

Fig. 1. The proposed algorithm for identifying broken bars.

4. EXPERIMENTAL RESULTS

Different experiments were developed at the laboratory by using a 4-pole, 1.1 kW induction motor which was coupled to a DC machine acting as a load. Different cage rotors (28 bars in each rotor) with diverse levels of failure were available, so that each specific rotor could be assembled to test the corresponding rotor fault condition. More specifically, in this work the considered cases are: healthy rotor and rotor with two broken bars. In this latter case, different

relative positions between the broken bars were tested, namely: Bars 1-2 broken (adjacent broken bars), bars 1-3 broken, bars 1-4 broken, bars 1-5 broken and bars 1-6 broken.

In each test, the machine was started until it reached the steady-state regime. The emf signal induced in an external coil sensor attached to the frame of the machine was captured using a digital oscilloscope. More specifically, two different sensor locations were considered: position A (sensor attached to the lateral part of the motor frame, in the shaft side, Fig. 2 (b)) and position B (sensor attached to the center of the frame, Fig. 2(c)). Both the experimental test bench and the two considered sensor positions are shown in Fig. 2.

(a)

(b) (c)

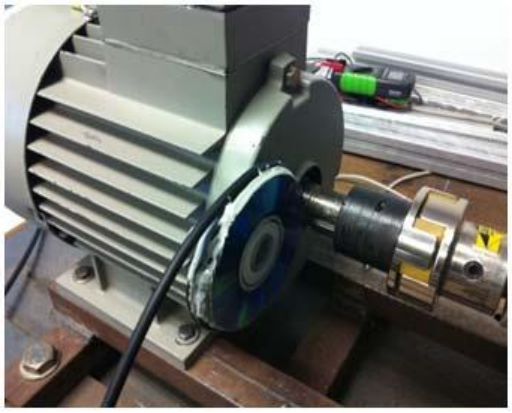

Fig. 2. a) Experimental test bench, b) Position A of the coil sensor, c) Position B of the coil sensor.

The idea of the proposed algorithm to identify the broken bar pattern is to take as a reference the healthy state of the motor, in order to detect the corresponding faulty condition. The objective is to detect differences in the power spectrum, taking into account that a motor in a healthy state will have a certain power spectrum; if the motor is faulty, it will no longer have the same spectrum, hence the foundation based on the rearrangement of the power spectrum and spectral subtraction, to obtain an identification pattern of broken bars

regardless of the relative position of the bars. The developed algorithm was conditioned by two goals: 1) it should be able to distinguish between healthy and faulty cases based on the analyses of flux data and 2) it should be able to detect the existence of the fault regardless of the position of the bars hat break.

A. Experimental results obtained from the measurement in position A

Regarding the position A, the resulting pattern obtained for each sample after application of the proposed algorithm (see Fig. 1) allows us to discern when we are in the presence of a motor with two broken bars, since all the samples converge to the same line (see Fig. 3).

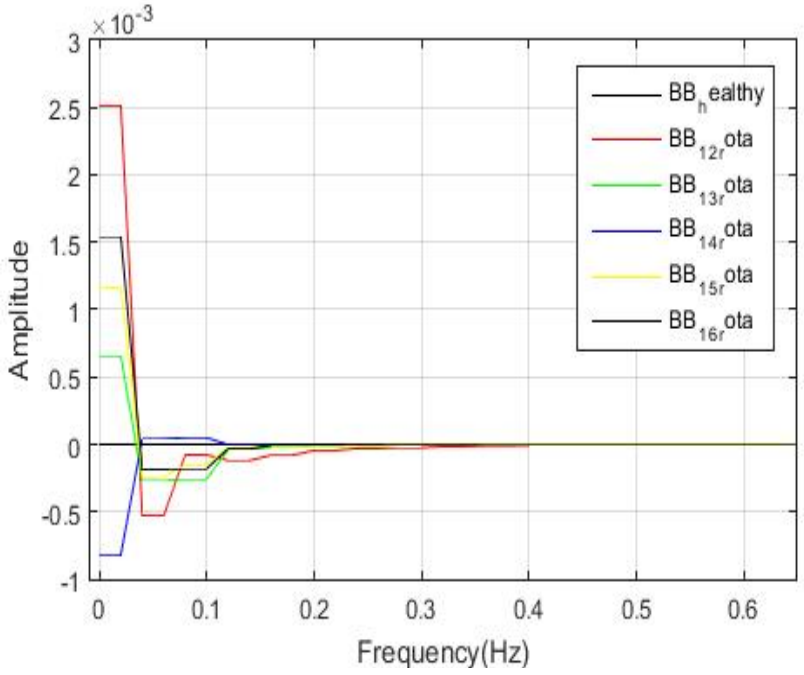

Fig. 3. Resulting spectral pattern obtained from position A.

In Fig.3 we can also see the stepped positioning of the obtained patterns from each sample according to the relative positions, whose difference lies in the amplitude, that is: first position_1_2 (red), position_1_6 (black), position_1_5 (yellow), position_1_3 (green), the above except for position_1_4 (blue) which reflects a total difference with the rest of the obtained patterns, from each sample. This result can be very useful for discrimination between the healthy and faulty cases and for the identification of the two broken bars case, regardless of the relative position of the broken bars.

To prove that we are in the presence of a motor with two broken bars, the Pearson correlation coefficient was applied between the resulting patterns obtained from the measurements carried out in position A. The correlation obtained between the resulting patterns is almost 1, except on the case of position 1_4. Table I shows the results obtained. In that table, CORRE_X_X is the correlation obtained from each pattern with respect to the resulting pattern of the bar BB_1_2. The measurement BB_1_2 was taken as reference, but another sample could have been taken, the correlation will give similar values with the exception of position 1_4, which has a certain difference as shown in the graph of Fig.3.

Now if we consider the mean value of the module of the obtained correlations, it gives as result: 0.9768

TABLE I: CORRELATION VALUES OBTAINED ACCORDING TO THE RESULTING PATTERNS. POSITION A

CORRE_12_16 = 1.0000 0.9933 0.9933 1.0000	CORRE_12_15 = 1.0000 0.9945 0.9945 1.0000
CORRE_12_13 = 1.0000 0.9344 0.9344 1.0000	CORRE_12_14 = 1.0000 -0.9849 -0.9849 1.0000

B. Experimental results obtained from the measurement in position B

As for the position B, it is verified by the resulting pattern (see Fig.4) that there are two broken bars and just as in the position A, we can discern in which relative position is the position 1_4 (blue) and the position 1_6 (black) which are differentiable from the rest of the others, since their correlation value is negative as well as the results of the measurement at position A.

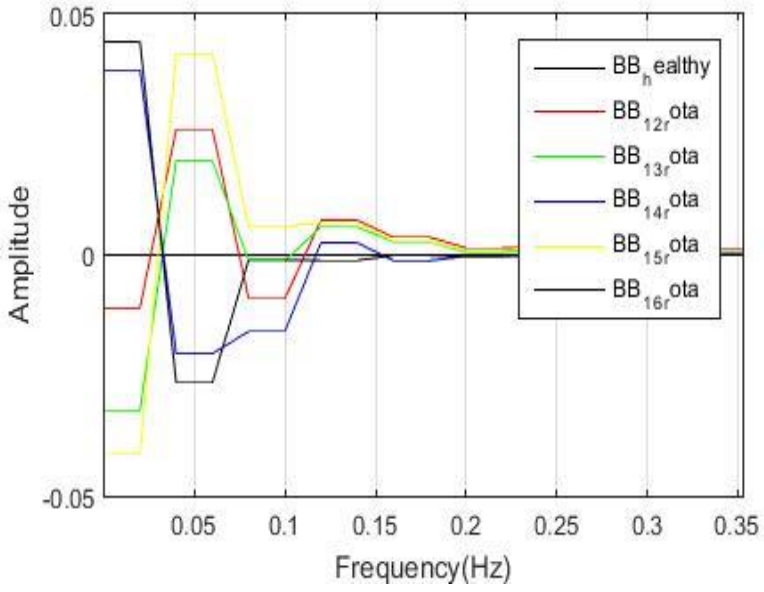

Fig. 4. Resulting spectral pattern obtained from position B.

With respect to the other positions, these follow a stepped descendently pattern as in Fig.2, although not in the same order. The correlation obtained between the resulting patterns as in position A is almost 1, except on the position 1_4 and position 1_6, whereby these two positions can be discerned. In Table 2 the results are shown. Now if we proceed in the same

way as for position A, with the average value of the module of the correlations obtained, it gives as result: 0.7309. The correlation levels obtained in the measurements made in both relative positions A and B respectively, oscillate between 0.7 and 0.98, which can be a variable indicator to identify broken bars using the flux signals.

TABLE II: CORRELATION VALUES OBTAINED ACCORDING TO THE RESULTING PATTERNS. POSITION B

CORRE_12_16 =	CORRE_12_15 =
1.0000 -0.7361 -0.7361 1.0000	1.0000 0.8457 0.8457 1.0000
CORRE_12_13 =	CORRE_12_14 =
1.0000 0.7875 0.7875 1.0000	1.0000 -0.5542 -0.5542 1.0000

C. *Discrimination between healthy and damaged state based on the spectra.*

The discrimination between healthy and faulty conditions can be carried out by simply comparing the corresponding spectra of the captured emf signals. However, this procedure may be influenced by the occurrence of non-adjacent breakages since, depending on the relative positions between the bars that break, the amplitudes of the fault harmonics may sensibly differ. However, as pointed out in previous works [8,
10, 11,26], the analyses of the FFT spectra may be helpful at least to have an evidence on if the anomaly may be present. A rough analysis of the characteristics of the FFT spectra for each one of the considered positions of the sensor is presented below.

Characteristics of the spectra for position A:

- All the analysed signals have little external interference or noise in the spectrum; this ripple noise can come from the same data acquisition system, from the AC line or from the sensor (see Figures 5 and 6).
- The same considerations are applicable to the signals captured for the sensor at position A, although, in this case, the amplitudes of all fault harmonics are less significant. This is due to the lower portion of flux that is captured at this position (see Fig. 5).

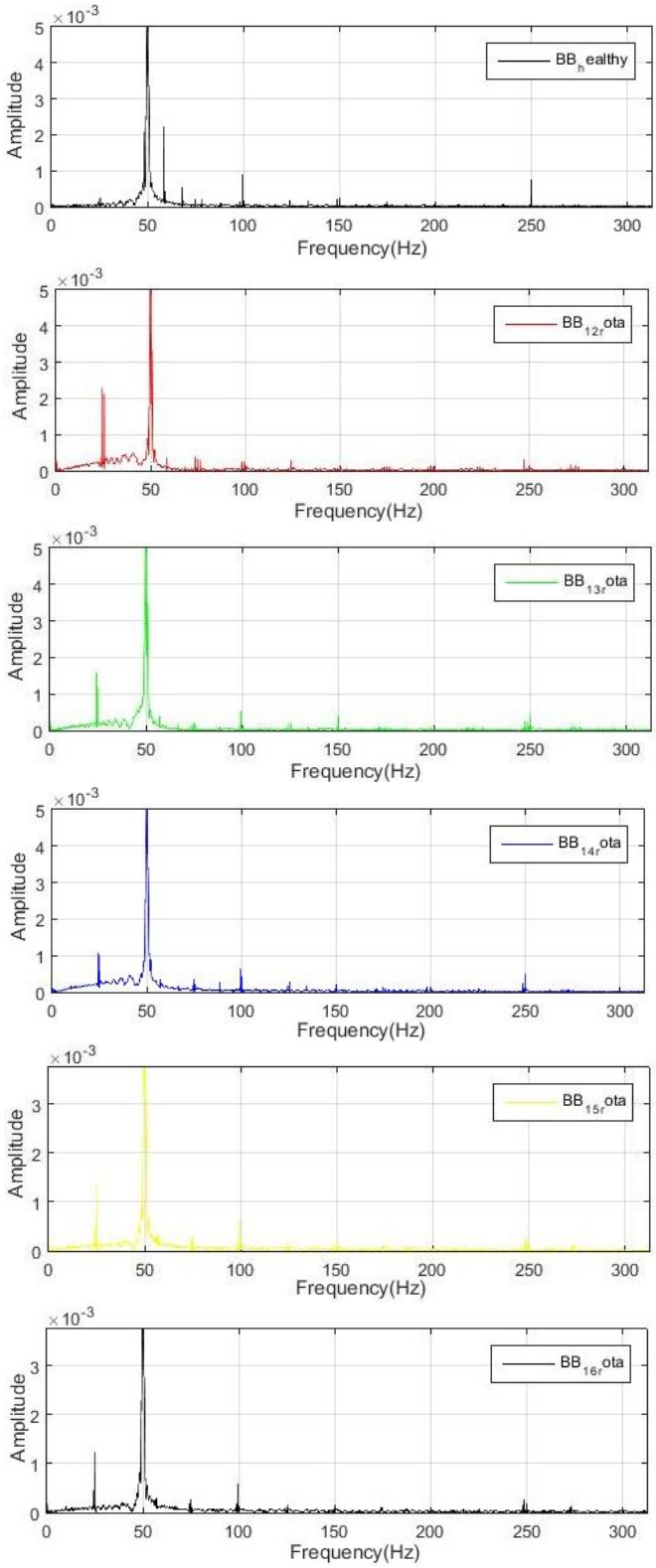

Fig. 5. Comparison of the spectrum of the healthy motor (a), with the broken bars spectrum((b) to (f)). Relative Position: A

Characteristics of the spectra for position B:

- All samples have the expected fundamental harmonic at 50Hz (see Figures 5 and 6), as well as a noticeable 150Hz component Sideband components are present for all faulty cases although their amplitudes vary depending on the relative position between broken bars (maximum amplitude for adjacent bars, in agreement with previous works [8, 10,11, 26].
- If the low frequency regions are zoomed fault harmonics are detectable at components $s \cdot f$ and $3s \cdot f$. Once again their amplitudes are influenced by the relative positions of the breakages. But their presence may be an evidence of the existence of the fault.
- The eccentricity harmonics at 25Hz and 75 Hz increase their amplitudes for all faulty cases but this is probably due to the assembly process of the rotor during the tests.
- The spectra corresponding to positions 1_6 and 1_5 are very similar. The same happens between the spectra of the position 1_3 and 1_5.

With the previously extracted characteristics, it is possible to distinguish visually between the spectrum of the healthy motor and the damaged one (see Fig.6).

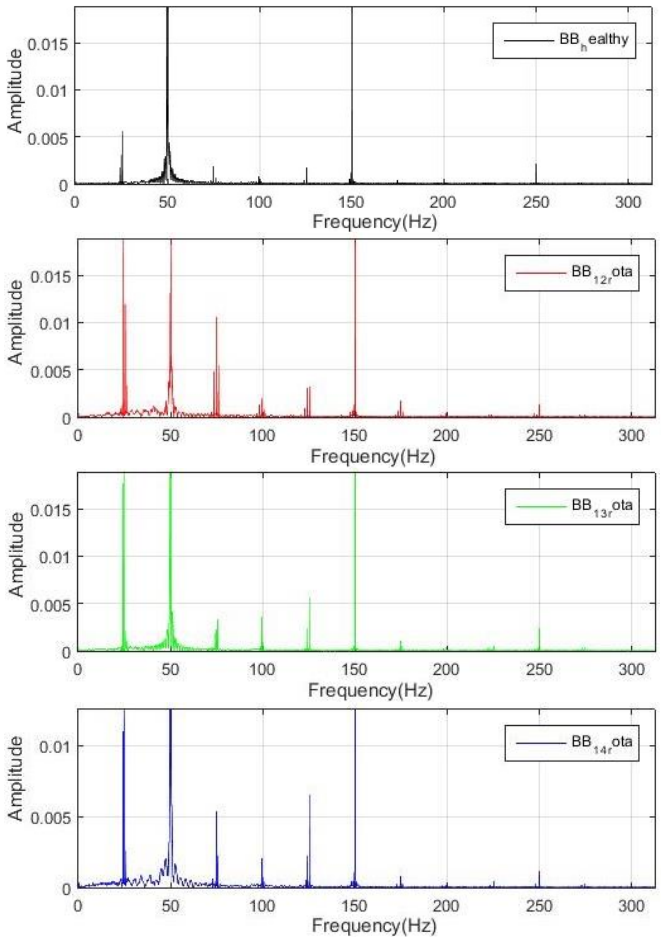

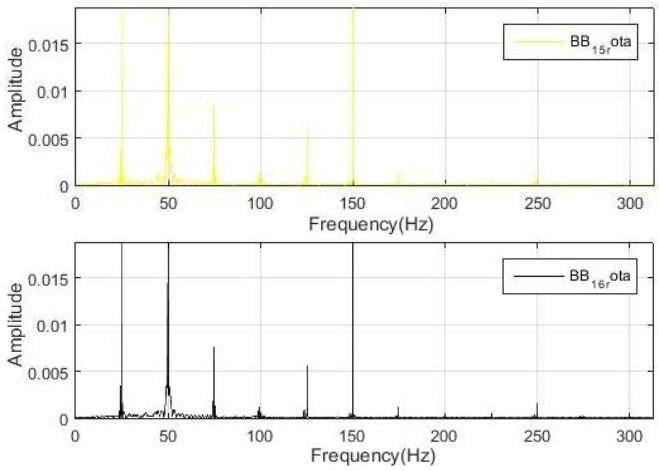

Fig. 6. Comparison of the spectrum of the healthy motor (a), with the broken bars spectrum ((b) to (f)). Relative Position: B

5. CONCLUSIONS

This work proposes the use of induction motor stray flux signals for the identification of bar breakages regardless of their relative position. During the experiments carried out, it was shown that it is possible with the proposed algorithm to detect the fault and even distinguish the relative position of the bars that break.

The proposed method is based on the frequency spectral subtraction of the power spectrum, furthermore it is use the Pearson correlation coefficient, which was applied to demonstrate the similarity of all the resulting patterns, obtained for two broken bars.
In order to identify between healthy and damaged state, the analysis of the Fourier spectrum may be sufficient; the differences between the spectrum of the healthy motor and the faulty states in both positions A and B can be noticed visually, by means of the harmonics appearing both at lower frequencies and around the main component

6. ACKNOWLEDGEMENTS

The first and fourth author are partially supported by MTM2016-75963-P.

7. REFERENCES

1. S. Nandi, H. A. Toliyat, and Xi. Li,:" Condition Monitoring and Fault Diagnosis of Electrical Motors—A Review", *IEEE Transactions on Energy Conversion*, vol. 20, no. 4, pp:719-729, December 2005.
2. M. Riera-Guasp, J.A. Antonino-Daviu,and G.A. Capolino:"Advances in Electrical Machine, Power Electronic, and Drive Condition Monitoring and Fault Detection: State of the Art", *IEEE Transactions on Industrial Electronics*, Vol. 62, No. 3,pp:1746-1759, March 2015
3. J. A. Antonino-Daviu, M. Riera-Guasp, J. R. Folch, and M. Pilar Molina Palomares, "Validation of a new method for the diagnosis of rotor bar failures via

wavelet transform in industrial induction machines," *IEEE Trans. Ind. Appl*., vol. 42, pp. 990-996, 2006.

4. C. Yang, T-J. Kang, D. Hyun, S. Lee, J. Antonino-Daviu, J. Pons- Llinares, "Reliable Detection of Induction Motor Rotor Faults Under the Rotor Axial Air Duct Influence," *IEEE Trans. Ind. Appl*., vol. 50, no. 4, pp. 2493-2502, Jul.-Aug. 2014
5. J. A. Antonino-Daviu, J. Pons-Llinares, Sungsik Shin, Kun Wang Lee and Sang Bin Lee, "Reliable detection of induction motor rotor faults under the influence of rotor core magnetic anisotropy," in Proc.of the 2015 IEEE 10th International Symposium on Diagnostics for Electrical Machines, Power Electronics and Drives (SDEMPED), Guarda, 2015, pp. 14-21.
6. T. J. Sobczyk, W. Maciolek, "Does the component (1-2s)f0 in stator current is sufficient for detection of rotor cage faults?", Proc. SDEMPED 2005, Vienna, Austria, pp. 1-5, Sep. 2005.
7. G. Y. Sizov, A. Sayed-Ahmed, C. C. Yeh and Nabeel A. O. Demerdash, "Analysis and Diagnostics of Adjacent and Nonadjacent Broken-Rotor-Bar Faults in Squirrel-Cage Induction Machines," *IEEE Trans. Ind. Elec*., Vol. 56, No. 11, pp. 4627-4641, Nov. 2009.
8. M. Riera-Guasp, M. F. Cabanas, J. A. Antonino-Daviu, M. Pineda- Sánchez and C. H. R. García, "Influence of Nonconsecutive Bar Breakages in Motor Current Signature Analysis for the Diagnosis of Rotor Faults in Induction Motors," in *IEEE Transactions on Energy Conversion*, vol. 25, no. 1, pp. 80-89, March 2010.
9. R. Romary, R. Pusca, J. P. Lecointe, and J. F. Brudny, "Electrical machines fault diagnosis by stray flux analysis," in *Proc. IEEE WEMDCD*, Paris, France, Mar. 11–12, 2013, pp. 247–256.
10. L. Frosini, A. Borin, L. Girometta, and G. Venchi, "A novel approach to detect short circuits in low voltage induction motor by stray flux measurement," in *Proc. ICEM*, Marseille, France, Sep. 2–5, 2012, pp.1538–1544.
11. R. Romary, R. Pusca, J. P. Lecointe, and J. F. Brudny, "Electrical machines fault diagnosis by stray flux analysis," in *Proc. IEEE WEMDCD*, Paris, France, Mar. 11–12, 2013, pp. 247–256.
12. R. Romary, R. Pusca, J. P. Lecointe, and J. F. Brudny, "Electrical machines fault diagnosis by stray flux analysis," in *Proc. IEEE WEMDCD*, Paris, France, Mar. 11–12, 2013, pp. 247–256.
13. L. Frosini, A. Borin, L. Girometta, and G. Venchi, "A novel approach to detect short circuits in low voltage induction motor by stray flux measurement," in *Proc. ICEM*, Marseille, France, Sep. 2–5, 2012, pp.1538–1544.
14. V. Kokko, "Condition monitoring of squirrel-cage motors by axial magnetic flux measurements," M.S. thesis, Dept. Elect. Eng., Optoelectron. Meas., Univ. Oulu, Oulu, Finland, 2006.
15. H. Henao, C. Demian, and G.-A. Capolino, "A frequency-domain detection of stator winding faults in induction machines using an external flux sensor," *IEEE Trans. Ind. Appl.*, vol. 39, no. 5, pp.1272–1279, Sep./Oct. 2003.
16. H. Henao, G.-A. Capolino, and C. S. Mar¸ti¸s, "On the stray flux analysis for the detection of the three-phase induction machine faults," in *Conf. Rec. 38th IEEE IAS Annu. Meeting*, 2003, vol. 2, pp. 1368–1373.
17. A. Yazidi *et al.*, "Detection of stator short-circuit in induction machines using an external leakage flux sensor," in *Proc. IEEE ICIT*, Hammamet, Tunisia, 2004, pp. 166–

169.
18. A. Yazidi, H. Henao, and G.-A. Capolino, “Broken rotor bars fault detection in squirrel cage induction machines,” in *Proc. IEEE IEMDC*, San Antonio, TX, USA, 2005, pp. 741–747.
19. S. H. Kia, H. Henao, G.-A. Capolino, and C. S. Mar¸ti¸s, “Induction machine broken bars fault detection using stray flux after supply disconnection,” in *Proc. IEEE IECON*, Paris, France, 2006, pp. 1498–1503.
20. S. M. J. Rastegar Fatemi, H. Henao, and G.-A. Capolino, “Gearbox monitoring by using the stray flux in an induction machine based electromechanical system,” in *Proc. IEEE MELECON*, Ajaccio, France, 2008, pp. 484–489.
21. Ch. Jiang, S.Li, T.G. Habetler:"A review of condition monitoring of induction motors based on stray flux", *In Energy Conversion Congress and Exposition (ECCE)*, 2017 IEEE, DOI: 10.1109/ECCE.2017.8096907
22. S.B. Salem, M. Salah, W. Touti:"Stray Flux analysis for monitoring eccentricity faults in induction motors: Experimental study", In Control, Automation and Diagnosis (ICCAD), 2017 International Conference on, DOI:10.1109/CADIAG.2017.8075673
23. J. A. Antonino-Daviu, Alfredo Quijano-López, Vicente Climente- Alarcon, Hubert Razik:"Evaluation of the detectability of rotor faults and eccentricities in induction motors via transient analysis of the stray flux", In *Energy Conversion Congress and Exposition (ECCE*),2017 IEEE, DOI: 10.1109/ECCE.2017.8096633
24. G. Mirzaeva , K. I. Saad,:”Advanced Diagnosis of Rotor Faults and Eccentricity in Induction Motors Based on Internal Flux Measurement”, *IEEE Transactions on Industry Applications*, Vol: 54, Issue: 3, pp: 2981 – 2991, May-June 2018.
25. [25] J. Faiz S.M.M.Moosavi,:”Eccentricity fault detection – From induction machines to DFIG—A review”, *Renewable and Sustainable Energy Reviews*, Vol.55, pp: 169-179, March 2016.
26. Siddique ; G.S. Yadava ; B. Singh,:”A review of stator fault monitoring techniques of induction motors”, *IEEE Transactions on Energy Conversion* , Vol.: 20, Issue: 1,pp: 106 – 114, March 2005.
27. J.A. Antonino-Daviu, H. Razik, A. Quijano-Lopez and V. Climente- Alarcon, "Detection of rotor faults via transient analysis of the external magnetic field," *IECON 2017 - 43rd Annual Conference of the IEEE Industrial Electronics Society*, Beijing, 2017, pp. 3815-3821.
28. H. Cherif, A. Menacer, R. Romary and R. Pusca, "Dispersion field analysis using discrete wavelet transform for inter-turn stator fault detection in induction motors," *2017 IEEE 11th International Symposium on Diagnostics for Electrical Machines, Power Electronics and Drives (SDEMPED)*, Tinos, 2017, pp. 104-109.
29. Ruonan Liu Boyuan Yang Enrico Zio Xuefeng Chen: “Artificial intelligence for fault diagnosis of rotating machinery: A review”, *Mechanical Systems and Signal Processing*, Vol.108, pp 33-47, August 2018.
30. K. C. Deekshit Kompella , M. Venu Gopala Rao , R. Srinivasa Rao:” SWT based bearing fault detection using frequency spectral subtraction of stator current with and without an adaptive filter”, TENCON 2017 - 2017 IEEE Region 10 Conference Electronic ISSN:2159-3450, DOI: 10.1109/TENCON.2017.8228277.

31. El Houssin, El Bouchikhi , Vincent Choqueuse , Mohamed El Hachemi Benbouzid,:"Current Frequency Spectral Subtraction and Its Contribution to Induction Machines' Bearings Condition Monitoring" *IEEE Transactions on Energy Conversion* , Vol.: 28, Issue: 1, March,2013.
32. A. Bellini, C. Concari, G. Franceschini, C. Tassoni and A. Toscani, "Vibrations, currents and stray flux signals to asses induction motors rotor conditions", IECON 2006 - 32nd Annual Conference on IEEE Industrial Electronics, Paris, 2006, pp. 4963-4968.
33. A. Ceban, R. Pusca and R. Romary, "Study of Rotor Faults in Induction Motors Using External Magnetic Field Analysis", *IEEE Trans. Ind. Electronics*, vol. 59, no. 5, pp. 2082-2093, 2012.

IEEE TRANSACTIONS ON INDUSTRY APPLICATIONS, VOL. 55, NO. 5, SEPTEMBER/OCTOBER 2019, pp: 4585 - 4594 , **DOI:** 10.1109/TIA.2019.2917861
Manuscript received January 12, 2019; revised March 26, 2019 and May 3, 2019; accepted May 14, 2019. Date of publication May 19, 2019; date of current version August 14, 2019. Paper 2018-EMC-1351.R2, presented at the 2018 International Conference on Electrical Machines, Alexandroupoli, Greece, and approved for publication in the IEEE TRANSACTIONS ON INDUSTRY APPLICATIONS by the Electric Machines Committee of the IEEE Industry Applications Society.
This work was supported in part by MEC under Project MTM 2016-7963-P and in part by the Spanish 'Ministerio de Ciencia Innovación y Universidades' and FEDER program in the framework of the 'Proyectos de I+D de Generación de Conocimiento del Programa Estatal de Generación de Conocimiento y Fortalecimiento Científico y Tecnológico del SistemadeI+D+i, Subprograma Estatal de Generación de Conocimiento'(ref: PGC2018-095747-B-I00). (Corresponding author: Jose A. Antonino-Daviu.)
M. E. Iglesias-Martínez is with the Departamento de Telecomunicaciones, Universidad de Pinar del Río Hermanos Saíz Montes de Oca, Pinar del Río 20100, Cuba (e-mail: migueliglesias2010@gmail.com) and with the Instituto Universitario de Matemática Pura y Aplicada, Universitat Politècnica de València, Valencia E-46022, Spain P.Fernández de Córdoba and J.A. Conejero are with the Instituto Universitario de Matemática Pura y Aplicada, Universitat Politècnica de València, Valencia E-46022, Spain (e-mail: pfernandez@mat.upv.es; aconejero@upv.es). J. A. Antonino-Daviu is with the Instituto Tecnológico de la Energía, Universitat Politècnica de València, Valencia E-46022, Spain (e-mail: joanda@ die.upv.es).
Color versions of one or more of the figures in this paper are available online at http://ieeexplore.ieee.org. Digital Object Identifier 10.1109/TIA.2019.2917861

Detection of Nonadjacent Rotor Faults in Induction Motors via Spectral Subtraction and Autocorrelation of Stray Flux Signals

Miguel Enrique Iglesias-Martínez, Pedro Fernández de Córdoba, Jose A. Antonino-Daviu , Senior Member, IEEE, and J. Alberto Conejero

***Abstract*—In this paper, statistical signal processing techniques are applied to electromotive force signals captured in external coil sensors for adjacent and nonadjacent broken bars detection in in- duction motors. An algorithm based on spectral subtraction anal- ysis is applied for broken bar identification, independent of the relative position of the bar breakages. Moreover, power spectrum analyses enable the discrimination between healthy and faulty con- ditions. The results obtained with experimental data prove that the proposed approach provides good results for fault detectability. Moreover, the identification of the faults, and the signal correla- tion indicator to prove the results are also presented for different positions of the flux sensor.**

***Index Terms*—Fault diagnosis, flux, induction motors, signals, spectral analysis.**

I. INTRODUCTION

A recent trend in the electric motor condition monitoring area relies on combining the information obtained from the analyses of different machine quantities (currents, vibrations,

temperatures, etc.) to reach a more reliable conclusion about its health. This is due to the fact that it has been proven that the analysis of a single quantity enables to diagnose specific faults or anomalies but it is not enough to determine the health of the whole motor. In this context, the analysis of classical quantities that are well known in the industry, such as currents or vibrations, has shown some problems or drawbacks for the diagnosis of certain faults [1].

With regards to the condition of the rotor, neither current nor vibration analyses have proven to be valid in all the cases that may rise in industry; it has been reported, for instance, the occasional occurrence of false indications when these techniques are used [2]–[5]. One of the cases where these techniques have not shown good results when detecting rotor damages is under the presence of nonadjacent bar breakages in the rotor cage. In this regard, over recent decades, several works have reported problems of current-based techniques to detect such fault: in the early 1980s Hargis *et al.* already pointed out that when the bro- ken bars are separated by $\pi/2$ electrical radians, current analysis may underestimate the number of broken bars and may even fail to detect the defect [6]. Years later, Benbouzid [7] ratified the previous statement, remarking that the lower sideband harmonic (LSH) may not be discernible when the breakages occur at spe- cific relative locations. The statement of the problem led several authors to deepen in the physical study of the phenomenon by developing suitable electric motor models that were aimed to analyze the relation between the relative positions of the broken bars and the results of *motor current signature analysis* (MCSA). This is the case of [8], in which a model of a 22-bar, four-pole machine was built considering all the potential cases of double breakages; the authors concluded again that the amplitude of the LSH greatly depends on the relative position between the bro- ken bars. Other physical analyses of the problem that reached analogous conclusions can be found in [9] and [10], while em- pirical analyses were performed in [11]. Finally, in [12], it is presented a physical analysis of the air gap magnetic anomaly for the case of any double bar breakage, including multiple ex- perimental tests that confirmed the effect of the bar breakage location on the MCSA results. This work proved that when two broken bars are separated by a distance equal to half the pole pitch, the LSH amplitude can be significantly lower than that reached for the case of only one broken bar.

In spite of the number of works dealing with the nonadjacent broken bars issue, note that most of them are focused on present- ing rigorous analyses of the problem which ratify the difficulties of classical diagnosis methods. However, none of the previous works has proposed reliable solutions to the problem, neither based on current analysis nor on analysis of other quantities.
More recently, several groups of authors have proposed novel strategies that were intended to solve the nonadjacent broken bars diagnosis issue. In this regard, Riera-Guasp *et al.* [13] proposed a method for detecting nonadjacent bar breakages, which relies on the study, both at steady-state and under starting, of high-order harmonics (located at $f\cdot(5–4\cdot s)$ and $f\cdot(5–6\cdot s)$, with f = supply frequency and s = slip) produced by the fault in the stator current. The problem of this approach is that these harmonics often have low amplitudes and are not always easily discernible neither on the Fourier spectrum of the steady-state current nor on the time-frequency analysis of the starting current. On the other hand, Antonino-Daviu *et al*. [14] compares the per- formance of MCSA and *zero sequence current* (ZSC) analysis to detect both adjacent and nonadjacent bars. This works con- cludes that the ZSC analysis may be promising to avoid potential false-negative indications of MCSA. However, this method re- quires the measurement of currents in all three motor phases (in delta configuration) for the later computation of the ZSC, which is not easy in many real industrial applications. In a more recent work, Gyftakis *et al.* [15] proposed a reliable indicator to detect nonadjacent broken bars based on the *filtered Park's/extended Park's vector approach*. This method relies on monitoring the higher harmonic index of the Park's vector. Their

results were confirmed via multiple experimental tests. Once again, the prob- lem is that measurement of all three currents is necessary, a requirement that may significantly complicate the industrial ap- plicability of the approach.

Due to the important problems of the methods relying of cur- rent analysis to detect nonadjacent broken bars, other technolo- gies based on alternative quantities are being explored. In this context, in [16], it is proposed the installation of a Hall Effect sensor between two stator slots and the subsequent *fast Fourier transform* (FFT) analysis of the registered data. The disadvan- tage of this method, which proves to be effective under low slip operating conditions, is the unpractical nature of the approach due to the necessity of sensor installation during motor assem- bly. However, this work demonstrates the potential of the flux analysis for such diagnosis, even though it is focused on the analysis of the internal flux in the machine.

An alternative flux-based method that could have a more prac- tical feasibility would rely on the analysis of the motor stray flux. In this regard, the study of the external magnetic field in the vicinity of the motor has been proposed as a very interesting al- ternative for the diagnosis of several motor faults, namely: adja- cent rotor faults [17]–[19], eccentricities [20], [21], stator faults [22]–[24] or even gearbox problems [25]. It has been proven that when certain faults are present, specific harmonics are am- plified in the Fourier spectra of the *electromotive force* (EMF) signals induced in external coil sensors installed at different po- sitions. The simplicity, low cost, and easy implementation of the technique make it a very interesting option to complement the information obtained with other well-known technologies, especially considering the progressive reduction in price of the available flux sensors that comes together with an increase of their features [26]. Though most of the previous works related to flux monitoring have explored the applicability of the tech- nique under stationary conditions, some recent works have also studied the viability of the method under transient operation, obtaining very promising results [27]–[29].

In spite of all these advances, very few works have deepened in the application of the stray-flux analysis technique to detect nonadjacent broken bars in induction motors. One of the few available papers in this topic is [30], which relies on the extrac- tion of certain spectral flux component over time. Once again, the main constraint is that it focuses on the amplitudes of high- order harmonics that may not always be easily detectable.

In this work, a new algorithm to detect rotor damages, in in- duction motors based on the analysis of stray flux signals, is proposed. It uses a spectral pattern recognition method based on the spectral subtraction of the power spectrum of the cap- tured flux signals. The proposed algorithm is applied not only to detect adjacent bar breakages, but also nonadjacent broken bars. In this paper, different positions of the considered sen- sor are assessed. The results, which are an extension of those already presented in [31], show the potential of this approach, which provides valuable information to detect nonadjacent rotor damages. One important advantage of the proposed approach, in comparison with other methods, is its simple implementation and practical feasibility, since only one sensor measurement is required. Moreover, this can be done in a non-invasive way, with- out perturbing the operation of the machine. This is a crucial advantage in industry, where non-invasive nature and simplicity are crucial requirements for the massive penetration of fault di- agnosis techniques. Finally, the method relies on clear variations of the detected patterns which are discernible even for low fault severity levels and that are based on the overall flux spectrum rather than on particular harmonics that could be easily affected by other phenomena or which may have reduced amplitudes. The validity of the proposed approach is proven through sev- eral experimental tests that have been developed with the aid of an in-house built sensor that enables to measure the necessary quantity in a simple and fast way.

II. ROTOR BAR BREAKAGE DETECTION VIA ANALYSIS OF FLUX SIGNALS

Different authors have proven that the presence of certain faults in the motor amplifies some components in the stray flux spectrum [17]–[25], [32]. Most of these works proposed the use of external coil sensors for the capture of the necessary signals and the subsequent Fourier analysis of these signals to detect the components amplified by rotor damages and other faults. Regarding the detection of bar damages, in [32], it is suggested the study of the sideband components appearing at $f\cdot(1\pm 2\cdot s\cdot f)$ (with s stands for the *slip* and f for the supply frequency) around the main frequency component in the FFT spectrum of the cap- tured EMF signals. More recent works such as [17] and [33] propose the study of other components in the low frequency re- gion of the FFT spectrum of the EMF induced in external coil sensors; according to these authors, when rotor faults are present, the components located at $s\cdot f$ and $3\cdot s\cdot f$ are amplified in that FFT spectrum. Therefore, the study of the amplitudes of these har- monics may become a reliable indicator of the presence of the fault.

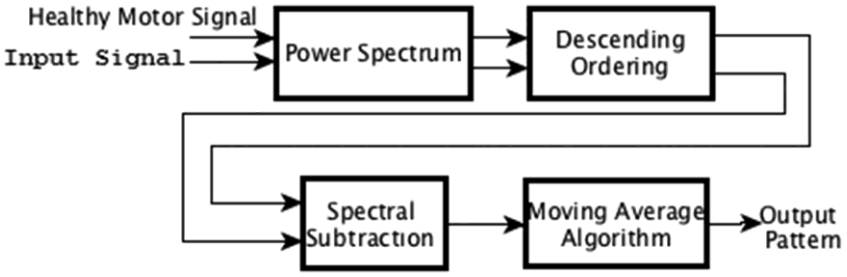

Fig. 1. Block diagram of the proposed algorithm for identifying broken bars.

Although most of the works developed in the literature are focused on the analysis of the EMF signals induced in external coil sensors at steady-state operation of the motor, some recent papers have explored the viability of the analysis of these signals under the startup, obtaining very promising results [27], [28], [34]. These works have proven that, during transient operation, the fault components follow particular trajectories that can be used as evidences of the failure.

The present work focuses on the flux-based detection of ro- tor faults but considering the case of nonadjacent broken bars. As commented above, despite several works have stated the dif- ficulties that conventional methods have under this situation, very few works have tried to proposed effective solutions to the problem.

III. PROPOSED ALGORITHM

To try to achieve some recognition criteria to classify the damages, a method based on the spectrum descending order is applied to the signal obtained after preprocessing (output signal after noise reduction). Later, a spectral subtraction operation with respect to the signal of the healthy motor is also performed [35], [36]. Finally, a moving average block is used as a smoothing filter to eliminate impulsive components of the spectral subtraction. The resulting algorithm given by these processes is described in Fig. 1.

The pattern recognition algorithm is based on the use, as a basic pattern, of the signal of the healthy motor. This is not a serious restriction under a practical point of view, since that signal

could be obtained after motor commissioning or after motor inspection, once the rotor is guaranteed to be healthy. In the method, once the actual samples have been captured, they can be compared with the healthy ones. The proposed method is based on searching for patterns, by looking at the differences in the spectrum of both signals (actual sample versus healthy one). The use of the signal of the healthy motor as a signal reference is analogous to the schemes of adaptive systems. What is obtained at the output, is a spectral pattern that identifies the number of broken bars present in the motor.

For finite duration discrete-time signals $\{x(n)\}_{n=0}^{N-1}$ (which represents the signal to be processed) and $\{y(n)\}_{n=0}^{N-1}$ (which represents the healthy motor signal that is taken as reference sig- nal), both of length *N* samples, the classic method for estimation of the power spectrum is the periodogram. The periodogram is defined as:

$$Pxx(f) = \frac{1}{N}\left|\sum_{m=0}^{N-1} x(m)e^{j2\pi f_m}\right|^2 = \frac{1}{N}|X(f)|^2 \quad (1)$$

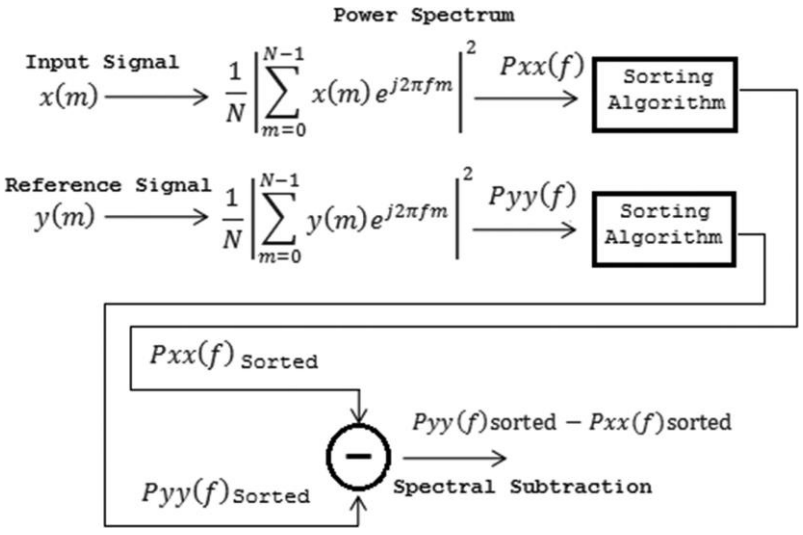

Fig. 2. Method to perform the proposed algorithm.

In our case, the algorithm is based on performing the power spectrum for both signals, namely: the input signal *x* and the reference signal *y*. Afterward, we proceed to sort the power spectrum using descend method. The obtained results for both signals after sorting the power spectrum are used for spectral subtraction. The overall process to perform the proposed algo- rithm is shown in Fig. 2. As a final step, we propose the application of a moving average filter for smoothing. The novelty of this algorithm relies on the use of a reference signal which controls the entire process, in addition to the use of spectral subtraction and the ordering of the power spectrum. Computational complexity of the algorithm is low, since it is based on second-order statistics.

IV. EXPERIMENTAL RESULTS

Different experiments were developed at the laboratory by using a four-pole, 1.1-kW induction motor which was coupled to a dc machine acting as a load. The detailed characteristics of the

tested motor and load can be found in the Appendix. Different cage rotors (28 bars in each rotor) with diverse levels of failure were available, so that each specific rotor could be assembled to test the corresponding rotor fault condition. More specifically, in this work, the considered cases are: healthy rotor and rotor with two broken bars. In this latter case, different relative positions between the broken bars were tested, namely: bars 1–2 broken (adjacent broken bars), bars 1–3 broken, bars 1–4 broken, bars 1–5 broken, and bars 1–6 broken.

In each test, the machine was started until it reached the steady-state regime. The EMF signal induced in an external coil sensor attached to the frame of the machine was captured using a digital YOKOGAWA DL-850 oscilloscope. The flux sensor was built in the laboratory and was based on a coil with 1000 turns with an external diameter of 80 mm and an internal diameter of 39 mm. Two different sensor locations were considered: Posi- tion A (sensor attached to the lateral part of the motor frame, in the shaft side, Fig. 3(b)) and Position B (sensor attached to the center of the frame, Fig. 3(c)). The signals were captured using a sampling rate of 5 kHz and the acquisition time for the steady-state signals was 40 s. Both the experimental test bench and the two considered sensor positions are shown in Fig. 3.

In order to detect the corresponding faulty condition, the idea of the proposed algorithm to identify the broken bar pattern

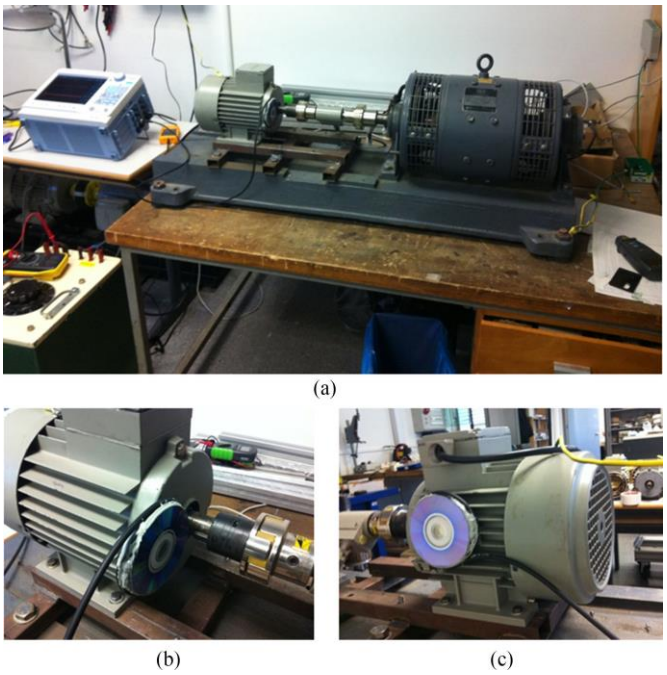

Fig. 3. (a) Experimental test bench. (b) Position A of the coil sensor. (c) Position B of the coil sensor.

is to take, as a reference, the healthy state of the motor. The objective is to detect differences in the power spectrum, taking into account that a motor in a healthy state will have a certain power spectrum. When the motor is faulty, it will no longer have the same spectrum. Hence, our method

will be based on the rearrangement of the power spectrum and spectral subtraction to obtain an identification pattern of broken bars regardless of the relative position of the bars. The developed algorithm was conditioned by two goals: 1) it should be able to distinguish between healthy and faulty cases based on the analyses of flux data; and 2) it should be able to detect the existence of the fault regardless of the position of the bars that break.

A. Experimental Results Obtained From the Measurement in Position A

Regarding Position A, the resulting pattern obtained for each sample after the application of the proposed algorithm (see Fig. 1) allows us to discern when we are in the presence of a motor with two broken bars, since all the samples converge to the same line (see Fig. 4).
In Fig. 4, we can also see the stepped positioning of the obtained patterns from each sample according to the relative positions, whose difference lies in the amplitude, that is: first position_1_2 (red), position_1_6 (black), position_1_5 (yellow), position_1_3 (green), the above except for position_1_4 (blue) which reflects a total difference with the rest of the obtained patterns, from each sample. This result can be very useful for discrimination between the healthy and faulty cases and for the identification of the two broken bars case, regardless of the rel- ative position of the broken bars.

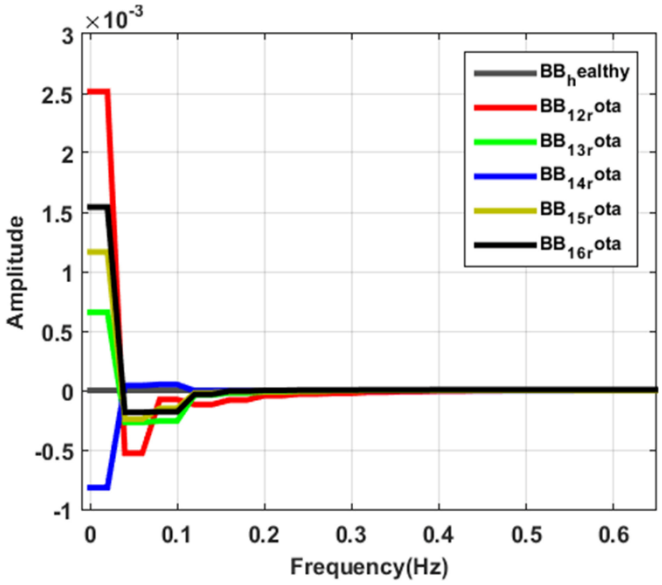

Fig. 4. Resulting spectral pattern obtained from Position A.

TABLE I. CORRELATION VALUES OBTAINED ACCORDING TO THE RESULTING PATTERNS: POSITION A.

CORR_POS_1_2 & 1_6 = 1.0000 0.9933 0.9933 1.0000	CORR_POS_1_2 & 1_5 = 1.0000 0.9945 0.9945 1.0000
CORR_POS_1_2 & 1_3= 1.0000 0.9344 0.9344 1.0000	CORR_POS_1_2 & 1_4= 1.0000 -0.9849 -0.9849 1.0000

To prove that we are in the presence of a motor with two broken bars, the Pearson correlation coefficient was applied between the resulting patterns obtained from the measurements carried out in Position A. The correlation obtained between the resulting patterns is almost 1, except on the case of Position 1_4. Table I shows the results obtained. In that table, CORR_POS_X_X is the correlation obtained from each pattern with respect to the resulting pattern of the bar BB_1_2. The measurement BB_1_2 was taken as reference, but another sample could have been taken; the correlation will give similar values with the excep- tion of Position 1_4, which has a certain difference as shown in the graph of Fig. 4. Now, if we consider the mean value of the module of the obtained correlations, it gives as result: 0.9768.

B. Experimental Results Obtained From the Measurement in Position B

As for Position B, it is verified by the resulting pattern (see Fig. 5) that there are two broken bars and just as in Position A, we can discern in which relative position is Position 1_4 (blue) and Position 1_6 (black) which are differentiable from the rest of the others, since their correlation value is negative as well as the results of the measurement at Position A.

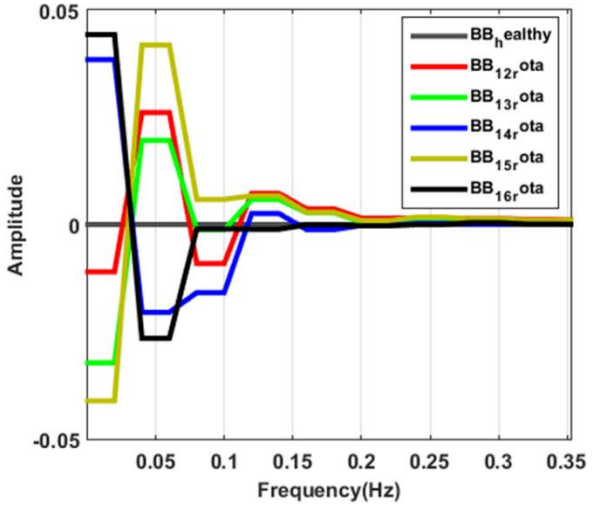

Fig. 5. Resulting spectral pattern obtained from Position B.

TABLE I I CORRELATION VALUES OBTAINED ACCORDING TO THE RESULTING PATTERNS: POSITION B

CORR_POS_1_2 & 1_6 = 1.0000 -0.7361 -0.7361 1.0000	CORR_POS_1_2 & 1_5 = 1.0000 0.8457 0.8457 1.0000
CORR_POS_1_2 & 1_3 = 1.0000 0.7875 0.7875 1.0000	CORR_POS_1_2 & 1_4 = 1.0000 -0.5542 -0.5542 1.0000

With respect to the other broken bar relative positions (1_2, 1_3, and 1_5), these follow a stepped descendent pattern as in Fig. 2, although not in the same order. The correlation obtained between the resulting patterns as in Position A is almost 1, except on Position 1_4 and Position 1_6, whereby these two positions can be discerned. In Table II, the results are shown. Now, if we proceed in the same way as for Position A, with the average value of the module of the correlations obtained, it yields: 0.7309. The correlation levels obtained in the measurements made in both relative Positions A and B, respectively, oscillate between 0.7 and 0.98, which can be a variable indicator to identify broken bars using the flux signals.

Note that the power spectra of Figs. 4 and 5 have been sorted according to the amplitude in descending form, as a way to organize the vector to evaluate the spectral subtraction, whose objective is to obtain differences in the spectrum in relation to the healthy state. By carrying out the spectral subtraction of the spectra, only the components in the failure bands will remain, since the components of fundamental frequencies as well as the noise that may exist in the spectrum are cancelled out.

The fault components appear in the spectrum in the bands adjacent to the fundamental frequency. When the spectrum is sorted, the frequency components are placed in descending order according to their amplitude value; the amplitude values of the components where there is a fault will take a new position in the new ordered amplitude vector, but this information is not relevant, since what is intended is to find out a common pattern for when there are two broken bars, regardless of their relative position, so, in this case, the information relative to the location in the frequency domain is not so relevant.

C. Discrimination Between Healthy and Damaged States Based on the Spectra

The discrimination between healthy and faulty conditions can be carried out by comparing the corresponding spectra of the captured EMF signals. However, this procedure is influenced by the occurrence of nonadjacent breakages since, depending on the relative positions between the bars that break, the amplitudes of the fault harmonics may sensibly differ [30]. However, as pointed out in previous works [17], [33], the analyses of the Fourier spectra may be helpful at least to have evidence that an anomaly may be present. A rough analysis of the characteristics of the Fourier spectra for each one of the considered positions of the sensor (see Figs. 6 and 7) is presented next. Table III synthesizes the conclusions of both figures and includes the case of a single broken bar for comparison purposes.

Characteristics of the spectra for Position A are as follows.

1) All the analyses show the presence of the main rotor fault component (LSH), which is typically used for diagnosing the fault and that is located at $f\cdot(1–2\cdot s)$. However, note that there are clear differences between the amplitude of this harmonic for healthy and faulty conditions, a fact that may enable to discriminate between both conditions (see Fig. 6).
2) Note that, for the different cases of broken bars, the am- plitude of the LSH significantly changes. The maximum amplitude is reached when the broken bars are consecutive (Positions 1–2), whereas the minimum amplitudes happen when the broken bars are at Positions 1–4 and 1–5. This fact clearly confirms the influence of the relative position of the broken bars on the fault component amplitude. In any case, in spite of these differences between faulty cases, the differences are evident versus healthy condition.

Characteristics of the spectra for Position B are as follows.

1) All samples have the expected fundamental harmonic at 50 Hz (see Fig. 7).
2) As in Position A, sideband components are present for all faulty cases although their amplitudes vary depending on the relative position between broken bars (maximum amplitude for adjacent bars, in agreement with the con- clusions of previous works focused on current analysis [12]).
3) Again, there is a significant variation between the lower sideband amplitude for the faulty cases. In some relative positions, the compensation effect between both break- ages may lead to very low amplitudes of the sideband that may lead to difficulties for discriminating versus healthy condition.
4) If the low frequency regions (not shown in the figures due to space restrictions) are studied, fault harmonics are detectable at components $s\cdot f$ and $3s\cdot f$ [33]. One again their amplitudes

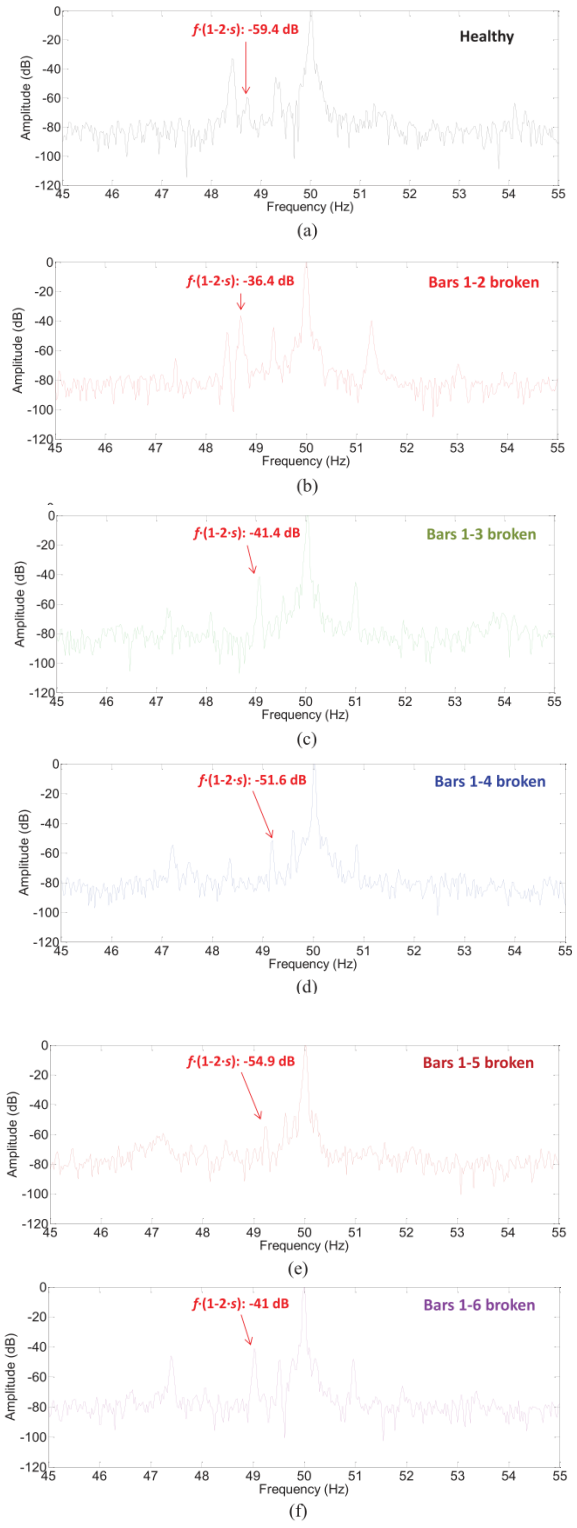

Fig. 6. Comparison of the spectrum of (a) healthy motor, with (b)–(f) broken bars spectra. Sensor Position: A

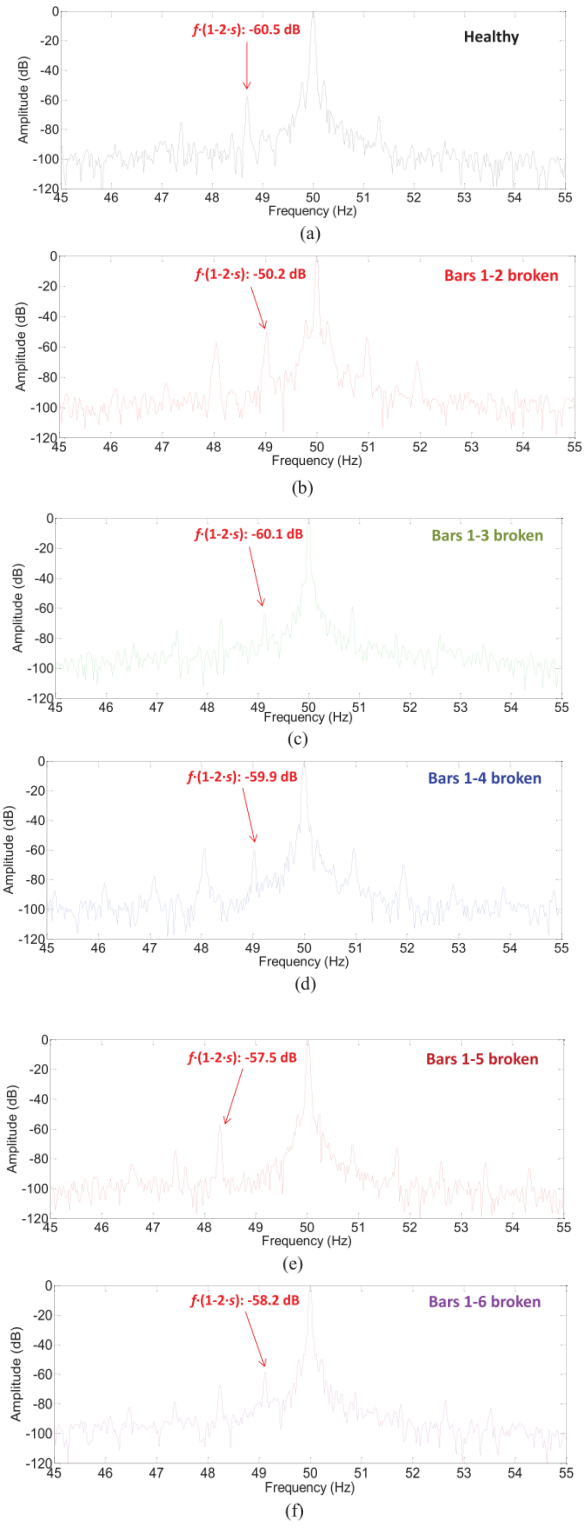

Fig 7. Comparison of the spectrum of (a) healthy motor, with (b)– (f) broken bars spectra. Sensor Position: B

TABLE III. LSH FREQUENCY AND AMPLITUDE FOR EACH TESTED CONDITION AND FOR EACH SENSOR POSITION

SENSOR POSITION A			
CONDITION	SPEED (RPM)	LSH FREQUENCY (HZ)	LSH AMPLITUDE (DB)
Healthy	1481	48,73	-59,4
1 broken bar	1480	48,67	-53,2
2 broken bars (1-2)	1480	48,67	-36,4
2 broken bars (1-3)	1487	49,13	-41,4
2 broken bars (1-4)	1488	49,20	-51,6
2 broken bars (1-5)	1488	49,20	-54,9
2 broken bars (1-6)	1486	49,07	-41
SENSOR POSITION B			
CONDITION	SPEED (RPM)	LSH FREQUENCY (HZ)	LSH AMPLITUDE (DB)
Healthy	1480	48,67	-60,5
1 broken bar	1486	49,07	-54,1
2 broken bars (1-2)	1484	48,93	-50,2
2 broken bars (1-3)	1488	49,20	-60,1
2 broken bars (1-4)	1485	49,00	-59,9
2 broken bars (1-5)	1479	48,60	-57,5
2 broken bars (1-6)	1486	49,07	-58,2

amplitudes are influenced by the relative positions of the breakages. But their presence is evidence of the existence of the fault.

In conclusion, the analyses of the spectra can enable to distinguish visually between healthy and faulty conditions but the influence of the relative position between broken bars may make the discrimination difficult in some cases. Due to this, the algo rithm proposed in the first part of this paper can be especially useful to diagnose this situation and avoid false-negative indications.

D. Discrimination Between Healthy and Damaged States Based on the Autocovariance Function.

From the previous results based on the information of the frequency spectrum, differences between both spectra can be visually appreciated for the healthy and damaged states. However, it is convenient to obtain an indicator that emits a constant or a variable value in a certain range when it is in the presence of a healthy motor and when the motor is damaged. In relation to this, in this section, an algorithm based on the square value of the median of the autocovariance of the flux signal is proposed. It is decided to use the median and not the mean value so that the amplitude peak in the flux signal has no influence at the time of the calculation of the indicator. The reason for using the quadratic value of the median of the autocovariance is explained by the fact that it is necessary to obtain a quantitative indicator which clearly differs between healthy and faulty conditions. Although other quantities such as the mean value, quadratic mean of variance have been also evaluated, they have not led to so sensitive results as the proposed quantity. The theoretical foundations of the proposed algorithm are described next: for a stationary periodic real signal, the autocovariance function of a random, stationary process $\{x(n)\}$ is a measure of the dispersion of the process around its mean value and is defined as a function dependent on the first and second-order moments as follows:

$$c_2^X(\tau) = m_2^X(\tau) - (m_1^X)^2$$

where $c_2^X(\tau)$ is the autocorrelation function. From the above equation, it can be noted that if the process is of value zero mean value, the autocovariance coincides with the autocorrelation function. Then, replacing in (2) and applying second-order statistics we have:

$$c_2^X(\tau) = \frac{1}{N}\sum_{t=0}^{N-1-\tau} x(t)\cdot x(t+\tau)$$

Then, after obtaining the autocovariance function, we proceed to calculate the square value of the median, for each sample used in the experiment, which is as follows:
Let *x*1 , *x*2 , *x*3 ,..., *xn* be the data of a sample ordered in in- creasing order and designating the median *Me* as: if *n* is odd, the median is the value occupied by the position :
$Me_{c_2^X(\tau)} = \frac{c_2^X(\tau)_{(n+1)}}{2}$ then if n is not odd, the median is the arithmetic mean of the two central values. Then, it would be:

$$Me_{c_2^X(\tau)} = \frac{c_2^X(\tau)_{(n/2)} + c_2^X(\tau)_{(n/2+1)}}{2}$$

Substituting to find out the temporary indicator:

$$Ind_t = (Me_{c_2^X(\tau)})^2$$

The obtained results applying the proposed algorithm as a temporary indicator for the detection of the healthy–damaged state of the motor are shown in Fig. 8, likewise these are summarized in Table IV.

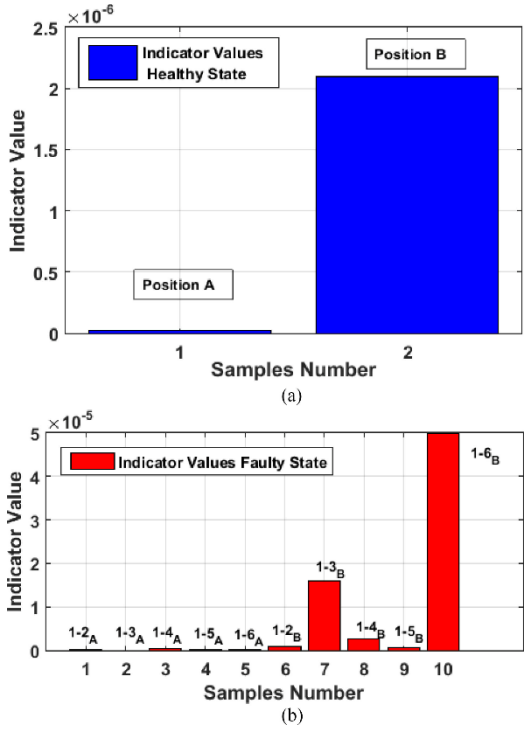

Fig. 8. Comparison between: (a) indicator for healthy state condition for both sensor positions A and B and (b) indicator for broke state condition for both sensor positions A and B.

TABLE IV VALUES OF THE INDICATOR AND MULTIPLICATION FACTOR FOR BOTH SENSOR POSITIONS A AND B

Sensor Position	Indicator for Faulty State	Indicator for Healthy State	Multiplication Factor
Healthy_A		2.7E-08	
1-2_A	6.8E-09		0.2519
1-3_A	1.7E-10		0.0063
1-4_A	4.4E-07		16.2963
1-5_A	3.4E-09		0.1259
1-6_A	4.65E-08		1.7222
Healthy_B		2.1E-06	
1-2_B	9.77E-07		0.4652
1-3_B	1.6E-05		7.6190
1-4_B	2.67E-06		1.2714
1-5_B	5.23E-07		0.2490
1-6_B	5E-05		23.8095

As it can be observed in Table IV, there is a notable difference in the values of the indicator obtained for Position A with respect to those obtained for Position B, even for the same condition. This indicates that the sensor position plays an important role. Note also that there are

important differences between the value of the indicator for healthy condition and its corresponding value for each fault condition (second and third columns). In order to obtain a measure of this difference, a multiplication factor is introduced (see fourth column); it is defined as the ratio between the value of the indicator for the corresponding faulty condition and its value for healthy state. This ratio gives an idea of the fault severity in comparison with the healthy condition.

Note that the relative Positions 1–3_A, 1–3_B, and 1–6_B, respectively, are the positions where more noticeable differences of the indicator are obtained in relation to the values obtained for the healthy condition. For the other relative positions, the differences are not so clear; a fact that indicates that, in addition to the sensor position, the relative position of the broken bar also has certain influence in the results.

V. CONCLUSION

This work proposes the use of induction motor stray flux sig- nals for the identification of bar breakages regardless of their rel- ative position. During the experiments carried out, it was shown that it is possible with the proposed algorithm to detect the fault and even distinguish the relative position of the bars that break. The proposed method is based on the frequency spectral sub- traction of the power spectrum and on the subsequent computa- tion of the Pearson correlation coefficient, which was calculated to demonstrate the similarity of all the patterns obtained for the case of two broken bars [37], [38].

In order to identify between healthy and damaged states, a rough analysis of the power spectrum may be sufficient in some situations; the differences between the spectrum of the healthy motor and the faulty states in both Positions A and B can be noticed visually, by means of the harmonics appearing both at lower frequencies and around the main component.

Furthermore in relation to this, a potential indicator to evalu- ate the condition of the motor and discriminate between healthy and damaged states has been evaluated experimentally. This in- dicator is based on the calculation of the square value of the median of the autocovariance function of the stray flux signal.

It is shown that there are quantitative differences in the obtained values when evaluating the indicator for both states (healthy and faulty) and it was demonstrated that the position of the flux sen- sor as well as the relative position of the broken bar may have influence at the time of calculation of the indicator. According to the obtained results, the indicator evaluated when the sensor is at Position B seems to be more sensitive than when the sensor is at Position A.

APPENDIX

See Tables V and VI.

TABLE V
RATED CHARACTERISTICS OF THE TESTED MOTOR

Model 1LA2080-4AA10	
Rated power (P_N)	1.1 kW
Rated speed (n_N)	1410 rpm
Rated voltage (U_N)	400(Y)/230 (Δ)
Rated current (I_N)	2.7(Y)/4.6 (Δ)
Rated power factor (Cos φ)	0.8
Number of rotor bars	28

TABLE VI
RATED CHARACTERISTICS OF THE LOAD (D.C. MACHINE)

Rated power (P_N)	3 kW
Rated speed (n_N)	2000 -3000 rpm
Rated voltage (U_N)	220 V
Rated excitation current	0.4 A
Rated armature current	13.6 A
Number of pole pairs	1

VI. REFERENCES

1. S. Nandi, H. A. Toliyat, and X. Li, "Condition monitoring and fault diag- nosis of electrical motors—A review," IEEE Trans. Energy Convers. 20, no. 4, pp. 719–729, Dec. 2005.
2. M. Riera-Guasp, J. A. Antonino-Daviu, and G. A. Capolino, "Advances in electrical machine, power electronic, and drive condition monitoring and fault detection: State of the art," IEEE Trans. Ind. Electron. 62, no. 3, pp. 1746–1759, Mar. 2015.
3. J. A. Antonino-Daviu, M. Riera-Guasp, J. R. Folch, and M. Pilar Molina Palomares, "Validation of a new method for the diagnosis of rotor bar failures via wavelet transform in industrial induction machines," IEEE Trans. Ind. Appl. 42, no. 4, pp. 990–996, Jul./Aug. 2006.
4. C. Yang, T.-J. Kang, D. Hyun, S. Lee, J. Antonino-Daviu, and J. Pons-Llinares, "Reliable detection of induction motor rotor faults under the rotor axial air duct influence," IEEE Trans. Ind. Appl. 50, no. 4, pp. 2493–2502, Jul./Aug. 2014.
5. J. A. Antonino-Daviu, J. Pons-Llinares, S. Shin, K. W. Lee, and S. B. Lee, "Reliable detection of induction motor rotor faults under the influence of rotor core magnetic anisotropy," in Proc. IEEE 10th Int. Symp. Diagnostics Elect. Mach. Power Electron. Drives, Guarda, Portugal, 2015, pp. 14–21.

6. C. Hargis, B. G. Gaydon, and K. Kamash, “The detection of rotor defects in induction motors,” in Proc. IEE Int. Conf. Elect. Mach. Des. Appl., London, U.K., pp. 216–220.
7. M. H. Benbouzid, “A review of induction motors signature analysis as a medium for fault detection,” IEEE Trans. Ind. Electron. 47, no. 5, pp. 984–993, Oct. 2000.
8. T. J. Sobczyk and W. Maciolek, “Does the component (1-2s)fo in stator current is sufficient for detection of rotor cage faults?” in Proc. IEEE 5th Int. Symp. Diagnostics Elect. Mach. Power Electron. Drives, Vienna, Austria, Sep. 2005, pp. 1–5.
9. J. Faiz and B. M. Ebrahimi, “Locating rotor broken bars in induction motors using finite element method,” Energy Convers. Manage. 50, no. 1, pp. 125–131, Jan. 2009.
10. G. Y. Sizov, A. Sayed-Ahmed, C. C. Yeh, and N. A. O. Demerdash, “Anal- ysis and diagnostics of adjacent and nonadjacent broken-rotor-bar faults in squirrel-cage induction machines,” IEEE Trans. Ind. Electron. 56, no. 11, pp. 4627–4641, Nov. 2009.
11. A. Menacer, S. Moreau, G. Champenois, M. S. N. Said, and A. Benakcha, “Experimental detection of rotor failures of induction machines by stator current spectrum analysis in function of the broken rotor bars position and the load,” in *Proc. Int. Conf. Comput. Tool*, Sep. 2007, pp. 1752–1758.
12. M. Riera-Guasp, M. F. Cabanas, J. A. Antonino-Daviu, M. Pineda- Sánchez, and C. H. R. García, “Influence of nonconsecutive bar breakages in motor current signature analysis for the diagnosis of rotor faults in in- duction motors,” *IEEE Trans. Energy Convers.* 25, no. 1, pp. 80–89, Mar.2010.
13. M. Riera-Guasp, J. Pons-Llinares, F. Vedreño-Santos, J. A. Antonino- Daviu, and M. Fernández Cabanas, “Evaluation of the amplitudes of high- order fault related components in double bar faults,” in *Proc. 8th IEEE Symp. Diagnostics Elect. Mach. Power Electron. Drives*, Bologna, Italy, 2011, pp. 307–315.
14. J. A. Antonino-Daviu, K. N. Gyftakis, R. Garcia-Hernandez, H. Razik, and A. J. M. Cardoso, “Comparative influence of adjacent and non-adjacent broken rotor bars on the induction motor diagnosis through MCSA and ZSC methods,” in *Proc. 41st Annu. Conf. IEEE Ind. Electron. Soc.*, Yoko- hama, Japan, 2015, pp. 1680–1685.
15. K. N. Gyftakis, J. A. Antonino-Daviu, and A. J. M. Cardoso, “A reliable indicator to detect non-adjacent broken rotor bars severity in induction motors,” in *Proc. 22nd Int. Conf. Elect. Mach.*, Lausanne, Switzerland, 2016, pp. 2910–2916.
16. C. G. Dias and C. M. de Sousa, “An experimental approach for diagnosis of adjacent and nonadjacent broken bars in induction motors at very low slip,” in *Proc. IEEE Int. Elect. Mach. Drives Conf.*, Miami, FL, USA, 2017, pp. 1–6.
17. R. Romary, R. Pusca, J. P. Lecointe, and J. F. Brudny, “Electrical machines fault diagnosis by stray flux analysis,” in *Proc. IEEE Workshop Elect. Mach. Des. Control Diagnosis*, Paris, France, Mar. 11–12, 2013, pp. 247–256.
18. A. Yazidi, H. Henao, and G.-A. Capolino, “Broken rotor bars fault detec- tion in squirrel cage induction machines,” in *Proc. IEEE Int. Conf. Elect. Mach. Drives*, San Antonio, TX, USA, 2005, pp. 741–747.
19. H. Henao, G.-A. Capolino, and C. S. Martis, “On the stray flux anal- ysis for the detection of the three-phase induction machine faults,” in *Proc. Conf. Rec. 38th IEEE IAS Annu. Meeting* 2, 2003, pp. 1368 –1373.
20. G. Mirzaeva and K. I. Saad, “Advanced diagnosis of rotor faults and ec- centricity in induction motors based on internal flux measurement,” *IEEE Trans. Ind. Appl.* 54, no. 3, pp. 2981–2991, May/Jun. 2018.

21. S. B. Salem, M. Salah, W. Touti, K. Bacha, and A. Chaari, "Stray flux anal- ysis for monitoring eccentricity faults in induction motors: Experimental study," in *Proc. Int. Conf. Control Autom. Diagnosis*, 2017, pp. 292–297, doi: 10.1109/CADIAG.2017.8075673.
22. L. Frosini, A. Borin, L. Girometta, and G. Venchi, "A novel approach to detect short circuits in low voltage induction motor by stray flux measure- ment," in *Proc. Int. Conf. Elect. Mach.*, Marseille, France, Sep. 2–5, 2012, pp. 1538–1544.
23. H. Henao, C. Demian, and G.-A. Capolino, "A frequency-domain de- tection of stator winding faults in induction machines using an external flux sensor," *IEEE Trans. Ind. Appl.* 39, no. 5, pp. 1272–1279, Sep./Oct.2003.
24. A. Yazidi, D. Thailly, H. Henao, R. Romary, G.-A. Capolino, and J.-F. Brudny, "Detection of stator short-circuit in induction machines using an external leakage flux sensor," in *Proc. IEEE Int. Conf. Ind. Technol.*, Hammamet, Tunisia, 2004, pp. 166–169.
25. S. M. J. Rastegar Fatemi, H. Henao, and G.-A. Capolino, "Gearbox monitoring by using the stray flux in an induction machine based electromechanical system," in *Proc. IEEE Mediterranean Electrotech. Conf.*, Ajaccio, France, 2008, pp. 484–489.
26. C. Jiang, S. Li, and T. G. Habetler, "A review of condition monitoring of induction motors based on stray flux," in *Proc. IEEE Energy Convers.Congr. Expo.*, Cincinnati, OH, USA, 2017, pp. 5424–5430.
27. J. A. Ramirez-Nunez *et al.*, "Evaluation of the detectability of electrome- chanical faults in induction motors via transient analysis of the stray flux," *IEEE Trans. Ind. Appl.* 54, no. 5, pp. 4324–4332, Sep./Oct. 2018.
28. H. Cherif, A. Menacer, R. Romary, and R. Pusca, "Dispersion field analysis using discrete wavelet transform for inter-turn stator fault detection in induction motors," in *Proc. IEEE 11th Int. Symp. Diagnostics Elect. Mach. Power Electron. Drives*, Tinos, Greece, 2017, pp. 104–109.
29. J. A. Antonino-Daviu, H. Razik, A. Quijano-Lopez, and V. Climente- Alarcon, "Detection of rotor faults via transient analysis of the external magnetic field," in *Proc. 43rd Annu. Conf. IEEE Ind. Electron. Soc.*, Bei- jing, China, 2017, pp. 3815–3821.
30. P. A. Panagiotou, I. Arvanitakis, N. Lophitis, J. A. Antonino-Daviu, and K. N. Gyftakis, "Analysis of stray flux spectral components in induction machines under rotor bar breakages at various locations," in *Proc. 23rd Int. Conf. Elect. Mach.*, Alexandroupoli, Greece, 2018, pp. 2345–2351.
31. M. E. Iglesias-Martínez, P. F. de Córdoba, J. A. Antonino-Daviu, and J. A. Conejero, "Detection of bar breakages in induction motor via spectral subtraction of stray flux signals," in *Proc. 23rd Int. Conf. Elect. Mach.*, Alexandroupoli, Greece, 2018, pp. 1796–1802.
32. A. Bellini, C. Concari, G. Franceschini, C. Tassoni, and A. Toscani, "Vi- brations, currents and stray flux signals to asses induction motors rotor conditions," in *Proc. 32nd Annu. Conf. IEEE Ind. Electron.*, Paris, France, 2006, pp. 4963–4968.
33. A. Ceban, R. Pusca, and R. Romary, "Study of rotor faults in induction mo- tors using external magnetic field analysis," *IEEE Trans. Ind. Electron.* 59, no. 5, pp. 2082–2093, May 2012.
34. J. A. Antonino-Daviu, H. Razik, A. Quijano-Lopez, and V. Climente- Alarcon, "Detection of rotor faults via transient analysis of the external magnetic field," in *Proc. 43rd Annu. Conf. IEEE Ind. Electron. Soc.*, Bei- jing, China, 2017, pp. 3815–3821.

35. K. C. Deekshit Kompella, M. Venu Gopala Rao, and R. Srinivasa Rao, "SWT based bearing fault detection using frequency spectral subtraction of stator current with and without an adaptive filter," in *Proc. IEEE Region 10 Conf.*, 2017, pp. 2472–2477, doi: 10.1109/TENCON.2017.8228277.
36. E H. El Bouchikhi, V. Choqueuse, and M. El Hachemi Benbouzid, "Current frequency spectral subtraction and its contribution to induction machines' bearings condition monitoring," *IEEE Trans. Energy Convers.* 28, no. 1, pp. 135–144, Mar. 2013.
37. H. Deborah, N. Richard, and J. Y. Hardeberg, "A comprehensive evalu- ation of spectral distance functions and metrics for hyperspectral image processing," *IEEE J. Sel. Topics Appl. Earth Observ. Remote Sens.* 8, no. 6, pp. 3224–3234, Jun. 2015.
38. G. Borelli, J. Jovic Bonnet, Y. Rosales Hernandez, K. Matsuda, and J. Damerau, "Spectral-distance-based detection of EMG activity from ca- pacitive measurements," *IEEE Sens. J.* 18, no. 20, pp. 8502–8509, Oct. 15, 2018.

energies

MDPI

Article

Rotor Fault Detection in Induction Motors Based on Time-Frequency Analysis Using the Bispectrum and the Autocovariance of Stray Flux Signals

Miguel E. Iglesias-Martínez [1,2], Jose Alfonso Antonino-Daviu [3,*], Pedro Fernández de Córdoba [2] and J. Alberto Conejero [2]

1 Departamento de Telecomunicaciones, Universidad de Pinar del Río, Pinar del Río, Martí #270, CP 20100, Cuba; migueliglesias2010@gmail.com

2 Instituto Universitario de Matemática Pura y Aplicada, Universitat Politècnica de València (UPV), Camino de Vera s/n, 46022 Valencia, Spain; pfernandez@mat.upv.es (P.F.d.C.); aconejero@upv.es (J.A.C.)

3 Instituto Tecnológico de la Energía, Universitat Politècnica de València (UPV), Camino de Vera s/n, 46022 Valencia, Spain

* Correspondence: joanda@die.upv.es; Tel.: +34-963877592

Received: 20 January 2019; Accepted: 11 February 2019; Published: 14 February 2019

Energies **2019**, *12*(4), 597; https://doi.org/10.3390/en12040597

Impact Factor: 2.707 (2018) ; 5-Year Impact Factor: 2.990 (2018)

Abstract: The aim of this work is to find out, through the analysis of the time and frequency domains, significant differences that lead us to obtain one or several variables that may result in an indicator that allows diagnosing the condition of the rotor in an induction motor from the processing of the stray flux signals. For this, the calculation of two indicators is proposed: the first is based on the frequency domain and it relies on the calculation of the sum of the mean value of the bispectrum of the flux signal. The use of high order spectral analysis is justified in that with the one-dimensional analysis resulting from the Fourier Transform, there may not always be solid differences at the spectral level that enable us to distinguish between healthy and faulty conditions. Also, based on the high-order spectral analysis, differences may arise that, with the classical analysis with the Fourier Transform, are not evident, since the high order spectra from the Bispectrum are immune to Gaussian noise, but not the results that can be obtained using the one-dimensional Fourier transform. On the other hand, a second indicator based on the temporal domain that is based on the calculation of the square value of the median of the autocovariance function of the signal is evaluated. The obtained results are satisfactory and let us conclude the affirmative hypothesis of using flux signals for determining the condition of the rotor of an induction motor.

Keywords: indicator; fault diagnosis; induction motors; bispectrum; autocovariance

1. Introduction

In the electric motor condition monitoring area, there is a continuous search for new techniques that are able to enhance the performance and to avoid the drawbacks of the currently existing ones. In this context, the analysis of alternative machine quantities is being explored, as a way to complement the information provided by the well-known methods that are widespread in the industry (currents and vibrations). This is especially important, taking into consideration that no single quantity has been proved to be reliable enough to diagnose the condition of the whole machine, and that the best option seems to be to combine the information obtained from different sources [1–3].

Induction motor fault detection (FD) methods, such as stray flux data analysis [4–8], have specific advantages that make them especially attractive for certain applications. Fault diagnosis and processing techniques based on stray flux signals are completely non invasive and their set up is relatively simple, although the application of this approach requires a specific sensor and a priori knowledge of the distribution of the magnetic field around the electrical machine, which depends, in general, on the manufacturing characteristics of the induction motor [1].

In reference [6], fault detection from the analysis of stray flux signals is based on the variation of the amplitude versus the load of a specific harmonic for two different positions of the flux sensor. The advantage of this method is that it does not require information about the machine behavior in a healthy state. In reference [4], the use of an analytical model that allows us to determine the magnetic flux approximation under conditions of healthy and faulty states for the case of a short circuit between the stator turns and the broken bars is explained. We also refer to [7] for another method for short circuitdetection using stray flux signals.

Fault diagnosis using stray flux signals is based on spectral analysis, through statistical methods, of the harmonics signals obtained from the flux sensor at different relative positions. Compared with classical methods based on analysis of currents such as MCSA (Monte Carlo Statistical Analysis), a disadvantage is that the results may depend on the position of the sensor, and it is not possible to theoretically establish a general rule to obtain the optimum position in the measurement. Moreover, there are no defined thresholds to determine the severity of the fault based on the analysis of these quantities.

In spite of the drawbacks of stray flux data analysis, the progressive cost decrement of necessary flux sensors together with the aforementioned advantages of this technique have led to a renewed dynamism in the research devoted to the study of this technique. Recent works have even extrapolated its application to transient analysis, showing especial advantages in comparison with other methods [9]. Stray flux analysis is adequate to avoid occasional false indications appearing when other techniques are applied to rotor fault detection [10]. Moreover, the suitability of stray flux analysis for

non-adjacent bar breakage detection has been explored in [11,12]. Regarding statistical analysis using stray flux signals, an algorithm has been proposed in [13] that relies on the use of the mean value and the standard deviation of the spectral components. Its performance has been tested with three levels of faults, see also [14,15].

In the present work, an algorithm to determine the rotor condition of induction motors from the analysis of stray flux signals is proposed. The detection of the healthy and faulty state conditions is based on a time-frequency analysis of the bispectrum and of the autocovariance function. The results are satisfactory and show the potential of this approach, which provides valuable information to detect the state of the rotor or, at least, to supplement the information provided by other quantities, improving the performance of classical techniques.

2. Materials and Methods

2.1. Data Acquisition

The experimental test bench was based on a 1.1 kW induction motor that was driving a direct current generator. Stray flux measurements were obtained by registering the electromotive force waveforms induced in an external coil sensor that was attached tovarious positions of the motor frame. The flux sensor was a coil with 1000 turns with an external diameter of 80 mm and an internal diameter of 39 mm.

Different operating conditions of the motor were considered. To differentiate the results by working regimes, our samples were taken during the motor startup (the motor was fed at 60% of the rated voltage) and at steady state (in this case the motor was fed 100% of the nominal voltage). We have obtained eight samples of flux signals of a healthy motor and sixteen samples of flux signals of a motor with damaged rotor (one broken bar). All the measurements in the experiments were taken under similar characteristics in both cases, in order to facilitate subsequent comparisons. In both experiments, the sampling frequency was 5 kHz.

We show in Tables 1 and 2 the different conditions of the experiments for capturing The flux signals of the healthy and faulty motors during start-up (60% of the supply voltage), as well as the corresponding sensor positions (see Figure 1).

Table 1. Characteristics of the experiment for the healthy motor during start-up

Sample	Position	Load	Speed (r/min)	Torque (Nm)	Supply Voltage(%)	Time(s)
0	DMA	NL	988	0.49	60	1
2	DM	NL	988	0.49	60	1
4	E	NL	987	0.51	60	1
6	L	NL	986	0.54	60	1

Table 2. Characteristics of the experiment for the damaged motor with a broken bar during start-up

Sample	Position	Load	Speed(r/min)	Torque (Nm)	Supply Voltage (%)	Time(s)
0	DMA	NL	985	0.49	60	1
2	DM	NL	988	0.49	60	1
4	E	NL	987	0.49	60	1
6	L	NL	985	0.49	60	1
8	DMA	FL	755	5.1	60	1
10	DM	FL	750	5	60	1
12	E	FL	760	5	60	1
14	L	FL	765	5	60	1

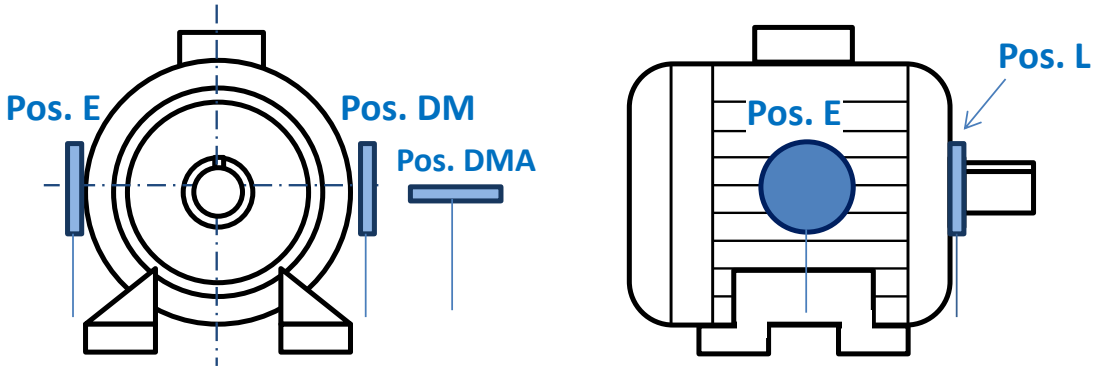

Figure 1. Different positions considered of the flux sensor

Similar experiments were carried out with the motor under permanent regime (100% of the supply voltage). We summarize in Tables 3 and 4 the experimental conditions of the motor operation at steady state.

Table 3. Characteristics of the experiments for the healthy motor at steady-state

Sample	Position	Load	Speed (r/min)	Torque (Nm)	Supply Voltage (%)	Time(s)
1	DMA	NL	994	0.49	100	8
3	DM	NL	994	0.48	100	8
5	E	NL	995	0.51	100	8
7	L	NL	995	0.5	100	8

Table4. Characteristics of the experiment for the damage motor with a broken bar at steady-state

Sample	Position	Load	Speed (r/min)	Torque (Nm)	Supply Voltage (%)	Time(s)
1	DMA	NL	994	0.52	100	8
3	DM	NL	994	0.53	100	8
5	E	NL	994	0.55	100	8
7	L	NL	997	0.58	100	8
9	DMA	FL	940	6.2	100	8
11	DM	FL	940	6.13	100	8
13	E	FL	940	6.1	100	8
15	L	FL	940	6.09	100	8

2.2 Analysis in the Frequency Domain: Theoretical Foundation

Let be $\{x(n)\}, n = 0,\pm1,\pm2,\pm3...$ a stationary random vector and its high-order moments exist, then[13-14]:

$$m_k^x(\tau_1,\tau_2,...,\tau_{k-1}) = E\{x(n)x(n+\tau_1)..x(n+\tau_{k-1})\} \quad (1)$$

represents, the moment of order k for that vector, which depends only on the different time intervals $\tau_{1,}\tau_2,...\tau_{k-1},\tau_i = 0,\pm1,...$for all i. Since, in practice cumulants are functions dependent on the expected value, they must be estimated, since we have a finite amount of data to process $\{x(n)\}_{n=0}^{N-1}$.
These estimators are of a stationary nature and are characterized by first and second order statistical functions such as mean value and variance.Then, be $x(n)$a stationary process of zero mean value. The third ordercumulant is given by [15]:

$$C_{3x}(\tau_1,\tau_2) = \frac{1}{N}\sum_{n=N1}^{N2} x(n)\cdot x(n+\tau_1)\cdot x(n+\tau_2) \quad (2)$$

whereN_1 y $N_2$are chosen in such a way that the summation involves onlyx(n) with$n \in [0, N-1]$, $N$is the number of samples in the cumulant region to be evaluated. Likewise, the bispectrum is defined by the Fourier Transform of the third order cumulant, which is given by [15]:

$$B_x^N(f_1,f_2) = \sum_{\tau_1=-N-1}^{N-1}\sum_{\tau_2=-N-1}^{N-1} C_{3x}(\tau_1,\tau_2)\cdot e^{-2\pi f_1\tau_1}\cdot e^{-2\pi f_2\tau_2} = \frac{1}{N^2}X(f_1,f_2)\cdot X(f_1)\cdot X(f_2) \quad (3)$$

where $X(f)$ is the Fourier Transform of the sequence $\{x(n)\}_{n=0}^{N-1}$.

For the detection of the healthy and damaged state condition of the induction motor, an algorithm based on the summation of the mean value of the bispectrum absolute vale of the flux

signal is proposed. The theoretical description is shown as follows from the obtained result of equation (3):

$$(B^N_{x-mean}(f)) = \frac{1}{N}\sum_{i=1}^{N}|B^N_x(f_1,f_2)|_i \ ,\nabla i = 1,\dots,N \quad (4)$$

where N is the number of rows of the square matrix (NxN) obtained from the bispectrum. The obtained result in (4) is a $1xN$ vector that contains the average frequency values of the amplitude bispectrum matrix of the flux signal. From the obtained result in (4), we define an indicator variable in the frequency domain by the following expression, as the summation of every average frequency values of the amplitude bispectrum:

$$Ind_f = \sum_{i=1}^{N} B^N_{x-mean}(f)_{(i)} \quad (5)$$

that will be used for the detection of the healthy and faulty condition of the induction motor.

2.3 Temporal Domain Analysis

First, we process the flux signals in the time domain, using the initial data of the experiment, see Tables 1-4. During the start-up, it is shown that the indicator variable in the frequency domain leads to good results and a palpable difference is observed, which enables us to discriminate between healthy and damaged state conditions of arotor. However, when the motor works at steady state, at 100% of the rated voltage, the method based on the analysis in the frequency domain is not completely effective.

Therefore, to solve the aforementioned issues and to obtain a reliable indicator to be applied in both situations, enabling the discrimination between healthy and damaged rotors, an algorithm based on the autocovariance function of the stray flux signals is proposed. This algorithm is based on the square value of the median of the autocovariance matrix of the flux signal. The theoretical foundations of the proposed are described below:

The autocovariance function of a random, stationary process $\{x(n)\}_{n=0}^{N-1}$ is a measure of the dispersion of the process around its mean value and is defined as a function dependent on the first and second order moments as follows [16]:

$$c_2^x(\tau) = m_2^x(\tau) - (m_1^x)^2 \quad (6)$$

where $m_2^x(\tau_1)$ is the autocorrelation function and (m_1^x) is the first order moment. From (6) it can be noted that if the process is of zero mean value, the autocovariance coincides with the autocorrelation function. Then replacing in (6) $m_2^x(\tau_1)$ and applying second order statistics we have:

$$c_2^x(\tau) = \frac{1}{N}\sum_{t=0}^{N-1-\tau} x(t) \cdot x(t+\tau) \quad (7)$$

Then, after obtaining the autocovariance function, we proceed to calculate the square value of the median, for each sample used in the experiment, which is as follows [16]:

Let be $x_1, x_2, x_3, \ldots, x_n$the data of a ordered sample in increasing order and designating the median as M_e, ifnit is odd the median is the value that the position occupies : $M_{e(c_2^x)} = \frac{c_2^x(\tau)_{(n+1)}}{2}$, then if nit is pair the median is the arithmetic mean of the two central values. Then, it would be like:

$$M_{e(c_2^x)} = \frac{c_2^x(\tau)_{\left(\frac{n}{2}\right)} + c_2^x(\tau)_{\left(\frac{n}{2}+1\right)}}{2} \quad (8)$$

substituting to find out the temporary indicator:

$$Ind_t = (M_{e(c_2^x)})^2 \quad (9)$$

The obtained result in (9) will be taken as the variable of indication in the time domain for the detection of the healthy and faulty conditions in the induction motor.

3. Results

3.1 Results in the frequency domain

Using the data obtained in the experiments, we have applied the algorithm described in the Section 2.2 in order to obtain the indication variable in the frequency domain, based on the bispectrum of the flux signal. This enabled us to discriminate between the healthy and faulty conditions of an induction motor. The bispectrum has been calculated in a window of 1024 samples, which results in a square matrix, where the number of rows and columns coincides with the data window to be processed, i.e.,$1024x1024$.

We have used the algorithm based on the bispectruminstead of the analysis based on the one-dimensional Fourier transform. The reason is the following: when applying the proposed method using the sum of the mean of the frequency spectrum absolute value, no relative differences were observed between the healthy and the damagedstates if the one-dimensional Fourier transform is used, as mentioned above.

This statement has been checked using sample 0 (position DMA of Table 1) corresponding to the samples of flux signals of the healthy motor and comparing the results with sample 0 (position DMA of Table 2) corresponding to the samples of flux signals of the motor with one broken rotor bar. The obtained results are shown in Figure 2 and Table 5, respectively.

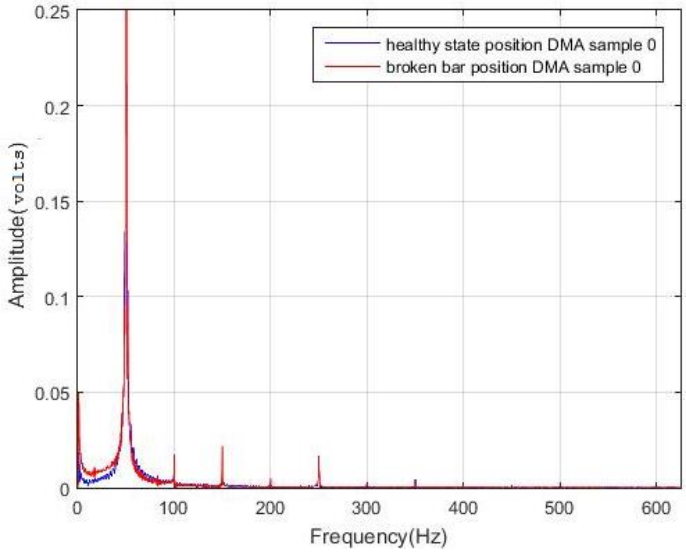

Figure 2. Comparison of the frequency spectra of the flux signals for the healthy state (Blue) and for the faulty state with one broken bar (red). Sample 0, DMA position.

Table5. Obtained results by applying the one-dimensional Fourier Transform and calculating the indicator (equation (4) and (5)).

Sample	Obtained Indicator in Frequency Domain
0, DMA position, healthy state	9.1160e-04
0, DMA position, damage state (one broken bar)	8.8375e-04

In Table 5, the difference that exists between both values of the indicator is 2.7857e-05, which is not significant to reliably discriminate between healthy and faulty conditions. Likewise, in figure 2, no relevant differences are observed at first sight in the spectra of both samples for the same position (DMA).

Taking into consideration the previous results, we decided to use the bispectrum of the flux signals.The algorithm of equations (4) and (5) was applied to obtain an indication variable that was able to detect differences between the healthy and damaged conditions. Figure 3 shows the bispectrum of the flux signal in the healthy state (sample 0, position DMA) and faulty state (sample 0, position DMA).

As can be seen in Figure 3, the bispectrum has two circles corresponding to fundamental frequency values of the form (f1, f2) in this case (0.01.0.01), which corresponds to the frequency of 50 Hz (normalized to 1), depicted in Figure 2, corresponding to the frequency spectrum using the one-dimensional Fourier transform.

Similarly, around these two points there are other four circles which correspond to the frequency values, multiples of the fundamental frequency of 50 Hz. As shown in Figure 3, there are differences between the bispectrum of the flux signal of the healthy motor and of the damaged motor. These six circles visualized in the contour of the bispectrum appear in all the analyzed samples, both in the healthy and in the faulty state conditions. This can be observed in Figures 4-9.

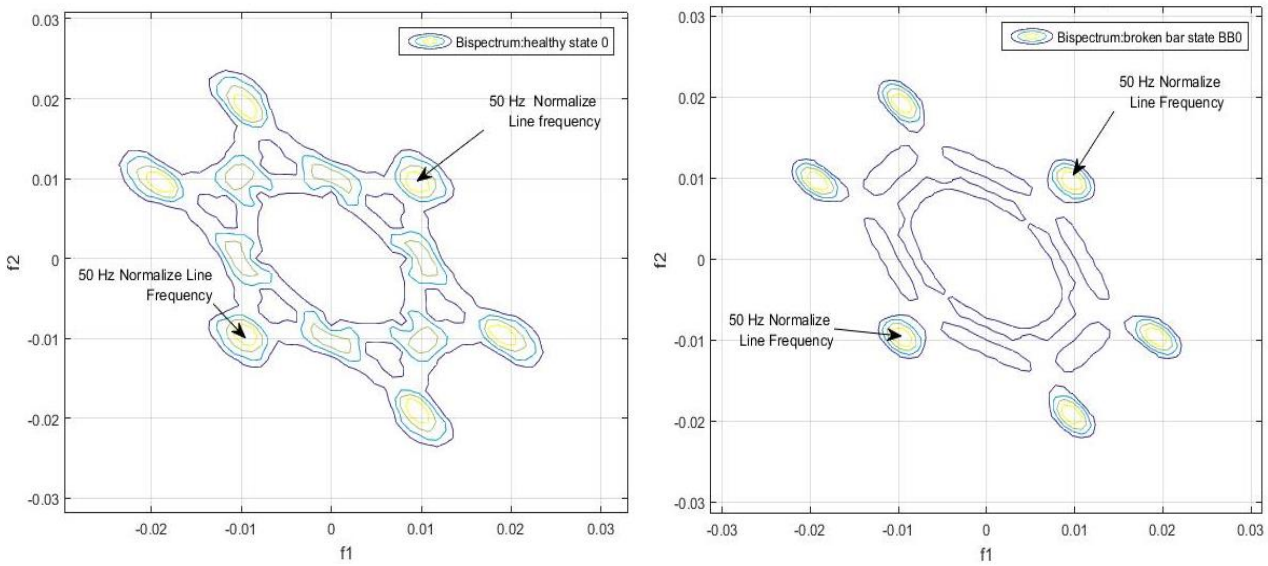

(**a**) (**b**)

Figure 3. (a) Contour of Bispectrum of the motor flux signal in healthy condition (sample 0, DMA position) (b) Contour of Bispectrum of the motor flux signal in faulty condition (sample 0, DMA position).

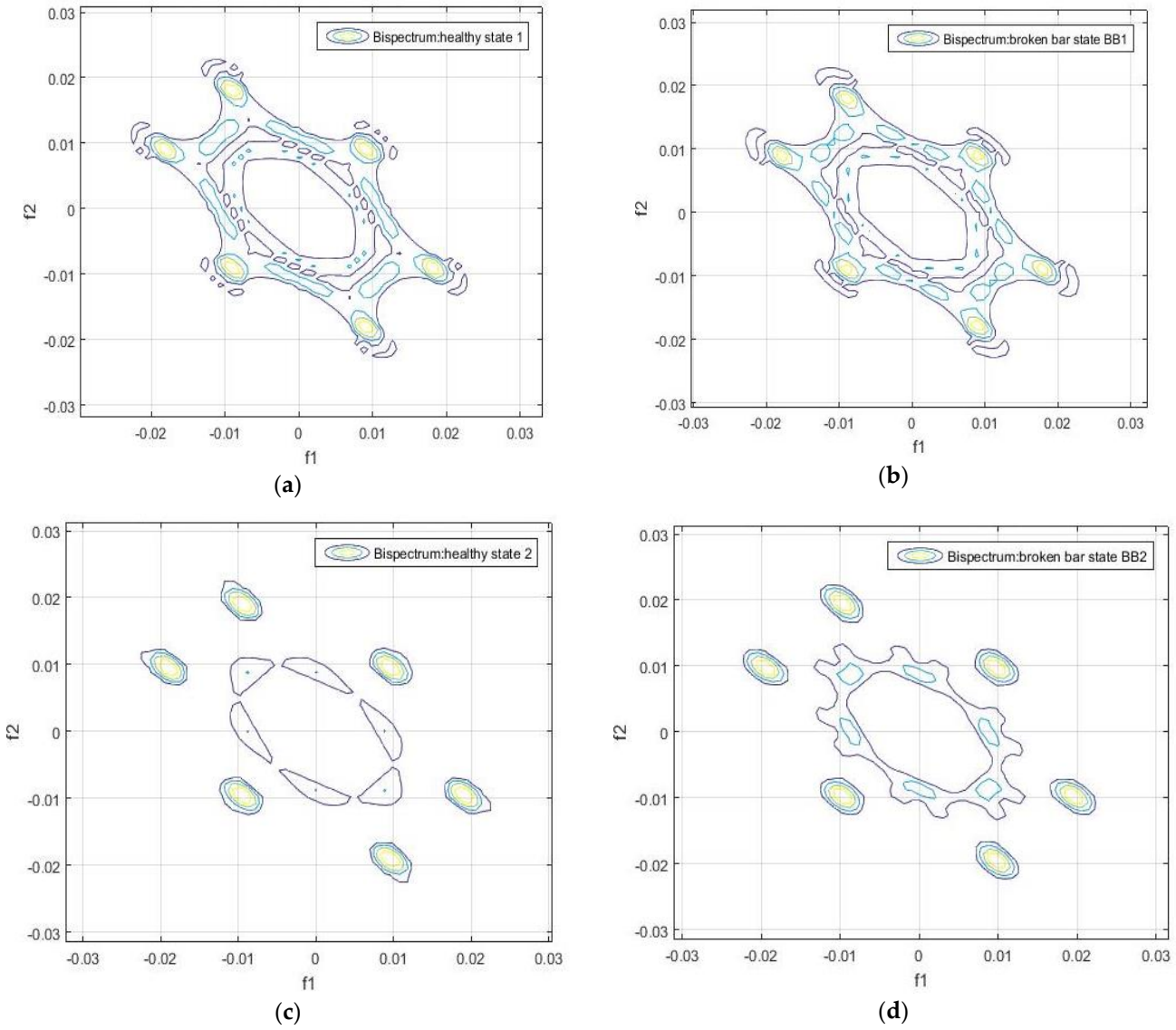

Figure 4. Contour of the bispectrum of the motor flux signal: (**a**) Sample 1 of the healthy motor, (**b**) Sample 1 of the damaged motor, (**c**) Sample 2 of the healthy motor, (**d**) Sample 2 of the damaged motor.

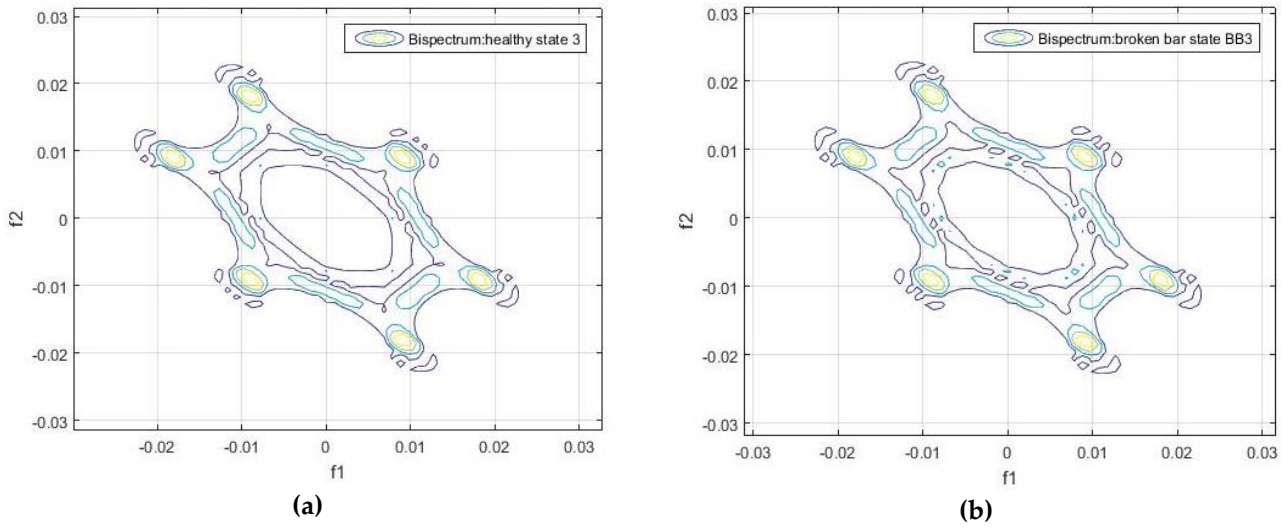

Figure 5. Contour of the bispectrum of the motor flux signal: a) Sample 3 of the healthy motor and b) Sample 3 of the damaged motor

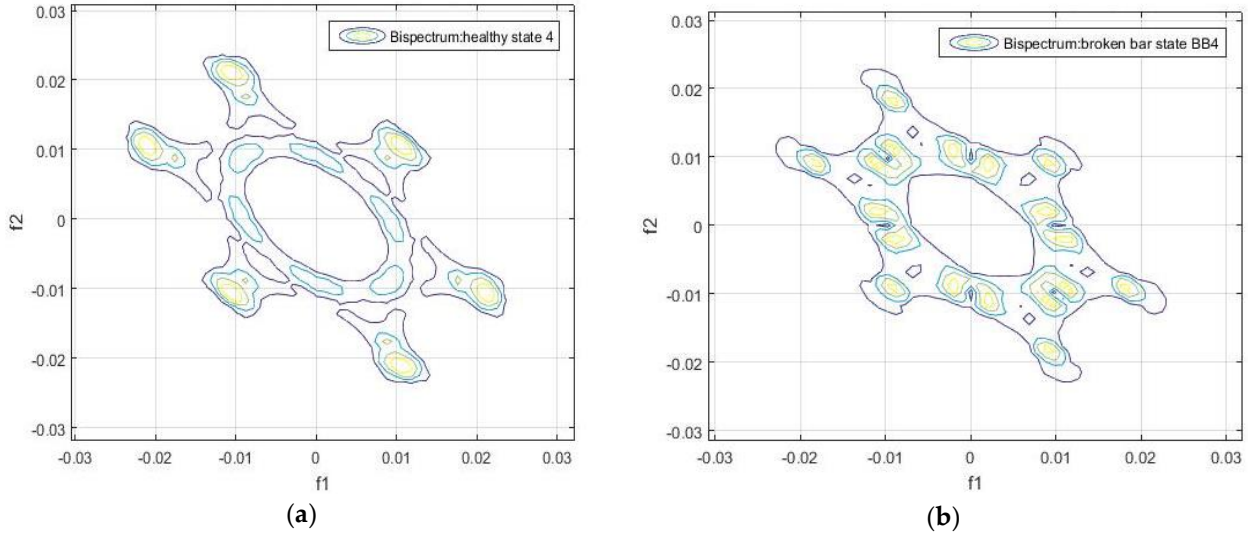

Figure 6. Contour of the bispectrum of the motor flux signal: a) Sample 4 of the healthy motor, b) Sample 4 of the damaged motor

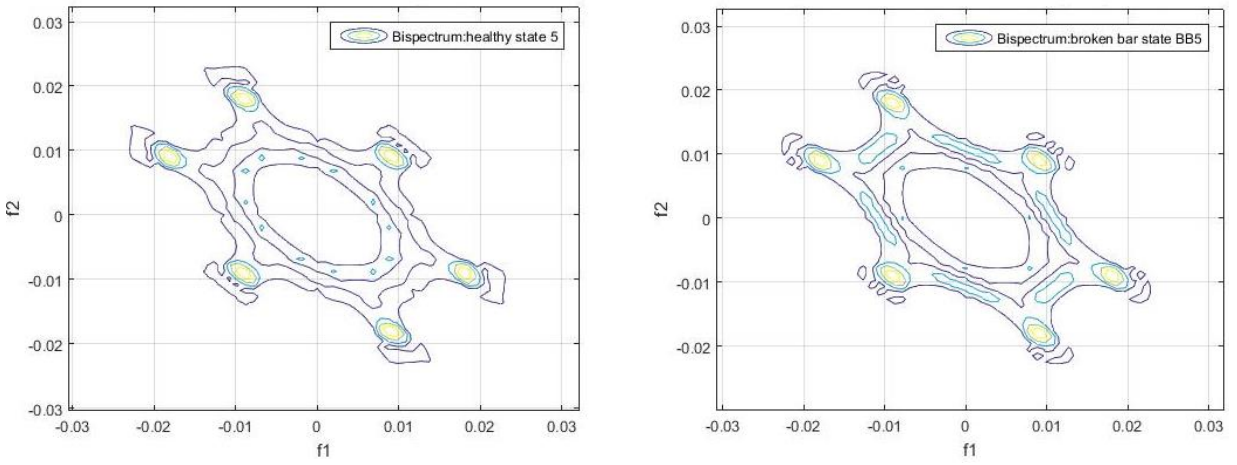

(**a**) (**b**)

Figure 7. Contour of the bispectrum of the motor flux signal: (**a**) Sample 5 of the healthy motor and (**b**) Sample 5 of the damaged motor.

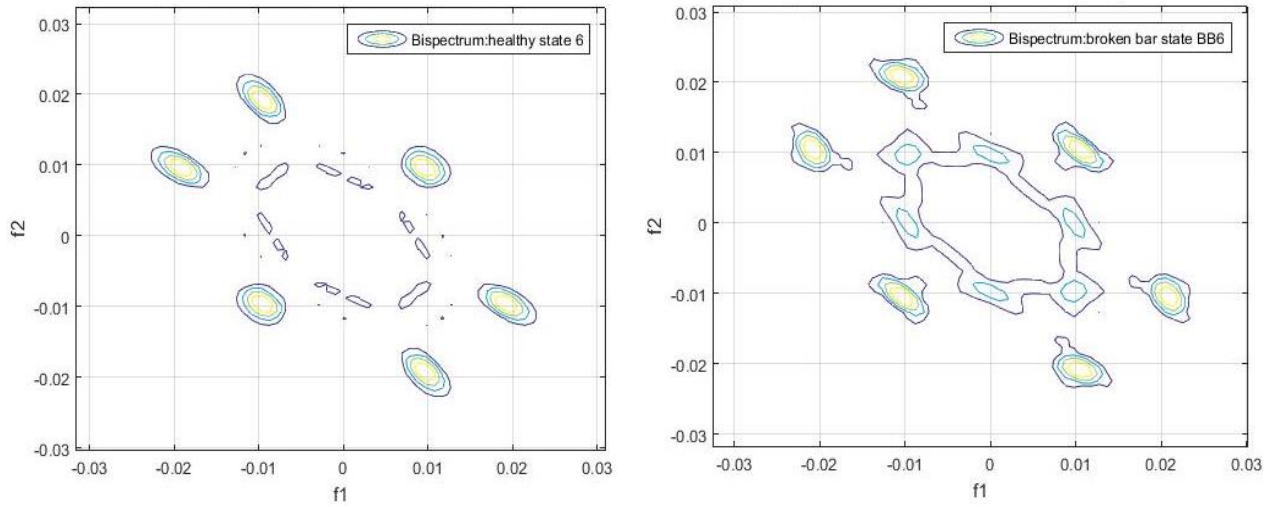

(**a**) (**b**)

Figure 8. Contour of the bispectrum of the motor flux signal: (a) Sample 6 of healthy the motor, (b) Sample 6 of the damaged motor.

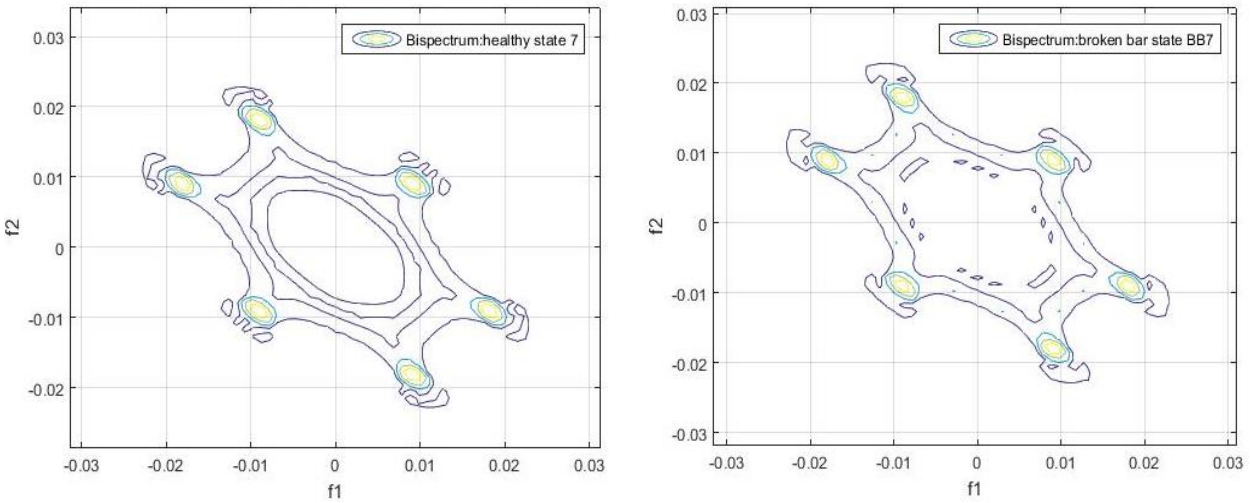

(**a**) (**b**)

Figure 9. Contour of the bispectrum of the motor flux signal: a) Sample 7 of healthy motor and b) Sample 7 of damaged motor

In Figures 3-6 we show the differences in the bispectrum between the healthy and the damaged motors, for the different positions at which the measurements of the flux signals were taken. Note that in some graphs there are more substantial differences, such as in Figure 3 as well as in Figure 4c,d. The differences depend on the position in which the measurement was taken, as well as on the load, and on the supply, and will also depend on obtaining a more or less significant difference in relation to the value of the indicator in the frequency domain (Equation (5)).

The calculation of the indicator in the frequency domain based on Equations (4) and (5) was performed for the data in Tables 1-4 which correspond to the motor under healthy and faulty conditions. The obtained results are shown in Tables 5 and 6.

Table 6. Results of the indicator in the frequency domain based on equations (4) and (5) for the data of the experiment with the healthy motor during start-up.

Sample	Position	Load	Speed(r/min)	Torque (Nm)	Supply Voltage (%)	Time(s)	Indicator
0	DMA	NL	988	0.49	60	1	30.38804
2	DM	NL	988	0.49	60	1	27.28881
4	E	NL	987	0.51	60	1	28.56996
6	L	NL	986	0.54	60	1	26.75429

From the results shown in Tables 6 and 7 it can be seen that for similar operating conditions, the indicator in the frequency domain depends on the position of the sensor, as can be seen for samples 0, 4, 8 and 14. In these cases, the relative differencesare appreciable and it is possible to discern between one state and the other.

On the other hand, the difference in the values of the indicator for the other positions, such as with samples 2 and 6, is not significant. In any case, the values of the indicator for the faulty condition are always greater than those of the equivalent healthy one.

Table 7. Results of the indicatorin the frequency domain based on equations (4) and (5) for the data of the experiment with the faulty motor with a broken bar, during start-up.

Sample	Position	Load	Speed(r/min)	Torque (Nm)	Supply Voltage (%)	Time(s)	Indicator
0	DMA	NL	985	0.49	60	1	38.15795
2	DM	NL	988	0.49	60	1	28.76003
4	E	NL	987	0.49	60	1	38.77947
6	L	NL	985	0.49	60	1	28.88013
8	DMA	FL	755	5.1	60	1	32.06025
10	DM	FL	750	5	60	1	25.04451
12	E	FL	760	5	60	1	23.42840
14	L	FL	765	5	60	1	41.01978

On the other hand, we show in Tables 8 and 9 show the values of the indicator when the motor works at steady-state (100% of the nominal voltage).

Table 8. Results of the indicatorin the frequency domain based on equations (4) and (5) for the data of the experiments with the healthy motor at steady state.

Sample	Position	Load	Speed(r/min)	Torque (Nm)	Supply Voltage (%)	Time(s)	Indicator
1	DMA	NL	994	0.49	100	8	1.152108
3	DM	NL	994	0.48	100	8	1.192266
5	E	NL	995	0.51	100	8	0.597756
7	L	NL	995	0.5	100	8	0.726403

Table 9. Results of the indicator in the frequency domain based on equations (4) and (5) for the data of the experimentswith the faulty motor with a broken bar at steady state.

Sample	Position	Load	Speed(r/min)	Torque (Nm)	Supply Voltage (%)	Time(s)	Indicator
1	DMA	NL	994	0.52	100	8	0.842987
3	DM	NL	994	0.53	100	8	0.854711
5	E	NL	994	0.55	100	8	0.975386
7	L	NL	997	0.58	100	8	0.709328
9	DMA	FL	940	6.2	100	8	3.707399
11	DM	FL	940	6.13	100	8	3.254082
13	E	FL	940	6.1	100	8	3.979508
15	L	FL	940	6.09	100	8	2.998851

From the results shown in Tables 8 and 9 it is noted that the differences between the values of the indicator in the frequency domain for healthy and faulty conditionsare not significant when the motor works at steady state. This may be due to the fact that, during startup, certain harmonics vary in frequency and amplitude [9]. This does not happen under the steady state regime, during which the harmonics maintain well-defined frequencies and amplitudes, as long as the load level does not change.

From the results shown in the above tables, it can be deduced that, under the healthy condition, the indicator in the frequency domainreachesa maximum value of 30.38804, and the minimum value is 0.597756. On the other hand, the indicator for the faulty condition (motor with a broken bar) ranges between 0.709328 and 41.0198. The value of the indicator for the healthy condition never exceeds the value of 31 for all measurements.

All the comparisons related to the values of the indicator have been carried out between measurements that were obtained under similar operating conditions. This leads to the conclusion that the position of the sensor plays a crucial role and that significant differences are not obtained in every position.

All the comparisons related to the values of the indicator have been carried out between measurements that were obtained under similar operating conditions. This leads to the conclusion that the position of the sensor plays a crucial role and that significant differences are not obtained in every position.

3.2 Results in the time domain

Taking into consideration the previous results obtained in the frequency domain, a new algorithm algorithm based on the square value of the median of the autocovariance matrix of the flux signal was proposed, as described in Equation (8). This gives a fault detection indicator in the time domain.

The results obtained after applying this last algorithmare shown in Figure 10, and they are summarized in Tables 10–13 based on the square value of the median of the autocovariance matrix of the flux signal was proposed.

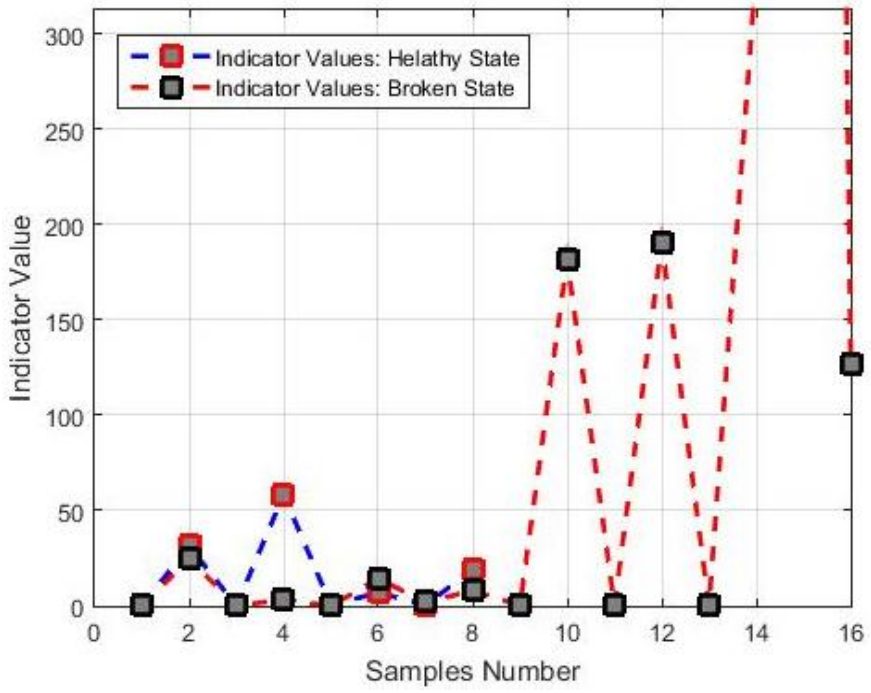

Figure 10 . Values of the indicator in the time domain for all the samples used in the experiments.

Table 10. Results of the indicatorin the time domain, based on equations (6), (7) and (8), for the data of the experiments with the healthy motor during startup.

Sample	Position	Load	Speed(r/min)	Torque (Nm)	Supply Voltage (%)	Time(s)	Indicator
0	DMA	NL	988	0.49	60	1	0.071959
2	DM	NL	988	0.49	60	1	0.027691
4	E	NL	987	0.51	60	1	0.435514
6	L	NL	986	0.54	60	1	0.537173

The previous results show that there is a notable difference between the values of the indicator when the motor works at steady-state (100% of the rated supply), but not during the start-up, when it works at 60% of the rated supply.

Table 11. Results of the indicatorin the time domain, based on equations (6)-(8), for the data of the experiments with the motorwith one broken bar during startup.

Sample	Position	Load	Speed(r/min)	Torque (Nm)	Supply Voltage(%)	Time(s)	Indicator
0	DMA	NL	985	0.49	60	1	0.003537
2	DM	NL	988	0.49	60	1	0.009451
4	E	NL	987	0.49	60	1	0.009606
6	L	NL	985	0.49	60	1	2.046191
8	DMA	FL	755	5.1	60	1	0.370122
10	DM	FL	750	5	60	1	0.033363
12	E	FL	760	5	60	1	0.005345
14	L	FL	765	5	60	1	2227.965

Table 12. Results of the indicator, based on equations (6)-(8), for the data of the healthy motor experimentsat steady state regime.

Sample	Position	Load	Speed(r/min)	Torque (Nm)	Supply Voltage (%)	Time(s)	Indicator
1	DMA	NL	994	0.49	100	8	31.38462
3	DM	NL	994	0.48	100	8	58.30218
5	E	NL	995	0.51	100	8	6.948441
7	L	NL	995	0.5	100	8	19.03505

Table 13. Results of the indicator, based on equations (6)-(8), for the data of the faulty motor experimentsat steady state regime.

Sample	Position	Load	Speed(r/min)	Torque (Nm)	Supply Voltage (%)	Time(s)	Indicator
1	DMA	NL	994	0.52	100	8	24.67371
3	DM	NL	994	0.53	100	8	3.342042
5	E	NL	994	0.55	100	8	14.26557
7	L	NL	997	0.58	100	8	7.897072
9	DMA	FL	940	6.2	100	8	181.7043
11	DM	FL	940	6.13	100	8	190.5501
13	E	FL	940	6.1	100	8	334.8858
15	L	FL	940	6.09	100	8	126.3791

4. Discussion

We group the previous results with respect to the flux sensor location in order to compare the indicator values obtained in the frequency and time domains, for different fault conditions and operating regimes, see Tables 14 and 15.

Table 14. Results of the time and frequency indicators for the DMA position

Sample	Position	Load	Speed (r/min)	Torque (Nm)	Supply Voltage. (%)	Time(s)	Frequency Indicator	Time Indicator	State
0	DMA	NL	988	0.49	60	1	30.38804	0.071959	Healthy
	DMA	NL	994	0.49			38.15795	0.003537	Faulty
1	DMA	NL	994	0.49	100	8	1.152108	31.38462	Healthy
	DMA	NL	994	0.52			0.842987	24.67371	Faulty

For the sample corresponding to the DMA position, the difference of the indicators values is noticeable at the startup, when working in the frequency domain. The difference in the temporal indicator between the healthy and faulty condition is preceded by a multiplication factor of 20. When the motor works at steady-state (with 100% of the rated supply), the difference in the values of the time indicator is appreciable. At startup, the indicator in the frequency domain is always greater for the faulty state; the opposite occurs with the temporary indicator at steady-state.

Table 15. Results of the time and frequency indicators for the DM position

Sample	Position	Load	Speed (r/min)	Torque (Nm)	Supply Voltge. (%)	Time(s)	Frequency Indicator	Time Indicator	State
2	DM	NL	988	0.49	60	1	27.28881	0.027691	Healthy
	DM	NL	988	0.49			28.76003	0.009451	Faulty
3	DM	NL	994	0.48	100	8	1.192266	58.30218	Healthy
	DM	NL	994	0.53			0.854711	3.342042	Faulty

For the sample corresponding to the DM position, the difference of the indicators values at startup is not as noticeable compared to the values obtained at the DMA position, when working in the frequency domain. The difference in the time indicator between the healthy and damaged state is preceded by a multiplication factor of 3. When the motor works at steady-state, the difference of the time indicator is as significant as for the DMA position. At startup, the indicator in the frequency domain is always greater for the faulty condition; the opposite occurs with the temporal indicator at steady-state.

For the sample corresponding to the E position, there is a significant difference between the values of the indicator in the frequency domain at the startup, as with the DMA position. The difference in the temporal indicator between the healthy and the faulty condition is preceded by a multiplication factor of 45. At steady-state, with 100% of the rated voltage, the differences of the temporal indicators are significant. At startup, the indicator in the frequency domain is always greater for the faulty state; the same occurs in this case for the time indicator at steady-state, contrary to what happens in positions DM and DMA.

For the sample corresponding to the L position, the difference of the indicator at start-up is not clearly noticeable when working in the frequency domain as with the DMA and E sensor positions. The difference in the temporal indicator between the healthy and the faulty conditions is preceded by a multiplication factor of 4. When working at steady-state, the difference of the temporal indicator is significant. The indicator in the frequency domain is higher for the faulty state during start-up; the opposite occurs with the temporal indicator at steady-state.

From the results obtained in Tables 14-17 for the four sensor positions analyzed (DMA, DM, E,L) the following can be concluded:

- The indicator in the frequency domain for the healthy condition varies in a range of $26 \leq Ind_f \leq 30$and for the faulty condition it varies from$28 \leq Ind_f \leq 38$ during start-up; in this regime, the values of the indicator in the frequency domain for the healthy state are always lower than its values for the faulty state.
- The indicator in the time domain for the healthy state varies by a factor of $6 \leq Ind_t \leq 58$ and for the faulty state $3 \leq Ind_t \leq 24$when the motor operates at steady state.
- The best results are obtained when the measurement is carried out in the DMA position, since the values of both indicators are within the limits of obtained values.
- In order to discern between the healthy and faulty conditions, the signal obtained from the flux sensor must first be evaluated during the start-up, for which the indicator is calculated based on the analysis in the frequency domain. At steady-state, the signal should be better evaluated using the time indicator.
- A diagnostic decision based on the limit valuesfor both indicators should be finally adopted. In order to obtain a more reliable conclusion of the rotor condition, the two indicators must be evaluated.

Table 16. Results of the time and frequency indicators for the E position.

Sample	Position	Load	Speed (r/min)	Torque (Nm)	Supply Voltage. (%)	Time(s)	Frequency Indicator	Time Indicator	State
4	E	NL	987	0.51	60	1	28.56996	0.435514	Healthy
	E	NL	987	0.49			38.77947	0.009606	Faulty
5	E	NL	995	0.51	100	8	0.597756	6.948441	Healthy
	E	NL	994	0.55			0.975386	14.26557	Faulty

Table 17. Results of the time and frequency indicators for the L position.

Sample	Position	Load	Speed (r/min)	Torque (Nm)	Supply Voltage (%)	Time(s)	Frequency Indicator	Time Indicator	State
6	L	NL	986	0.54	60	1	26.75429	0.537173	Healthy
	L	NL	985	0.49			28.88013	2.046191	Faulty
7	L	NL	995	0.5	100	8	0.726403	19.03505	Healthy
	L	NL	997	0.58			0.709328	7.897072	Faulty

The accuracy of the proposed method as a classification of the condition of the damaged-healthy state of the induction motor depends, to a large extent, on the relative position where the measurement is made. Although regardless of the obtained results and the relative positions of each measurement, it can be noted that the average of the indication values obtained for the indicator in the frequency domain never exceeds the value of 28.250275 for the healthy state and 33.644395 for the damaged case. Similarly, if the analysis is performed for the indicator in the time domain, we have an average value of 28.91757275 for the healthy state, and of 12.5445985 for the faulty one. That is, in an a priori analysis, a result of the indication variable greater than these values, both for the frequency and time domains, can be concluded as an affirmative diagnosis of failure, as shown for the cases of the DMA and E positions.

5. Conclusions

The spectral analysis based on the bispectrum of the flux signals captured at external positions of an induction motor was proposed in order to provide a criterion to discriminate between healthy and faulty rotor conditions in induction motors. To this end, an algorithm based on the sum of the mean value of the bispectrum module of the induction motor flux signal was theoretically described and implemented.

To demonstrate the results experimentally, several real samples of flux signals were registered, both for healthy and faulty conditions of the rotor cage, and for different operating conditions. The proposed algorithms are based on the sum of the mean value of the bispectrum module of the flux signal and on the square value of the median of the autocovariance function. The results have shown they can be considered as indicators that enable us to provide a criterion for the discrimination between healthy and faulty conditions of the motor. We can also conclude that the position where the measurement of the flux signal is carried out is an important factor, as well as the operating regime of the motor.
In conclusion, the study carried out in this paper implies that, with the analysis of stray flux signals, it is possible to obtain indicator variables that discriminate between faulty and healthy motors, which is an improvement and a complementtoexisting results obtained by using classical techniques for the diagnosis of failures in electrical machines and, in the future, may be a contribution to the development of portable industrial diagnostic devices.

As future work, it is proposed to carry out an estimation analysis of the accuracy of the proposed method and to obtain an algorithm for the optimization of the relative position of the flux sensor at the time of the measurement.

Author Contributions: Conceptualization, M.E.I.M., J.A.A.D., P.F.d.C., and J.A.C.; Methodology, M.E.I.M.; Software, M.E.I.M.; Validation, M.E.I.M., J.A.A.D., P.F.d.C., and J.A.C.; Formal Analysis, M.E.I.M.; Investigation, M.E.I.M., J.A.A.D., P.F.d.C., and J.A.C.; Resources, M.E.I.M., J.A.A.D., P.F.d.C. and J.A.C.; Data Curation, M.E.I.M. and J.A.A.D.; Writing—Original Draft Preparation, M.E.I.M., J.A.A.D., P.F.d.C., and J.A.C.; Writing—Review & Editing, M.E.I.M., J.A.A.D.,P.F.d.C., and J.A.C.; Visualization, M.E.I.M.; Supervision, J.A.A.D., J.A.C.

Funding: This research was funded by MEC, grant number MTM 2016-7963-P.

Conflicts of Interest: The authors declare no conflict of interest.The funders had no role in the design of the study; in the collection, analyses, or interpretation of data; in the writing of the manuscript, or in the decision to publish the results.

6. References

1. S. Nandi, H. A. Toliyat, and Xi. Li,:" Condition Monitoring and Fault Diagnosis of Electrical Motors—A Review", IEEE Transactions on Energy Conversion, vol. 20, no. 4, pp:719-729, December 2005.
2. H. Henao, G.-A. Capolino, M. Fernández-Cabanas, F. Filippetti, C.Bruzzese, E. Strangas, R. Pusca, J. Estima, M. Riera-Guasp, and S.H.Kia, "Trends in Fault Diagnosis for Electrical Machines," IEEE Ind. Electron. Magazine, June 2014, pp. 31–42.
3. Riera-Guasp, M.; J. Antonino-Daviu; Capolino, G. (2015). Advances in Electrical Machine, Power Electronic, and Drive Condition Monitoring and Fault Detection: State of the Art. IEEE Transactions on Industrial Electronics. 62(3):1746-1759. doi:10.1109/TIE.2014.2375853
4. Chen Jiang ; Sufei Li ; Thomas G. Habetler," A review of condition monitoring of induction motors based on stray flux". in: 2017 IEEE Energy Conversion Congress and Exposition (ECCE), DOI: 10.1109/ECCE.2017.8096907 ,1-5 Oct. 2017
5. R. Romary, R. Pusca, J. P. Lecointe, and J. F. Brudny, "Electrical machines fault diagnosis by stray flux analysis," in Proc. IEEEWorkshop Electrical Machines Design, Control and Diagnosis (WEMDCD'2013), Paris, France, Mar. 11–12, 2013, pp. 245–254.
6. M.F. Cabanas, J.G. Norniella, M.G. Melero, C. H. Rojas, J.M. Cano, F.Pedrayes, G. A. Orcajo, " Detection of Stator Winding InsulationFailures: On–line and Off–line Tests", in Proc. IEEE Workshop Electrical Machines Design, Control and Diagnosis (WEMDCD'2013), Paris, France, March 11–12, 2013, pp. 208–217.
7. R. Pusca,C. Demian, D. Mercier, E. Lefevre, and R. Romary, "An improvement of a diagnosis procedure for AC machines using twoexternal flux sensors based on a fusion process with belief functions" in Proc. IEEE Annu.Conf. Ind. Electron. (IECON'2012), Montréal,Canada, Oct.25–28, 2012, pp.5096–5101.
8. L. Frosini, A. Borin, L. Girometta, G. Venchi, "A novel approach to detect short circuits in low voltage induction motor by stray fluxmeasurement", in Proc. Int. Conf. Electrical Machines (ICEM'2012), Marseille, France, Sept. 2–5, pp. 1536–1542.
9. J. A. Ramirez-Nunez et al., "Evaluation of the Detectability of Electromechanical Faults in Induction Motors Via Transient Analysis of the Stray Flux," in IEEE Transactions on Industry Applications, vol. 54, no. 5, pp. 4324-4332, Sept.-Oct. 2018.
10. Y. Park et al., "Stray Flux Monitoring for Reliable Detection of Rotor Faults under the Influence of Rotor Axial Air Ducts," in IEEE Transactions on Industrial Electronics. To be published in 2019.

11. Iglesias-Martínez, Miguel E., Fernández de Córdoba, Pedro; Antonino-Daviu, Jose A., Conejero, J. Alberto."Detection of Bar Breakages in Induction Motor via Spectral Subtraction of Stray Flux Signals", 2018 XIII IEEE International Conference on Electrical Machines (ICEM), 2018, pp.1796-1802.
12. P. A. Panagiotou, I. Arvanitakis, N. Lophitis, J. A. Antonino-Daviu and K. N. Gyftakis, "Analysis of Stray Flux Spectral Components in Induction Machines under Rotor Bar Breakages at Various Locations," *2018 XIII International Conference on Electrical Machines (ICEM)*, Alexandroupoli, 2018, pp. 2345-2351.
13. Mendel, J.M.Tutorial on higher- order statistics (spectra) in signal processing and system theory: Theoretical results and some applications. *IEEE Proc.* 1991, *79*, 278–305.
14. Nikia, C.L.; Mendel, J.M.Signal Processing with higher-order spectra.*IEEE Signal Process. Mag.* 1993, *10*, 10–37.
15. Swami,A.;Mendel,J.M.;Nikias,C.L.*Higher-Order Spectral Analysis Toolbox User's Guide, Version 2*;United Signals & Systems,Inc.: Ranco Palos Verde, CA, USA,2001.
16. Vaseghi, S.V. *Advanced Digital Signal Processing and Noise Reduction*,4thed.; JohnWiley&Sons: Hoboken, NJ, USA, 2008.

sensors

MDPI

Article

Feature Extraction and Similarity of Movement Detection during Sleep, Based on Higher Order Spectra and Entropy of the Actigraphy Signal: Results of the Hispanic Community Health Study/Study of Latinos

Miguel Enrique Iglesias Martínez [1], Juan M. García-Gomez [2,*], Carlos Sáez Silvestre [2], Pedro Fernández de Córdoba [3] and J. Alberto Conejero [3]

[1] Departamento de Telecomunicaciones, Universidad de Pinar del Río, Pinar del Río, Cuba, Martí #270, CP: 20100; Instituto Universitario de Matemática Pura y Aplicada, Universitat Politècnica de València (UPV), Camino de Vera s/n, 46022 Valencia, España; migueliglesias2010@gmail.com

[2] Biomedical Data Science Lab (BDSLab), Instituto Universitario de Tecnologías de la Información y Comunicaciones (ITACA), Universitat Politècnica de València (UPV), Camino de Vera s/n, 46022 Valencia, España; carsaesi@ibime.upv.es

[3] Instituto Universitario de Matemática Pura y Aplicada, Universitat Politècnica de València (UPV), Camino de Vera s/n, 46022 Valencia, España; pfernandez@mat.upv.es (P.F.d.C.); aconejero@upv.es (J.A.C.)

* Correspondence: juanmig@ibime.upv.es; Tel.: +34-963-877-000 (ext. 75278)

Received: 19 October 2018; Accepted: 30 November 2018; Published: 6 December 2018

Impact Factor: 3.031 (2018); 5-Year Impact Factor: 3.302 (2018)

Sensors **2018**, 18, 4310; doi:10.3390/s18124310 www.mdpi.com/journal/sensors

Abstract: The aim of this work was to develop a new unsupervised exploratory method of characterizing feature extraction and detecting similarity of movement during sleep through actigraphy signals. We here propose some algorithms, based on signal bispectrum and bispectral entropy, to determine the unique features of independent actigraphy signals. Experiments were carried out on 20 randomly chosen actigraphy samples of the Hispanic Community Health Study/Study of Latinos (HCHS/SOL) database, with no information other than their aperiodicity. The Pearson correlation coefficient matrix and the histogram correlation matrix were computed to study the similarity of movements during sleep. The results obtained allowed us to explore the connections between certain sleep actigraphy patterns and certain pathologies.

Keywords: actigraphy; bispectrum; entropy; feature extraction

1. Introduction

Actigraphy is now being increasingly used to explore sleep patterns in sleep laboratories. Its main advantages include its easy setup, its low cost, and the fact that prolonged records can be obtained over time, permitting patient activity in ambulatory conditions without interfering with their daily routines. It is considered to be a valuable tool for

controlling and monitoring circadian alterations and insomnia, as well as avoiding false positives in the assessment of daytime sleepiness tests, such as the multiple sleep latency test, and the wakefulness maintenance test [1–5].

Many recent studies have validated the practice of actigraphy, for example, in [6] several wrist-worn sleep assessments, actigraphy devices were compared. A relationship has been found between sleep disorders and their effects on certain conditions, such as hypertension and obesity [7], and it is now even possible to analyze sleep depth by actigraphy signals [8].

A review of the current state of higher-order statistics (HOS) and their use in biosignal analysis can be found in [9]. As most of the biomedical signals are non-linear, non-stationary, and non-Gaussian in nature, iHOS (Higher Order Statistics) analysis is preferable to second-order correlations and power spectra [9]. On this issue, several studies, such as [10] have been published on the screening of pediatric sleep apnea–hypopnea syndrome, and the automated classification of glaucoma stages in [11].

Concerning the detection of similarity of movements, in [12,13] although classification patterns were obtained from sleep/awake states according to the characteristics of the actigraphy signal, they were not based on higher order spectra. In fact, the common approach is to analyze individual actigraphy records over several days, so that the studies cited above were not focused on the analysis of the activity signal as a random process that is dependent on the movement of a certain part of the body.

The present work is based on the bispectral analysis of actigraphy signals and their relationship with bispectral entropy. The increase of movements as a form of feature extraction measurement, and the detection of similarities of movements during sleep are shown as features to be considered. The results obtained indicate the potential of this approach for the study of sleep disorders, and their connection with other conditions. The work is organized as follows: Materials and Methods are described in Section 2, the results are given in Section 3, the Discussion in Section 4, and the Conclusions and future work are outlined in Section 5.

2. Materials and Methods

2.1. Data Acquisition

The experiments were carried out on 20 samples of actigraphy signals obtained from the Hispanic Community Health Study/Study of Latinos (HCHS/SOL) Database [14–17] chosen at random, through the use of the "randi" Matlab function. The Sueño Ancillary Study recruited 2252 HCHS/SOL participants to wear wrist-worn actigraphy devices (Actiwatch Spectrum, Philips Respironics, Royal Philips, Netherlands,) between 2010 and 2013. The participants were instructed to wear the watch for a week. Records were scored by a trained technician of the Boston Sleep Reading Center [17].

2.2. Methods

Actigraphy signals have a random nature that can be visualized in terms of uniformity in the bispectrum. This uniformity depends on the non-impulsive

characteristics of the signal, which are reflected in the spectrum as frequency peaks. Since the bispectrum is a function that presents unique characteristics for each signal in terms of frequency and phase it can easily be seen in a graph. This led us to explore an entire methodology based on calculating the bispectrum and the bispectral entropy, which would be able to detect similar characteristics in movement patterns during sleep. Twenty cases of actigraphy signals were analyzed to extract their characteristics, which were then used to determine similarities and differences among the signals.

The activity signals were first normalized to 1, and then segmented to determine the subjects' daily activity record. The bispectrum of the total sample of the activity signal recorded was seven days. The experiments were conducted on two age groups between 18 and 44 years old, and 45 and 64 years old.

2.3. Theoretical Foundations: Bispectrum

Let $\{x(n)\}_n,\ n = 0, \pm1, \pm2, ...$ be a stationary random vector and let us also suppose that we can compute its *higher order moments* [19], where:

$$m_k^x(\tau_1, \tau_2, \dots, \tau_{k-1}) = E(x(n) \cdot x(n+\tau_1) \dots x(n+\tau_{k-1})) \quad (1)$$

represents the *moment of order* k of that vector. This moment only depends on the different time slots $\tau_1, \dots, \tau_{k-1}$ where $\tau_i = 0, \pm1, ...$ for all i. The *cumulants* are similar to the moments, but the difference is that the moments of a random process are derived from the characteristic function of the random variable, while the cumulants generating function is defined as the logarithm of the characteristic function of that random variable. The *k-th order cumulant* of a stationary random process $\{x(n)\}_n$ can be written as [20]:

$$(\tau_1, \tau_2, \dots, \tau_{k-1}) = m_k^x(\tau_1, \tau_2, \dots, \tau_{k-1}) - m_k^G(\tau_1, \tau_2, \dots, \tau_{k-1}), \quad (2)$$

where $m_k^G(\tau_1, \tau_2, \dots, \tau_{k-1})$ is the k-th order moment of a process with an equivalent Gaussian distribution that presents the same mean value and autocorrelation function as the vector $\{x(n)\}_n$.

It is evident from (2) that a process following a Gaussian distribution has null cumulants for orders greater than 2, since $m_k^x(\tau_1, \tau_2, \dots, \tau_{k-1}) = m_k^G(\tau_1, \tau_2, \dots, \tau_{k-1})$, and so that $c_k^x(\tau_1, \tau_2, \dots, \tau_{k-1}) = 0$ [20-21].

In practice, we estimate cumulants and polyspectra from a finite amount of data $\{x(n)\}_{n=0}^{N-1}$. These estimates are also random and are characterized by their *bias* and *variance* [22]. Let $\{x(n)\}_n$. denote a zero mean stationary process; we assume that all relevant statistics exist and have finite values. The third order cumulant sample estimates is given by [21]:

$$C_3(\tau_1, \tau_2) = \frac{1}{N} \sum_{n=N_1}^{N_2} x(n) \cdot x(n+\tau_1) \cdot x(n+\tau_2) \quad (3)$$

where N_1 y N_2 are chosen such that the sums only involve $x(n)$ for $n = 0, \dots, N-1$, being N the number of samples in the cumulant region. Likewise, the *bispectrum estimation* is defined as the Fourier Transform of the third-order cumulant sequence [22]:

$$B_x^N(f_1, f_2) = \sum_{\tau_1=-N-1}^{N-1} \sum_{\tau_2=-N-1}^{N-1} C_3(\tau_1, \tau_2) \cdot e^{-2\pi f_1 \tau_1} \cdot e^{-2\pi f_2 \tau_2} = \frac{1}{N^2} X^*(f_1 + f_2) \cdot X(f_1) \cdot X(f_2) \quad (4)$$

where f_1 y f_2 are the spectral frequencies vectors of the sequence $\{x(n)\}_{n=0}^{N-1}$, and $X(f_i)$, i=1,2, is its Fourier Transform.

2.3 Bispectral Entropy Analysis

Entropy provides a measure for quantifying the information content of a random variable in terms of the minimum number of bits per symbol required to encode the variable. It is an indicator of the amount of randomness or uncertainty of a discrete random process [23]. Consider a random variable Z with M states $z_1, z_2, \dots z_M$ and state probabilities $p_1, p_2, \dots p_M$, that is $P(Z = z_i) = p_i$, the *entropy of Z* is defined as:

$$H(Z) = -\sum_{i=1}^{M} p_i \log_2(p_i) \quad (5)$$

The entropy of a discrete-valued random variable attains a maximum value for a uniformly distributed variable. In order to extend this notion from the spatial to the frequency domain, we introduce bispectral entropy as a way to measure the uniformity of the spectrum [21]. The *bispectral entropy* is defined as:

$$E_{bx}^N(f_1, f_2) = -\sum_{\tau_1=-N-1}^{N-1} \sum_{\tau_2=-N-1}^{N-1} P_x^N(f_1, f_2) \cdot \log_2 P_x^N(f_1, f_2) \quad (6)$$

where the energy probability is computed in terms of the bispectrum estimation

$$P_x^N(f_1, f_2) = \frac{B_x^N(f_1, f_2)}{\sum_{\tau_1=-N-1}^{N-1} \sum_{\tau_2=-N-1}^{N-1} B_x^N(f_1, f_2)}. \quad (7)$$

3. Results

The actigraphy signals that measured the movements of individuals while sleeping were analyzed. These movements have an intrinsically random nature, since they can occur with non-specific probabilities and durations. This can be checked by analyzing the frequency spectrum of the activity signal and comparing it with a noise pattern. The probabilistic distribution function of the spectral pattern depends on the nature and uniformity of the movements, which may follow a normal distribution or another, such as a uniform distribution, depending on the random nature of the process.

3.1. Application of the Bispectrum to the Actigraphy Signal

A spectral analysis based on the one-dimensional Fourier transform is not recommended for the the detection of traits in a random signal, such as the actigraphy signal. For these, this analysis

only provides information relative to the magnitude-frequency or phase-frequency distribution. In other words, what is visualized in the spectrum is noise, which in our case, is in fact the useful information from which certain characteristics and features have to be extracted. The frequency spectrum of two actigraphy signals is shown in Figure 1 here it can be seen that the one-dimensional Fourier Transform is not able to identify the discriminant features in this type of signal.

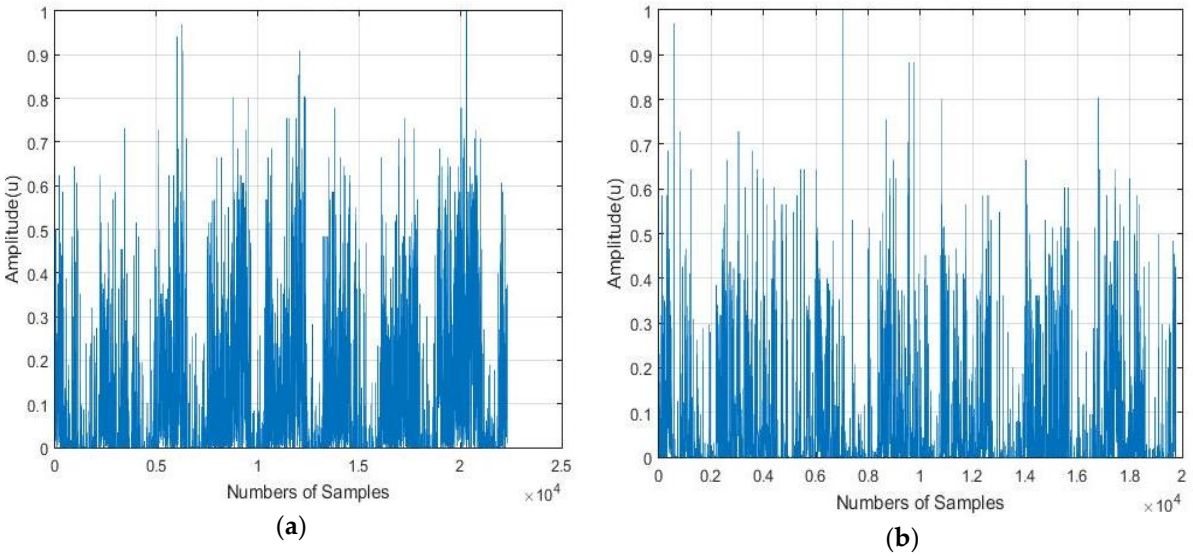

(**a**) (**b**)

Figure 1. Ilustration of: (**a**) and (**b**) Examples of the frequency spectrum of two actigraphy signals obtained from their respective one-dimensional Fourier t.

Unlike the one-dimensional frequency spectrum, the bispectrum of an activity signal can provide information on the spatial distribution of the amplitude, and on the frequency components (see Equation (4)). This information can be represented in a matrix that can be used to obtain the particular identification features of each signal. The bispectrum of the actigraphy signal was simulated in MatLab, using the Higher Order Spectra Analysis toolbox. Figures 2 and 3 show the contours of the bispectrum surface of the actigraphy signal, where f1 and f2 are the normalized spectral frequency vectors generated from the calculation of the bidimensional Fourier Transform.

We found that the bispectrum can indicate variables that measure specific characteristics of the movement during sleep, based on the uniformity of the activity data and the disorder of the sample. Here, a greater frequency disorder at a bispectral level may imply an excess of movement during the analyzed period, which can even be an identifying feature of sleep, and be linked to patients. For the sake of completeness, we can see in Figures 2-5 that the bispectrum is a unique variable for each actigraphy signal.

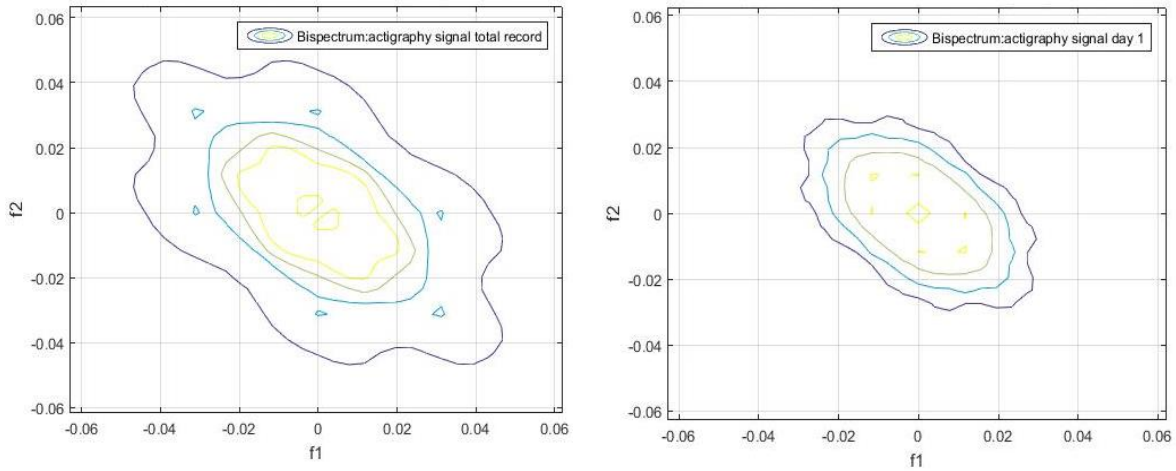

(**a**) (**b**)

Figure 2. (**a**) Bispectrum of the activity record over seven days and (**b**) bispectrum of the activity record day 1 of the actigraphy data sample *hchs-sol-sueno-00163225*.

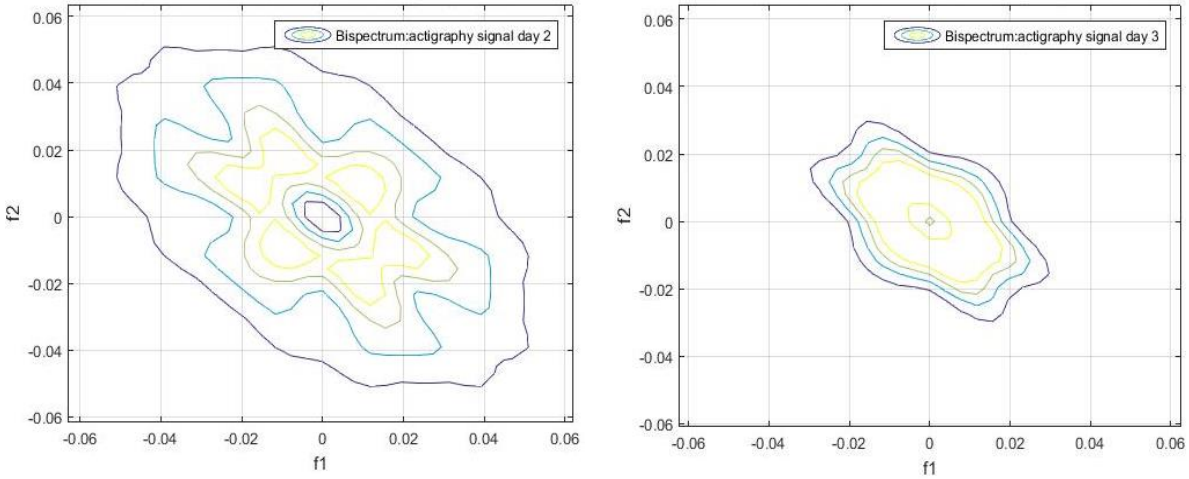

(**a**) (**b**)

Figure 3. (**a**) Bispectrum of the activity record day 2 and of (**b**) bispectrum of the activity record day 3 of the actigraphy data sample *hchs-sol-sueno-00163225*.

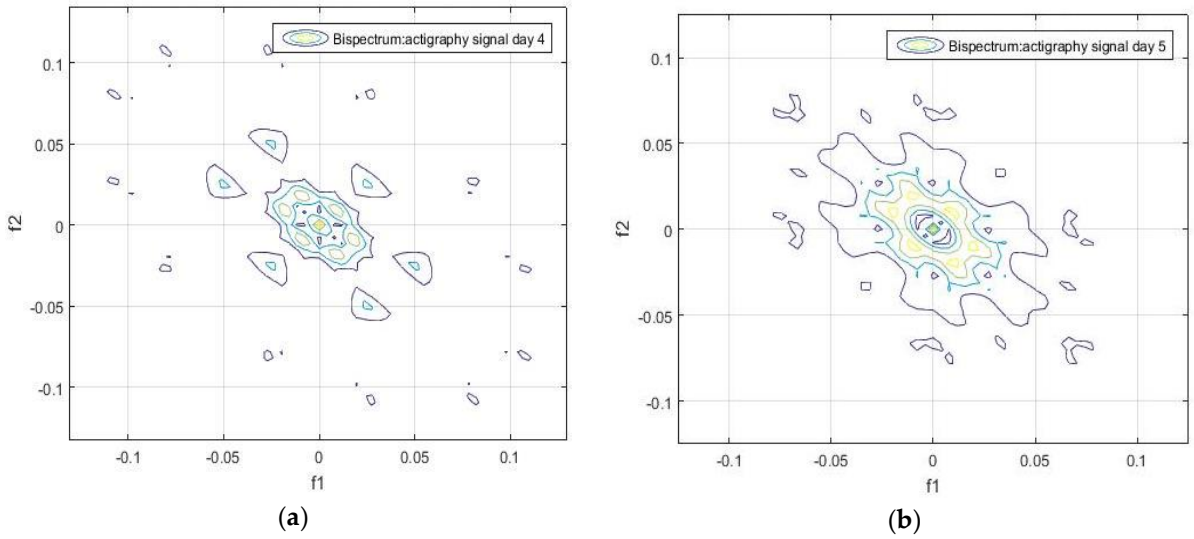

Figure 4. (**a**) Bispectrum of the activity record day 4 and (**b**) bispectrum of the activity record day 5 of the actigraphy data sample *hchs-sol-sueno-00163225*.

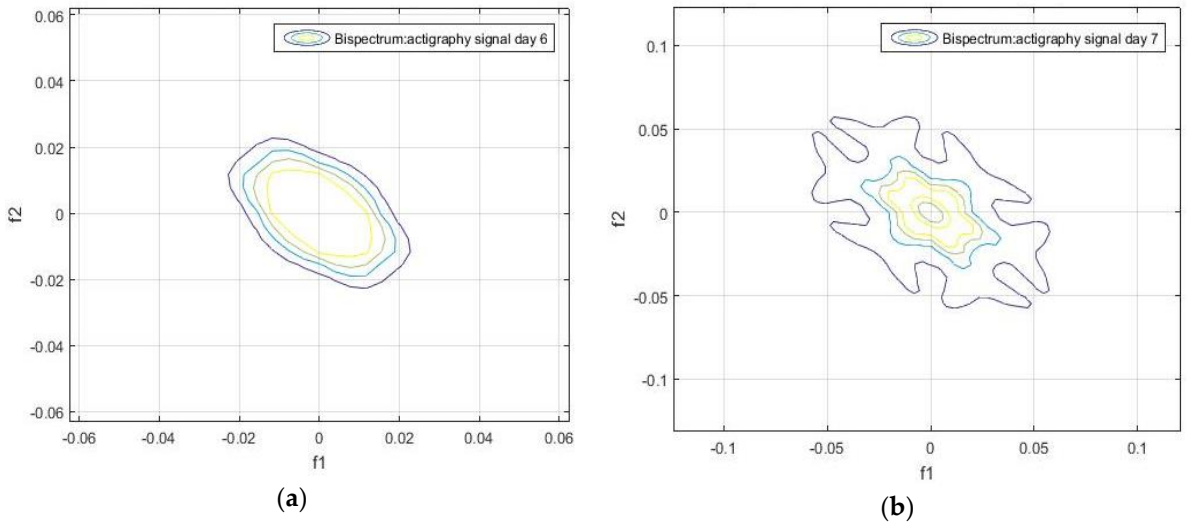

Figure 5. Bispectrum of the activity record day 6 and (**b**) bispectrum of the activity record day 7 of the actigraphy data sample *hchs-sol-sueno-00163225*.

It can also be seen that the daily bispectrum registrations are all different from each other, showing that all these registers form an identification pattern, which we have named the bispectral pattern of the activity signal.

A bispectrum analysis was performed on 20 different activity signal records. We tried to identify each one with a specific spectral sleep pattern per day, and to find a possible relationship between an individual's movement patterns during sleep. The results obtained are shown in Figure 6-8 which give the bispectrum of the actigraphy signal for the first 10 of the 20 analyzed actigraphy signals from the HCHS/SOL database

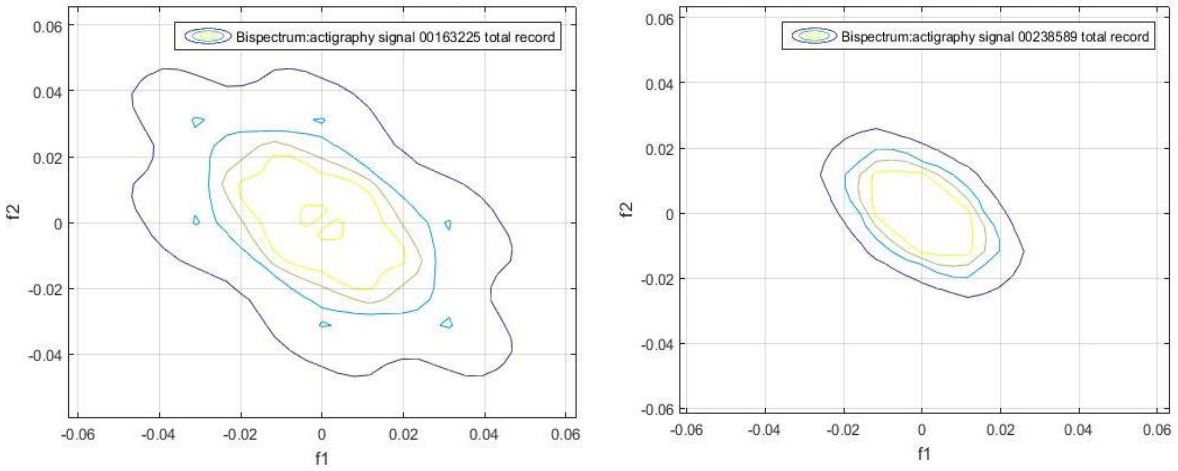

Figure 6. Bispectrum obtained from the activity record during seven analyzed days of the samples (**a**) *hchs-sol-sueno-00163225* and (**b**) *hchs-sol-sueno-00238589***.**

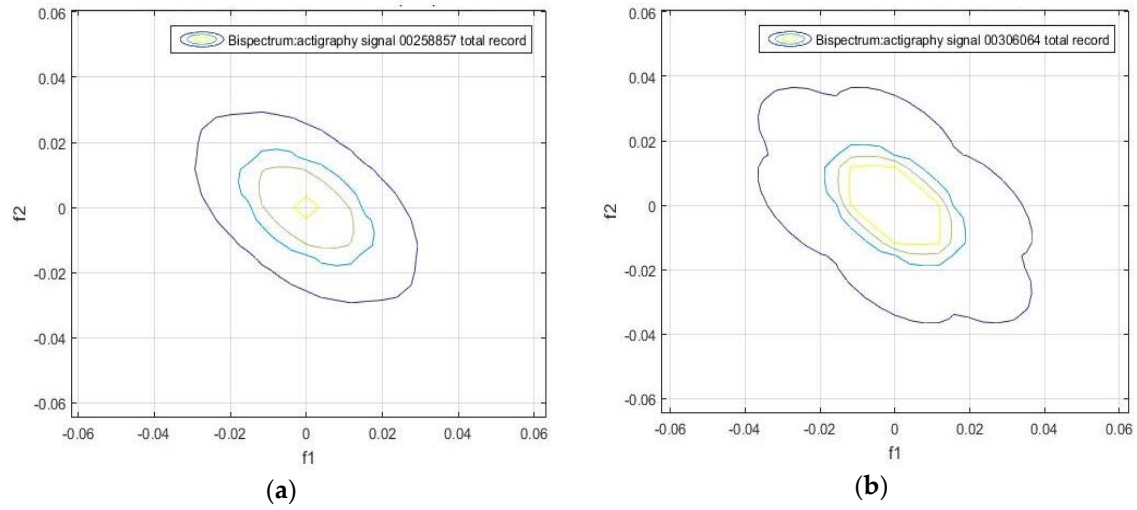

Figure 7. Bispectrum obtained from the activity record during seven analyzed days of the samples (**a**) *hchs-sol-sueno-00258857*, (**b**) *hchs-sol-sueno-00306064***.**

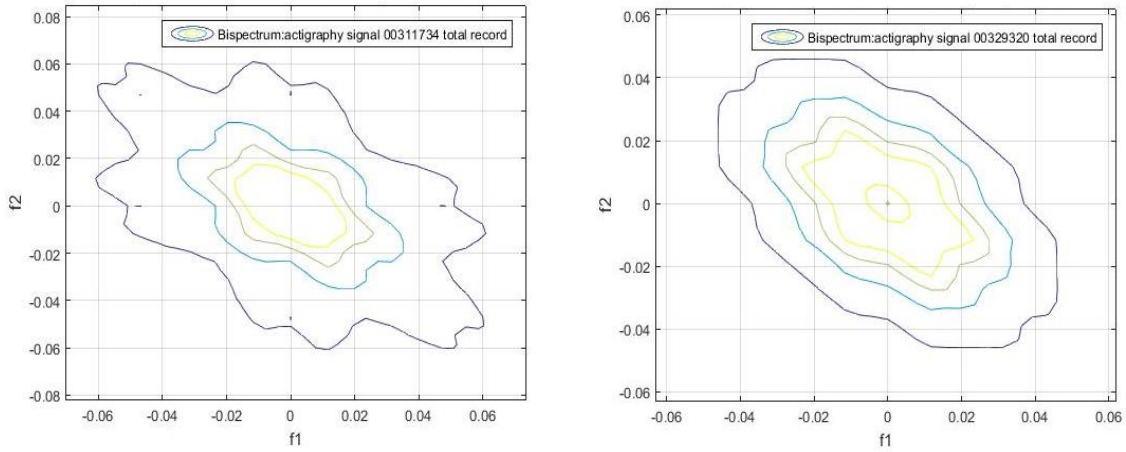

(**c**) (**d**)

Figure 7.cont. Bispectrum obtained from the activity record during seven analyzed days of the samples (**c**) *hchs-sol-sueno-00311734*, and (**d**) *hchs-sol-sueno-00329320***.**

It can be seen that there are unique identifiable characteristic features that can be used to obtain patterns of movement during sleep. For instance, Figures 5-8 have similar contours. This means individuals can be divided into groups according to the similarity of their sleep patern.

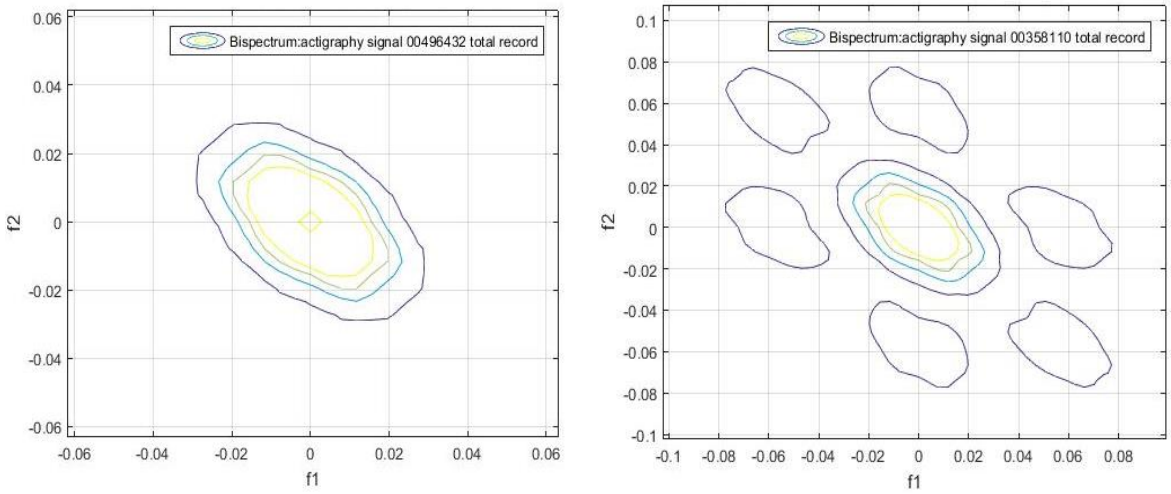

(**a**) (**b**)

Figure 8. Bispectrum obtained from the activity record during seven analyzed days of the samples (**a**) *hchs-sol-sueno-00349159* (**b**) *hchs-sol-sueno-00358110* .

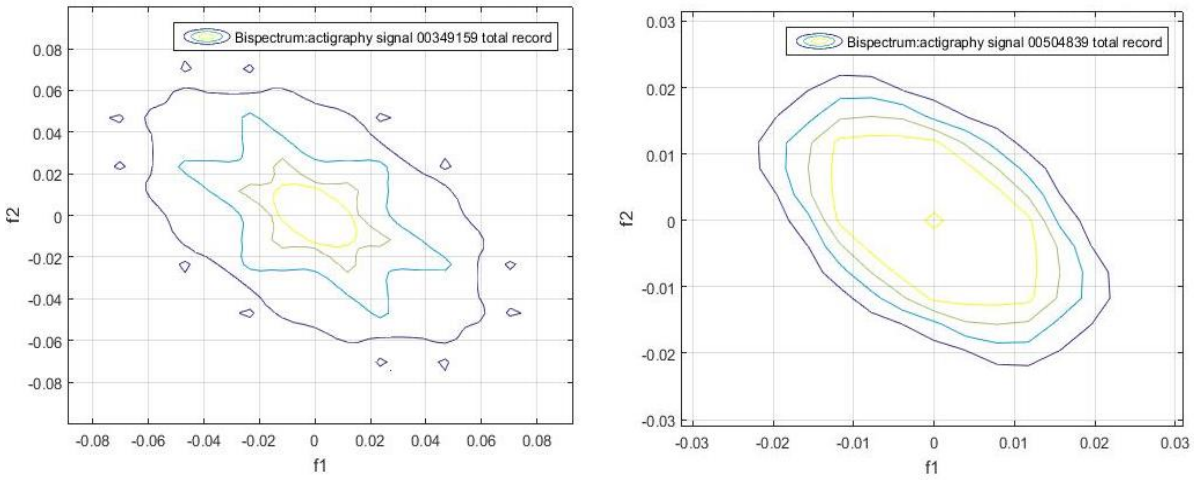

(**c**) (**d**)

Figure 8.cont Bispectrum obtained from the activity record during seven analyzed days of the samples (**c**) *hchs-sol-sueno-00496432* (**d**) *hchs-sol-sueno-00504839*.

To further illustrate these results, we correlated the bispectrum of the seven days of signals by computing the Pearson correlation coefficients for every pair of samples to find similarities between the two signals. The results are given in the correlation matrix R in Table 1. For example, R_{1-2} is the Pearson correlation coefficient between the bispectrum of samples 1 and 2 from hchs-sol-sueno-00163225 and hchs-sol-sueno-00238589.

Table 1. Correlation matrix obtained from the analysis of the bispectrum comparison of the 7-day activity signal for the 20 Hispanic Community Health Study/Study of Latinos (HCHS/SOL) database

0.898	0.944	0.934	0.965	0.957	0.899	0.899	0.947	0.825	0.966	0.976	0.971	0.950	0.979	0.911	0.972	0.970	0.973	0.945	
0.961	0.935	0.875	0.881	0.767	0.860	0.957	0.981	0.823	0.935	0.953	0.949	0.869	0.991	0.884	0.876	0.923	0.919	-	
0.965	0.944	0.914	0.837	0.911	0.961	0.909	0.892	0.970	0.976	0.970	0.917	0.970	0.937	0.925	0.959	0.933	-	-	
0.931	0.886	0.860	0.899	0.949	0.887	0.886	0.949	0.954	0.950	0.895	0.945	0.920	0.916	0.936	0.885	-	-	-	
0.938	0.914	0.926	0.927	0.809	0.962	0.969	0.951	0.945	0.949	0.890	0.973	0.965	0.967	0.913	-	-	-	-	
0.847	0.832	0.899	0.817	0.948	0.951	0.936	0.915	0.971	0.896	0.974	0.926	0.945	0.972	-	-	-	-	-	
0.849	0.844	0.688	0.889	0.892	0.854	0.864	0.870	0.773	0.889	0.888	0.863	0.799	-	-	-	-	-	-	
0.908	0.799	0.887	0.929	0.911	0.904	0.862	0.867	0.881	0.921	0.920	0.849	-	-	-	-	-	-	-	
0.913	0.891	0.957	0.976	0.956	0.913	0.965	0.912	0.921	0.955	0.926	-	-	-	-	-	-	-	-	
0.739	0.871	0.898	0.905	0.791	0.966	0.819	0.810	0.861	0.860	-	-	-	-	-	-	-	-	-	
0.946	0.924	0.892	0.964	0.841	0.960	0.960	0.941	0.922	-	-	-	-	-	-	-	-	-	-	
0.977	0.964	0.958	0.942	0.964	0.963	0.976	0.953	-	-	-	-	-	-	-	-	-	-	-	
0.975	0.953	0.966	0.957	0.954	0.981	0.949	-	-	-	-	-	-	-	-	-	-	-	-	
0.921	0.954	0.952	0.944	0.970	0.906	-	-	-	-	-	-	-	-	-	-	-	-	-	
0.888	0.970	0.961	0.960	0.957	-	-	-	-	-	-	-	-	-	-	-	-	-	-	
0.899	0.886	0.937	0.931	-	-	-	-	-	-	-	-	-	-	-	-	-	-	-	
0.962	0.971	0.937	-	-	-	-	-	-	-	-	-	-	-	-	-	-	-	-	
0.967	0.912	-	-	-	-	-	-	-	-	-	-	-	-	-	-	-	-	-	
0.938	-	-																	

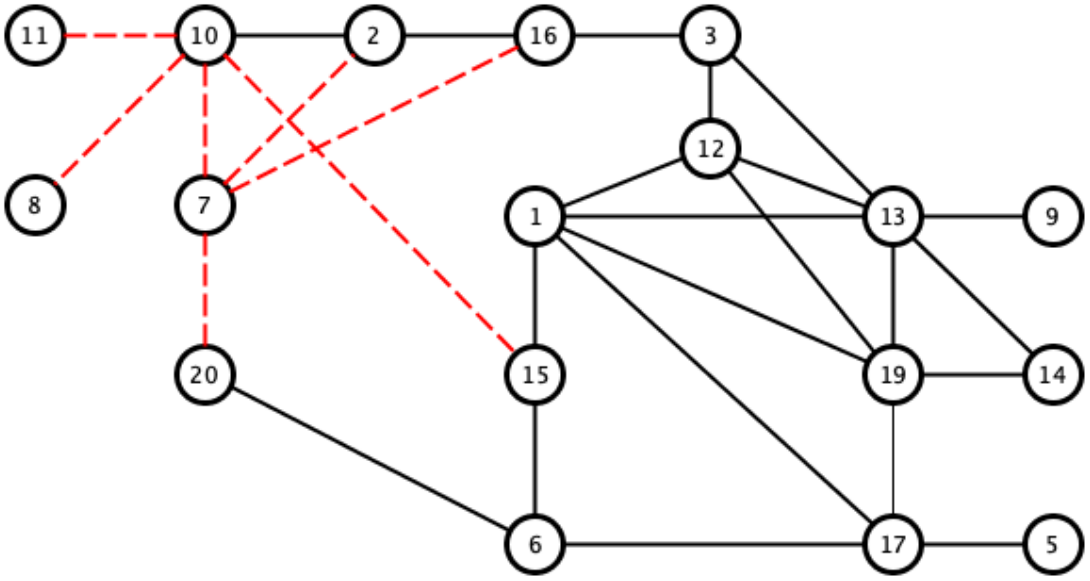

Figure 9. Visualization of pairs with Pearson correlation coefficients greater than 0.97 (black line) and lower than 0.8 (red dashed line).

The correlation values given in Table 1 and figure 9 show that there may be a similarity in sleep movement patterns. In Table 1 the maximum distance value is 0.3122 and the minimum is 10^{-6} the mean is 0.0538, and the statistical mode (the most frequent value in an array) is 0.001. Figure 10 give a comparative measurement of the values in Table 1 by rearranging the columns of the matrix into a vector, and considering it as a time series, in which the x-coordinate is the position in the vector and the y-coordinate, the corresponding value of the coefficient. In this arrangement, and the y-coordinate, the corresponding value of the coefficient. In this arrangement, the groups indicate almost repetitive terms that represent signals with similar characteristics.

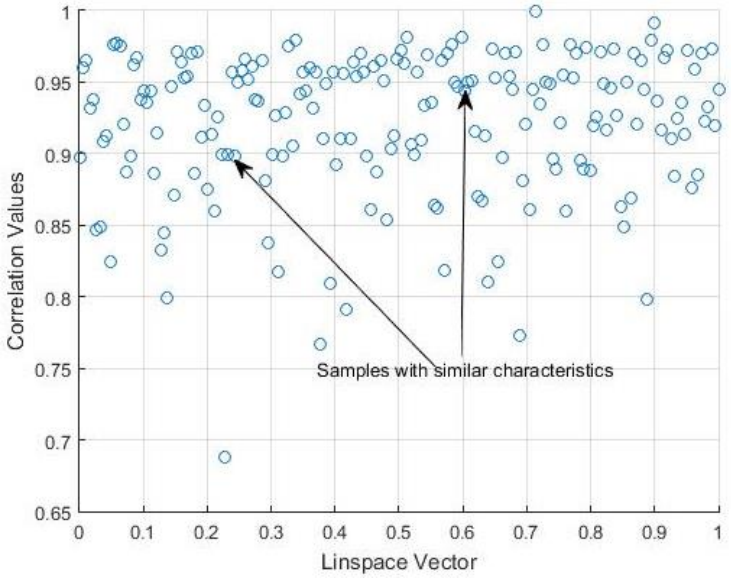

Figure 10. Scatter plot for the correlation matrix shown in Table 1.

In order to better distinguish the differences and similarities between the sleep signals, we performed another analysis using the bispectral entropy as the method of characterizing the disorder/uniformity of the processed signals.

3.2. Application of bispectral entropy as a measure of actigraphy disorder

The experiment was based on a similarity analysis, analogous to that of the bispectrum. We calculated the bispectral entropy of each activity sample for the whole period of seven days, to obtain a measure of the degree of uniformity of the sleep movement pattern, taking the degree of randomness of the activity signal into account. We considered the maximum value of the Bispectral entropy as a way of describing the degree of uniformity of a random process. The bispectral entropy of the signals was computed in a minimum window of eight samples, to represent the temporal displacement index of the signals. The results obtained are shown in Figure 11 together with the mean value of the bispectral entropy of each actigraphy signal.

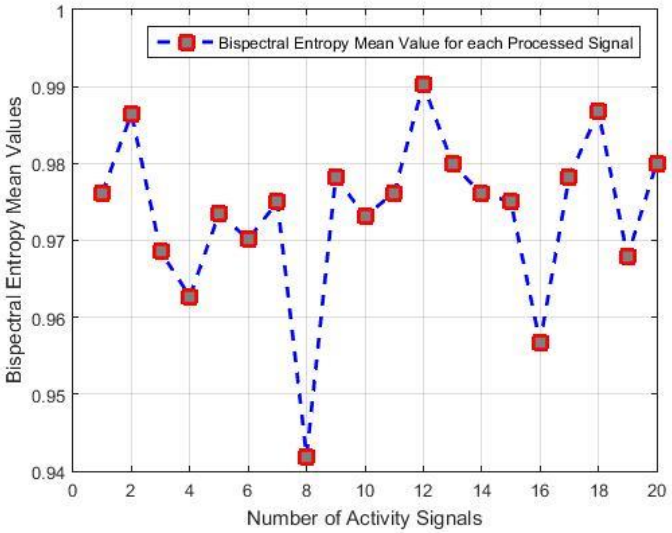

Figure 11. Mean bispectral entropy values of the 20 actigraphy signals considered

It can be seen that signals 8 and 16 have the lowest bispectral entropy values, due to the non-uniformity of the bispectrum frequency distribution. This can also be identified in some of the previous graphs; for instance, in Figure 8 he high-frequency components are characterized by the outer points (in blue), and the disconnected regions are the lowest frequency values.
In Figure 11 there are also samples with similar values of bispectral entropy of between 0.98 and 0.99, which indicates that they may be related to the hypothesis that activity samples with a similar correlation at the bispectral level may have the same level of uniformity of their value distributions. The opposite is also true with the minimum values of bispectral entropy, shown in Figure 11 as are those of samples 8, 10, 7, and 16, and other visible relationships, whose correlation values are under 0.8 in Table 2 and in Figure 11 are related to different uniformity patterns.

Given the analogy of the activity signal with the random process, the maximum entropy value would mean a greater uniformity of movement in the subject in the time interval studied, i.e., a

high uniformity in the randomness of the movements. Conversely, occasional movements would be associated with impulsive noise, which has a non-uniform randomness, and thus, it would be associated with minimum entropy.

To also visualize the frequency of the maximum uniformity of sleep movements, histograms were made of the 7-day bispectral entropy of each activity signal. The frequencies of the entropy values for each processed sample are shown in Figures 12 and 13. These histograms provide information on the number of repetitions of the entropy values in each sample, i.e., the number of times the value in the data vector is repeated.

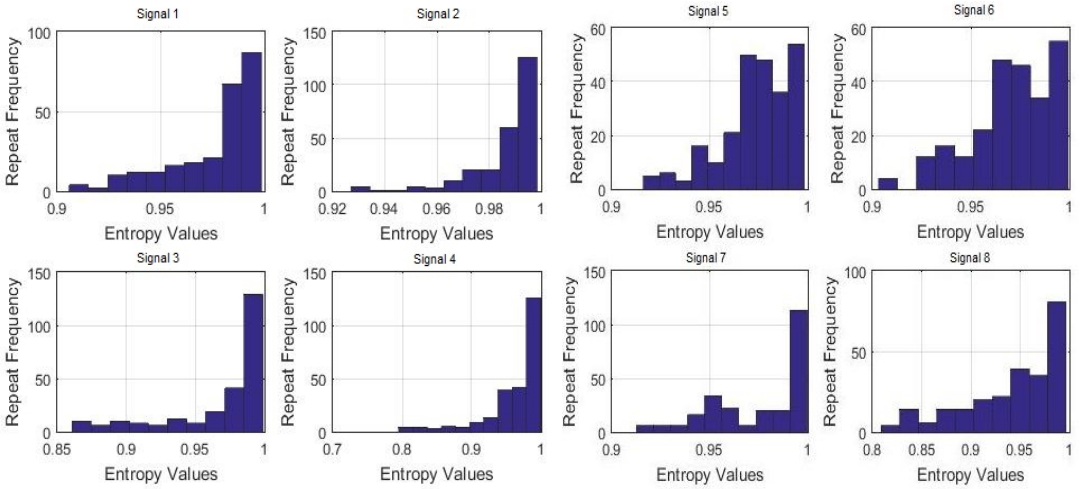

Figure 12. Illustration of: Histogram of the Bispectral Entropy of each activity signal (Signal 1 to Signal 8, processed samples) performed during seven records days.

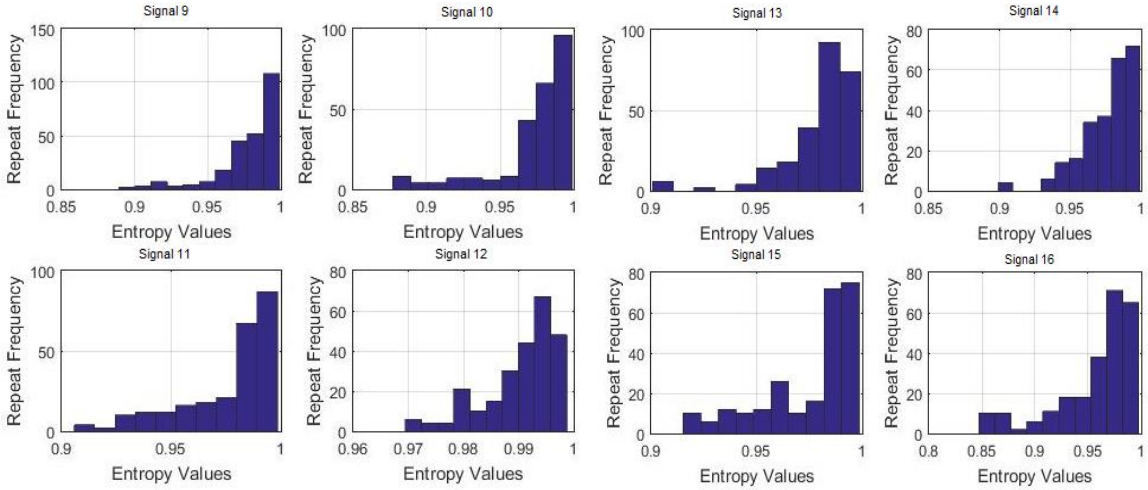

Figure 13. Illustration of: Histogram of the Bispectral Entropy of each activity signal (Signal 9 to Signal 16, processed samples) performed during seven records days.

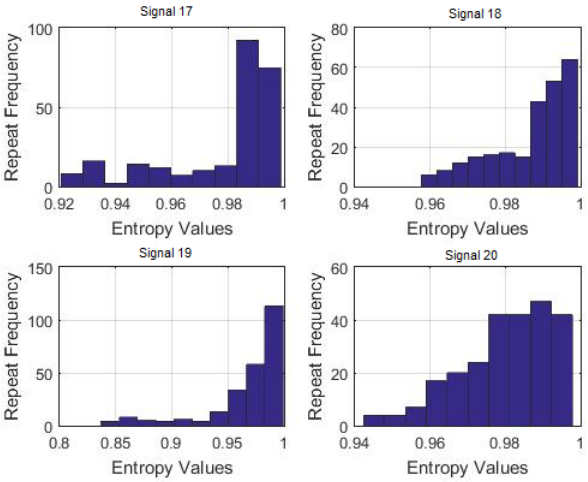

Figure 13.cont Illustration of: Histogram of the Bispectral Entropy of each activity signal (Signal 17 to Signal 20, processed samples) performed during seven records days.

Although none of the histograms is repeated in Figures 12 and 13 some of them show certain similarities that could indicate similar sleep patterns. To verify this, the histograms were correlated to each other, with the criteria for the entropy values as well as for the data repetition frequency. The results are shown below in Table 2.

Table 2. Correlation matrix obtained from the analysis of the bispectral entropy histograms of the 20 analyzed samples from the HCHS/SOL database.

0.966	0.906	0.908	0.681	0.702	0.791	0.889	0.934	0.957	1.000	0.828	0.928	0.938	0.972	0.931	0.927	0.931	0.957	0.720
0.976	0.973	0.699	0.714	0.880	0.944	0.967	0.948	0.966	0.725	0.842	0.893	0.906	0.865	0.841	0.889	0.985	0.650	-
0.979	0.593	0.623	0.937	0.930	0.943	0.906	0.906	0.583	0.731	0.783	0.840	0.763	0.748	0.827	0.964	0.504	-	-
0.715	0.732	0.913	0.979	0.985	0.945	0.908	0.677	0.780	0.845	0.824	0.818	0.740	0.894	0.983	0.621	-	-	-
0.981	0.514	0.802	0.774	0.711	0.681	0.816	0.706	0.853	0.558	0.730	0.511	0.762	0.703	0.934	-	-	-	-
0.553	0.805	0.790	0.715	0.702	0.793	0.697	0.848	0.575	0.708	0.490	0.773	0.713	0.926	-	-	-	-	-
0.886	0.845	0.788	0.791	0.429	0.559	0.665	0.709	0.615	0.589	0.729	0.863	0.430	-	-	-	-	-	-
0.975	0.929	0.889	0.731	0.786	0.874	0.798	0.834	0.717	0.913	0.958	0.720	-	-	-	-	-	-	-
0.976	0.934	0.779	0.859	0.908	0.855	0.887	0.789	0.947	0.989	0.714	-	-	-	-	-	-	-	-
0.957	0.840	0.927	0.925	0.912	0.947	0.878	0.975	0.980	0.708	-	-	-	-	-	-	-	-	-
0.828	0.928	0.938	0.972	0.931	0.927	0.931	0.957	0.720	-	-	-	-	-	-	-	-	-	-
0.937	0.932	0.796	0.928	0.825	0.898	0.756	0.910	-	-	-	-	-	-	-	-	-	-	-
0.955	0.934	0.992	0.931	0.937	0.865	0.800	-	-	-	-	-	-	-	-	-	-	-	-
0.889	0.962	0.863	0.939	0.897	0.899	-	-	-	-	-	-	-	-	-	-	-	-	-
0.929	0.950	0.887	0.892	0.646	-	-	-	-	-	-	-	-	-	-	-	-	-	-
0.924	0.954	0.892	0.802	-	-	-	-	-	-	-	-	-	-	-	-	-	-	-
0.846	0.845	0.618	-	-	-	-	-	-	-	-	-	-	-	-	-	-	-	-
0.932	0.801	-	-	-	-	-	-	-	-	-	-	-	-	-	-	-	-	-
0.657	-	-	-	-	-	-	-	-	-	-	-	-	-	-	-	-	-	-

Table 2 contains the results based on the histogram of the bispectral entropy of the activity signals to provide a criterion for the similarity of the data, based on the uniformity of the

bispectrum. This table can be interpreted similarly to Table 1 which was based on the algorithm that describes the matrix correlation in Figure 9.

According to the previous analysis, the upper threshold was 0.97, and the lower threshold was a little lower than previously found. We considered 0.8 to distinguish between the similarities and clear differences among the signals (see Figure 14).

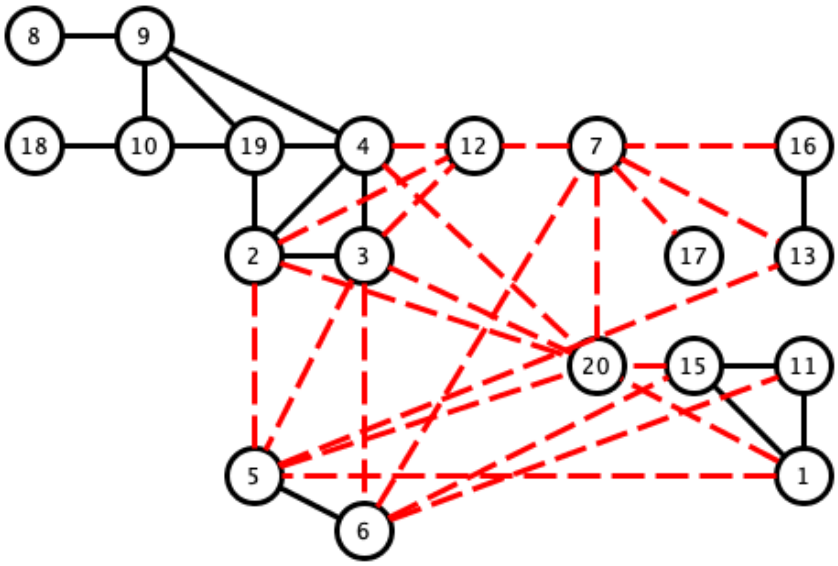

Figure 14. Visualization of pairs with Pearson correlation coefficients greater than 0.97 (black line) and lower than 0.8 (red dashed line).

It can thus be seen that several histograms are highly correlated, which indicates that this activity signal presents a high level of data uniformity, i.e., bispectral entropies with similar values, and also a high correlation value in terms of the bispectrum comparison. The dispersion graph of the correlation values obtained from Table 2 is shown in Figure 15. The data with similar values are seen to be grouped. The maximum value of the distance matrix is 0.6715, and the minimum is 10^{-5} . The mean value of the distance matrix was 0.1407 and the statistical mode was 10^{-5}, which indicates, as in the previous analysis, that there are data groups with similar characteristics associated with the same characteristic of movement, as can be seen in Figure 15.

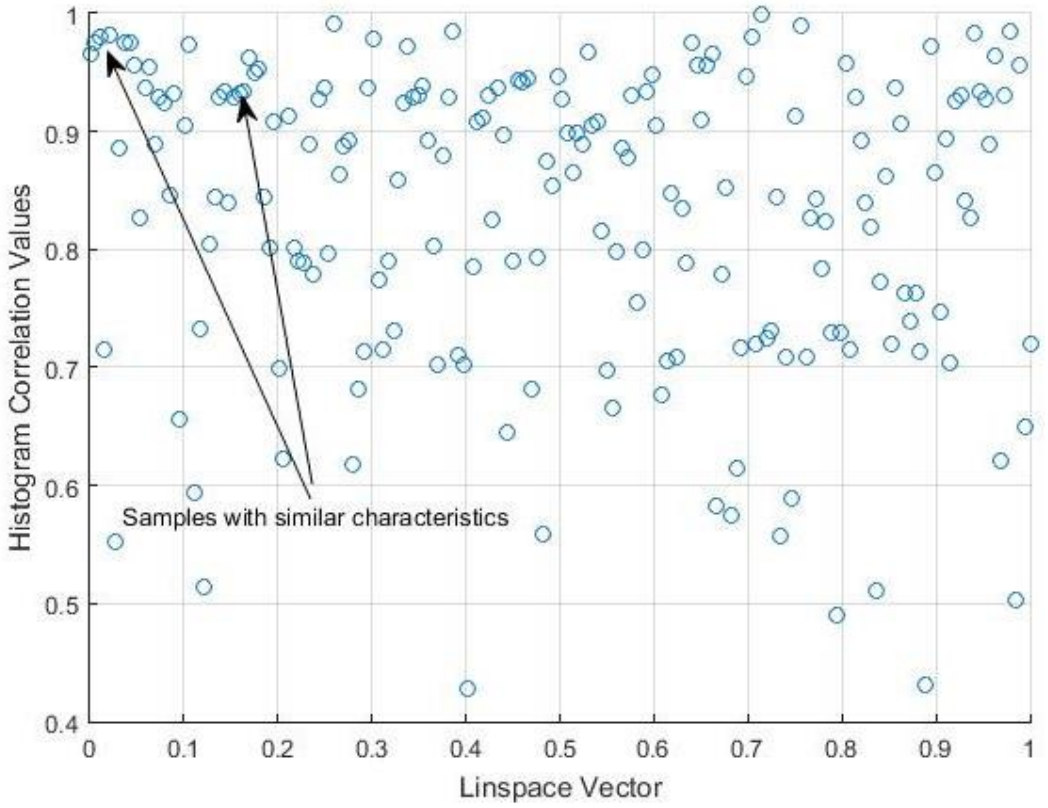

Figure 15. Scatter plot for the correlation matrix shown in Table 2

4. Discussion

In order to associate the results with clinical diagnoses, several variables were taken from the HCHS/SOL database as the clinical characteristics of the 20 actigraphy samples. First, we considered the following variables:

- CDCR_SUENO: self-report of cerebrovascular disease & carotid revascularization. CHD_SELF_SUENO: combination of self-reports of coronary revascularization or heart attack. DIABETES_SELF_SUENO: indicates a self-report of diabetes.
- DIABETES _SUENO: indicates diabetes. DM_AWARE_SUENO: describes the awareness of diabetes. Hypertension_SUENO: indicates hypertension status. STROKE_SUENO: checks for a self-report of stroke history.
- STROKE_TIA_SUENO: checks for medical history of stroke, mini-stroke or TIA (transient ischemic attack).

These variables are of the 0/1 type, i.e., '0' for a negative response and '1' for a positive. Their values for the 20 individuals whose actigraphy signals were processed can be found in Table 3.

Table 3. Clinical characteristics of each individual analyzed for each actigraphy sample.

Samples	CDCR_ SUENO	CHD_ SELF_ SUENO	DIABETES_ SELF_ SUENO	DIABETES_ SUENO	DM_ AWARE_ SUENO	HYPERTENSION_ SUENO	STROKE_ SUENO	STROKE_ TIA_ SUENO
1	0	0	0	0	0	1	0	0
2	1	1	1	1	1	1	0	0
3	0	0	0	0	0	1	0	0
4	0	0	0	0	0	0	0	0
5	0	0	0	0	0	0	0	0
6	0	0	0	0	0	0	0	0
7	0	0	0	1	0	1	0	0
8	0	0	0	0	0	1	0	0
9	0	0	0	0	0	0	0	0
10	0	0	0	0	0	1	0	0
11	0	0	0	0	0	0	0	0
12	0	0	0	0	0	0	0	0
13	0	0	0	0	0	0	0	0
14	0	0	0	0	0	0	0	0
15	0	0	0	0	0	0	0	0
16	0	0	0	0	0	1	0	0
17	0	0	0	1	0	0	0	0
18	0	1	0	0	0	1	0	0
19	0	0	1	1	1	1	0	0
20	0	0	0	0	0	1	0	0

To relate the clinical characteristics of the patients with the obtained results, the correlation was first used, which is a measure of the similarity of data. We show these results, although the obtainedcorrelations are weak, in part, for the limited number of signals used, and for the limitations of the information content embedded in the used signals database. We opted to consider the HYPERTENSION_SUENO variable to study relationships within the actigraphy signals, since its value varies in several samples. First, we saw that 47.62% of the pairs whose bispectrum correlates with a value greater than 0.97 share the same clinical diagnosis. However, in Figure 9 it can be seen that the pairs with the same positive or negative diagnosis tend to cluster, which indicates a stronger hidden relationship that cannot be obtained by simply correlating the bispectrum of the signals (see Figure 16).

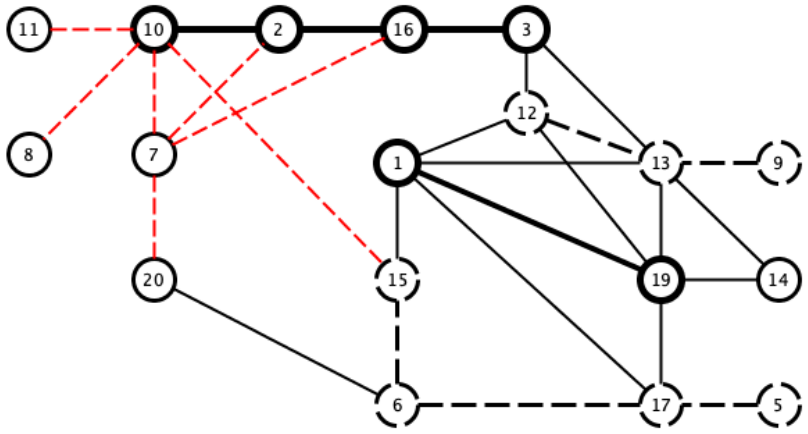

Figure 16. Pairs of bispectrum signals correlated with a coefficient that is greater than 0.97 (black lines) or lower than 0.7 (red dashed line). The thick black line indicates pairs that share a hypertension diagnosis, while the dashed black line indicates pairs in which neither has hypertension.

A similar effect was found in the comparison of the bispectral entropy histograms. Only 41.17% of the pairs correlated with a coefficient of 0.97 or higher present the same hypertension diagnoses. However, in the pairs with the same diagnosis in Figure 14 those sharing the hypertension diagnosis are seen to be connected (see Figure 17).

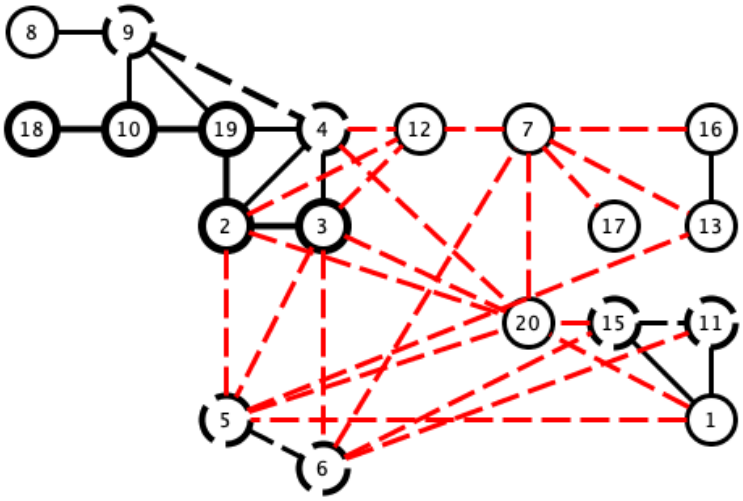

Figure 17. Pairs of bispectral entropy histograms correlated with a coefficient greater than 0.97 (black lines), and lower than 0.7 (red dashed line). The thick black line indicates pairs with a shared hypertension diagnosis, while the dashed black line indicates pairs in which neither has hypertension.

Although, the results shown in Figures 16 and 17 are not conclusive, they do suggest a further in-depth study of the characteristics of bispectrum signals that can contribute most to these similarities. It is also worth mentioning that the limited number of cases considered in this study advise a more systematic study of larger database samples.

5. Conclusions

This paper has shown that the application of higher-order statistical analysis to actigraphy can contribute to determining the traits and patterns of movement during sleep. These criteria can be based on part of the spatial information provided by the bispectrum and the bispectral entropy, both of which can help us to determine effective criteria for measuring the uniformity of data randomness signals can contribute to determining the traits and patterns of movement during sleep.
These criteria can be based on part of the spatial information provided by the bispectrum and the Bispectral entropy, both of which can help us to determine effective criteria for measuring the uniformity of data randomness.

The actigraphy signal experiments suggest the possible application of these criteria for the extraction and comparison of patterns of sleep movements. This would have a potential use in medicine, since similar pathologies may have similar associated movement patterns.

In future work we propose to use high-order statistical techniques, as for instance in [23]. We also want to experiment with data from chest actigraphy or other actigraphy signal measures, to corroborate the potential use of sleep actigraphy signals for purposes of diagnosis. Our next step will be to increase the number of cases analyzed to cover the entire HCHS/SOL database, and also to experiment with other clinical characteristics in patients and pathologies associated with specific sleep disorders or brain-associated diseases.

Author Contributions: Conceptualization, M.E.I.M., J.M.G.-G., C.S.S., P.F.d.C., and J.A.C.; Methodology, M.E.I.M.; Software, M.E.I.M.; Validation, M.E.I.M., J.M.G.-G., C.S.S., P.F.d.C., and J.A.C.; Formal Analysis, M.E.I.M.; Investigation, M.E.I.M., J.M.G.-G., C.S.S., P.F.d.C., and J.A.C.; Resources, M.E.I.M., J.M.G.-G., C.S.S., P.F.d.C. and J.A.C.; Data Curation, M.E.I.M. and C.S.S.; Writing—Original Draft Preparation, M.E.I.M., J.M.G.-G., C.S.S., P.F.d.C., and J.A.C.; Writing—Review & Editing, M.E.I.M., J.M.G.-G., C.S.S., P.F.d.C., and J.A.C.; Visualization, M.E.I.M.; Supervision, C.S.S., J.A.C.; Project Administration, J.A.C.

Funding: Funding for this study was provided by the authors' departments. J.A.C. acknowledges support from the Ministerio de Economía, Industria y Competitividad, Grant MTM2016-75963-P. J.M.G.-G. y C.S.S. Ministerio de Ciencia Tecnología y Telecomunicaciones, Grant DPI2016-80054-R. J.A.C., J.M.G.-G. and C.S.S. acknowledge support from the European Commission, CrowdHealth project (H2020-SC1-2016-CNECT No. 727560).

Acknowledgments: Special thanks to the Hispanic Community Health Study/Study of Latinos (HCHS/SOL) Database. The HCHS/SOL dataset was used under the Data Access and Use Agreement approval from the National Sleep Research Resource.

Conflicts of Interest: The authors declare no conflict of interest. The founding sponsors had no role in the design of the study, in the collection, analyses or interpretation of data, in the writing of the manuscript, or in the decision to publish the results.

6. References

1. Kushida, C.A.; Chang, A.; Gadkary, C.; Guilleminault, C.; Carrillo, O.; Dement, W.C. Comparison of actigraphic, polysomnographic, and subjective assessment of sleep parameters in sleep-disordered patients. Sleep Med. **2001**, 2, 389–396. [CrossRef]
2. Jean-Louis, G.; Kripke, D.F.; Mason, W.J.; Elliott, J.A.; Youngstedt, S.D. Sleep estimation from wrist movement quantified by different actigraphic modalities. J. Neurosci. Methods **2001**, 105, 185–191. [CrossRef]
3. Ancoli-Israel, S.; Cole, R.; Alessi, C.; Chambers, M.; Moorcraft, W.; Pollak, C.P. The role of actigraphy in the study of sleep and circadian rhythms. Sleep **2003**, 26, 342–392. [CrossRef] [PubMed]
4. de Souza, L.; Benedito, A.A.; Nogueira, M.L.; Poyares, D.; Tufik, S.; Calil, H.M. Further validation of actigraphy for sleep studies. Sleep **2003**, 26, 1–5. [CrossRef]
5. Taraldsen, K.; Chastin, S.F.; Riphagen, I.I.; Vereijken, B.; Helbostad, J.L. Physical activity monitoring by use of accelerometer-based body-worn sensors in older adults: A systematic literature review of current knowledge and applications. Maturitas **2012**, 71, 13–19. [CrossRef]
6. Martin, J.L.; Hakim, A.D. Wrist Actigraphy. Chest **2011**, 139, 1514–1527. [CrossRef]
7. Ray, M.A.; Youngstedt, S.D.; Zhang, H.; Robb, S.W.; Harmon, B.E.; Jean Louis, G.; Bo, C.; Hurley, T.G.; Herbert, J.R.; Bogan, R.K.; et al. Examination of wrist and hip actigraphy using a novel sleep estimation procedure. Sleep Sci. **2014**, 7, 74–81. [CrossRef]

8. Giménez, S.; Romero, S.; Alonso, J.F.; Mañanas, M.Á.; Pujol, A.; Baxarias, P.; Antonijoan, R.M. Monitoring sleep depth: Analysis of bispectral index (BIS) based on polysomnographic recordings and sleep deprivation. J. Clin. Monit. Comput. **2017**, 31, 103–110. [CrossRef]
9. Chua, K.C.; Chandran, V.; Acharya, U.R.; Lim, C.M. Application of higher order statistics/spectra in biomedical signals: A review. Med. Eng. Phys. **2010**, 32, 679–689. [CrossRef]
10. Vaquerizo-Villar, F.; Álvarez, D.; Kheirandish-Gozal, L.; Gutiérrez-Tobal, G.C.; Barroso-García, V.; Crespo, A.; Del Campo, F.; Gozal, D.; Hornero, R.G. Utility of bispectrum in the screening of pediatric sleep apnea-hypopnea syndrome using oximetry recordings. Comput. Methods Programs Biomed. **2018**, 156,141–149. [CrossRef]
11. Noronha, K.P.; Acharya, U.R.; Nayak, K.P.; Martis, R.J.; Bhandary, S.V. Automated classification of glaucoma stages using higher order cumulant features. Biomed. Signal Process **2014**, 10, 174–183. [CrossRef]
12. Long, X.; Fonseca, P.; Foussier, J.; Haakma, R.; Aarts, R. Sleep and wake classification with actigraphy and respiratory effort using dynamic warping. IEEE J. Biomed. Health **2014**, 18, 1272–1284. [CrossRef] [PubMed]
13. Matthews, K.A.; Patel, S.R.; Pantesco, E.J.; Buysse, D.J.; Kamarck, T.W.; Lee, L.; Hall, M.H. Similarities and differences in estimates of sleep duration by polysomnography, actigraphy, diary, and self-reported habitual sleep in a community sample. Sleep Health **2018**, 4, 96–103. [CrossRef] [PubMed]
14. Dean, D.A., 2nd; Goldberger, A.L.; Mueller, R.; Kim, M.; Rueschman, M.; Mobley, D.; Sahoo, S.S.; Jayapandian, C.P.; Cui, L.; Morrical, M.G.; et al. Scaling up scientific discovery in sleep medicine: The National Sleep Research Resource. Sleep **2016**, 39, 1151–1164. [CrossRef] [PubMed]
15. Zhang, G.Q.; Cui, L.; Mueller, R.; Tao, S.; Kim, M.; Rueschman, M.; Mariani, S.; Mobley, D.; Redline, S. The National Sleep Research Resource: Towards a sleep data commons. J. Am. Med. Inform. Assoc. **2018**, to appear. [CrossRef]
16. Redline, S.; Sotres-Alvarez, D.; Loredo, J.; Hall, M.; Patel, S.R.; Ramos, A.; Shah, N.; Ries, A.; Arens, R.; Barnhart, J.; et al. Sleep-disordered breathing in Hispanic/Latino individuals of diverse backgrounds. The Hispanic Community Health Study/Study of Latinos. Am. J. Respir. Crit. Care Med. **2014**, 189, 335–344. [CrossRef]
17. Patel, S.R.; Weng, J.; Rueschman, M.; Dudley, K.A.; Loredo, J.S.; Mossavar-Rahmani, Y.; Ramirez, M.; Ramos, A.R.; Reid, K.; Seiger, A.N.; et al. Reproducibility of a standardized actigraphy scoring algorithm for sleep in a US Hispanic/Latino Population. Sleep **2015**, 38, 1497–1503. [CrossRef]
18. Mendel, J.M. Tutorial on higher-order statistics (spectra) in signal processing and system theory: Theoretical results and some applications. IEEE Proc. **1991**, 79, 278–305. [CrossRef]
19. Nikia, C.L.; Mendel, J.M. Signal Processsing with higher-order spectra. IEEE Signal Process. Mag. **1993**, 10, 10–37. [CrossRef]
20. Swami, A.; Mendel, J.M.; Nikias, C.L. Higher-Order Spectral Analysis Toolbox User's Guide, Version 2; United Signals & Systems, Inc.: Ranco Palos Verde, CA, USA, 2001.

21. Vaseghi, S.V. Advanced Digital Signal Processing and Noise Reduction, 4th ed.; John Wiley & Sons: Hoboken, NJ, USA, 2008.
22. Bao, M.; Zheng, C.; Li, X.; Yang, J.; Tian, J. Acoustical vehicle detection based on bispectral entropy. IEEE Signal Process. Lett. **2009**, 16, 378–381. [CrossRef]
23. Murua, A.; Sanz-Serna, J.M. Vibrational resonance: A study with high-order word-series averaging. Appl. Math. Nonlinear Sci. **2016**, 1, 239–246. [CrossRef]

Chapter 3
General Discussion of the Results

Firstly, with regards to the electric machines fault diagnosis area (and, more especifically, regarding the detection of adjacent and non-adjacent bars breakages), two methods were provided, the first method based on the use of the power spectrum and a spectral subtraction process, based on the spectrum ordering. The second based on the analysis of the bispectrum of the flux signal.

In turn, two types of indicators, one based on the quadratic value of the median of the auto-covariance fuction and the other based on the sum of the mean value of the bispectrum of the flux matrix were proposed, as a discrimination mode between the healthy and damaged state of the motor. Both indicators were experimentally tested and validated, giving positive results in each case.

As a way to generalize what has been obtained, future studies will be carried out with different levels of load and during motor start-up, since the analyses were carried out at stedy-state.

Regarding the theoretical application of the algorithms to biomedical signals, it was proposed to perform an analysis of the Results of the Hispanic Community Health Study / Study of Latinos database, to detect patterns that may be common during sleep activity in the different patients which collects the database.

For this, it was proposed to use the bispectrum of the actigraphy signal for each weekly patient record to correlate all the analyzed samples to form a matrix with the degree of similarity existing in each movement pattern during sleep.

These results were then associated to specific groups where the movement characteristics were similar, obtaining reliable results that linked the patterns obtained with the same pathology associated with a patient in this case, hypertension was analyzed.

From the theoretical-practical proposal made in this thesis, general algorithms have been obtained that can be applied in different branches for the patterns recognition in time series, with the only limitation for the work, in principle, of the periodic nature of the signal to be study.

Chapter 4
Conclusions

This chapter analyzes the level of compliance with the research objectives set out in the introduction. The main conclusions reached are also collected, the most relevant contributions of the work are presented and several future lines of work are proposed.

Regarding the first objective “Review of the state of the art of the field to be treated”, in the general introduction, the reference to high-order statistical analysis and the detection of failures in electrical machines by means of stray flux signals has been initially addressed, as well as the analysis of actigraphy signals.

Regarding the second objective "Theoretical development of the algorithms to evaluate", in this research, several theoretical algorithms have been proposed that link the second-order classical and higher-order statistical analysis, with processes of espectral analysis and entropy, each of them theoretically explained and supported.

Regarding the third objective “Preparation and description of the data”, several experiments have been carried out for the verification of the developed algorithms, which have been described in each article published and mentioned in Chapter 2, describing each data or sample used in particular .

Regarding the fourth objective “Application of the algorithms that allow analyzing the available data through different methods”, each available data has been verified with every algorithm developed. It should be noted that, as the algorithms described are general, they can be applied to any type of signal since they only depend on the periodic nature of the sample to be analyzed.

As for the fifth objective "Validation and other possible uses of the methods described", each algorithm was validated with simulated and real samples experimentally obtained as well as databases available in each case.

4.1 Main Contributions

From the use of the developed algorithms for the detection and diagnosis of failures in electrical machines, based on the statistical and spectral signal processing, progress has been achieved in relation to the models currently existing, in the identification of faults through the use of stray flux signals

Moreover, through the use of higher order statistics for the extraction of anomalies in actigraphy signals, alternative parameters have been found identifying processes that can be related to a specific pathology, specifically the case of hypertension has been shown.

4.2 Future Research Lines

On the other hand and as results derived from the doctoral research, several works have been carried out, some already published, others accepted and others in the process of revision or elaboration, which are the result of the research lines that have been taken and will be carried out in a future. These works are summarized below:

1. S. Sahu, C. E. López Fortín, M. E. Iglesias Martínez, S. Nagataki and P. Fernández de Córdoba, "*The VHE SED modelling of Markarian"* 501 in 2009, MNRAS 492, 2261–2267 (2020), doi:10.1093/mnras/staa023. **Impact Factor: 5.231 Q1**

2. Iglesias-Martínez, M.E.; Castro-Palacio, J.C.; Scholkmann, F.; Milián-Sánchez, V.; Fernández de Córdoba, P.; Mocholí-Salcedo, A.; Mocholí Belenguer, F.; Kolombet, V.A.; Panchelyuga, V.A.; Verdú, G. Correlations between Background Radiation Inside a Multilayer Interleaving Structure, Geomagnetic Activity, and Cosmic Radiation: A Fourth-Order Cumulant-Based Correlation Analysis. *Mathematics* **2020**, *8*, 344. **Impact Factor: 1.105 Q1**

3. V. Milián-Sánchez, F. Scholkmann, P. Fernández de Córdoba, A. Mocholí-Salcedo, F. Mocholí, M.E. Iglesias-Martínez, J. C. Castro-Palacio, V. A. Kolombet, V. Panchelyuga, and G. Verdú, *"Fluctuations in measured radioactive decay rates inside a modified Faraday cage: Correlations with space weather*". **Accepted in Scientific Reports-Nature, Impact Factor: 4.525 Q1**

4. Miguel Enrique Iglesias Martínez, Pedro Fernández de Córdoba, Jose Alfonso Antonino-Daviu and J. Alberto Conejero, "*Detection of adjacent and non-adjacent bar breakages in induction motors via convolutional analysis of sound signals*", **(Sent to Applied Science MDPI, under Revision).**

5. Miguel Enrique Iglesias Martínez, Pedro Fernández de Córdoba, Jose Alfonso Antonino-Daviu and J. Alberto Conejero, "*Bispectrum Analysis of Stray Flux Signals for the Robust Detection of Winding Asymmetries in Wound Rotor Induction Motors*" **(Accepted in ECCE 2020 IEEE Energy Conversion Congress and Exposition Conference, Detroit, Michigan , October 11-15, 2020).**

6. M. E. Iglesias Martínez et al.:"*Flux Sensor Position Influence for Faults Detection. A Power Spectral Entropy Analysis: Case Study using the Asymmetries of Wound Rotor Induction Motor*." **(In the drafting phase to send to Energies, MDPI)**

7. M. E. Iglesia Martínez, J. C. Castro-Palacio, P. Fernández de Córdoba, J. M. Isidro y E. Navarro Pardo *"Reaction time dynamics on the milisecond scale over consecutive visual stimuli"*. **(In the drafting phase to send to Journal of the International Neuropsychological Society)**

8. M. E. Iglesias Martínez et al.:*"Probable anomalies in radioactive decay rates and electronic filters time constant measurements inside a modified faraday cage"* **(In the drafting phase)**
9. M. E. Iglesias Martínez et al.:*"Correlations between the 226Ra decay rates inside a Multilayer Interleaving Structure, the Geomagnetic Activity and the Cosmic Radiation*". **(In the drafting phase)**

The obtained results in this research are intended to extend the analysis to experimental psychology and biomedical signals in addition to actigraphy.

Chapter 5
Bibliography

1. M. A. Alsaedi. Fault diagnosis of three-phase induction motor: A review. Optics. Special Issue: Applied Optics and Signal Processing, 4(1-1):1–8, 2015.
2. J. Cusidó, L. Romeral, J. A. Ortega, A. García, and J. Riba. Signal injection as a fault detection technique. Sensors, 11(3):3356–3380, 2011.
3. P. A. Delgado-Arredondo, D. Morinigo-Sotelo, R. A. Osornio-Rios, J. G. Avina-Cervantes, H. Rostro-González, and R. de Jesús Romero-Troncoso. Methodology for fault detection in induction motors via sound and vibration signals. Mechanical Systems and Signal Processing, 83:568–589, 2017
4. V. Kokko, "Condition monitoring of squirrel-cage motors by axial magnetic flux measurements," M.S. thesis, Dept. Elect. Eng., Optoelectron. Meas., Univ. Oulu, Oulu, Finland, 2006.
5. H. Henao, C. Demian, and G.-A. Capolino, "A frequency-domain detection of stator winding faults in induction machines using an external flux sensor," *IEEE Trans. Ind. Appl.*, vol. 39, no. 5, pp. 1272–1279, Sep./Oct. 2003.
6. H. Henao, G.-A. Capolino, and C. S. Martis, "On the stray flux analysis for the detection of the three-phase induction machine faults," in *Conf. Rec. 38th IEEE IAS Annu. Meeting*, 2003, vol. 2, pp. 1368–1373.
7. A. Yazidi *et al.*, "Detection of stator short-circuit in induction machines using an external leakage flux sensor," in *Proc. IEEE ICIT*, Hammamet, Tunisia, 2004, pp. 166–169.
8. A. Yazidi, H. Henao, and G.-A. Capolino, "Broken rotor bars fault detection in squirrel cage induction machines," in *Proc. IEEE IEMDC*, San Antonio, TX, USA, 2005, pp. 741–747.
9. S. H. Kia, H. Henao, G.-A. Capolino, and C. S. Martis, "Induction machine broken bars fault detection using stray flux after supply disconnection," in *Proc. IEEE IECON*, Paris, France, 2006, pp. 1498–1503.
10. S. M. J. Rastegar Fatemi, H. Henao, and G.-A. Capolino, "Gearbox monitoring by using the stray flux in an induction machine based electromechanical system," in *Proc. IEEE MELECON*, Ajaccio, France, 2008, pp. 484–489.
11. Shao, M., Nikias, C.L.: "Signal processing with fractional lower order moments: stable processes and their applications", Proceedings of the IEEE, Vol. 81,No. 7 , pp 986 – 1010, 2002.
12. Sandgren, N., Stoica, P., Babu, P.: "On moving average parameter estimation". In: Proceedings of The 20th European Signal Processing Conference (EUSIPCO), 2012, pp 2348 – 2351, 27-31 Aug. 2012.
13. Ross S. Bowden ,Brenton R. Clarke.: "A single series representation of multiple independent ARMA processes". Journal of Time Series Analysis, Vol.33 No.2, pp 304-311, March 2012.
14. Yue Chen , Yang Xu, Mierop, A.J., Theuwissen, A.J.P.: "Column-Parallel Digital Correlated Multiple Sampling for Low-Noise CMOS Image Sensors". Sensors Journal, IEEE, Vol.12, No. 4, pp 793 – 799, April 2012.

15. Vidhi Sharma; Dinesh Kumar Dhaka:" Review Paper on Second Order Statistics of Various Fading Channels", International Journal of Advanced Research in Electrical, Electronics and Instrumentation Engineering, Vol. 3, No. 7, pp:10885-10887, July 2014.
16. M. Sanaullah:" A Review of Higher Order Statistics and Spectra in Communication Systems", Global Journal of Science Frontier Research Physics and Space Science, Vol.13 No. 4, pp: 31-50, 2013.
17. Plante DT. Leg actigraphy to quantify periodic limb movements of sleep: a systematic review and meta-analysis. Sleep medicine reviews. 2014:18(5):425-434.
18. Sonia Ancoli-Israel, Jennifer L. Martin, Terri Blackwell, Luis Buenaver, Lianqi Liu, Lisa J. Meltzer, Avi Sadeh, Adam P.Spira, and Daniel J. Taylor. The SBSM Guide to Actigraphy Monitoring: Clinical and Research Applications Behavioral Sleep Medicine Vol. 13, Iss. Sup1, 2015.
19. S. Sahu, C. E. López Fortín, M. E. Iglesias Martínez, S. Nagataki and P. Fernández de Córdoba, "*The VHE SED modelling of Markarian"* 501 in 2009, MNRAS 492, 2261–2267 (2020), doi:10.1093/mnras/staa023.
20. Iglesias-Martínez, M.E.; Castro-Palacio, J.C.; Scholkmann, F.; Milián-Sánchez, V.; Fernández de Córdoba, P.; Mocholí-Salcedo, A.; Mocholí Belenguer, F.; Kolombet, V.A.; Panchelyuga, V.A.; Verdú, G. Correlations between Background Radiation Inside a Multilayer Interleaving Structure, Geomagnetic Activity, and Cosmic Radiation: A Fourth-Order Cumulant-Based Correlation Analysis. *Mathematics* 2020, *8*, 344.
21. V. Milián-Sánchez, F. Scholkmann, P. Fernández de Córdoba, A. Mocholí-Salcedo, F. Mocholí, M.E. Iglesias-Martínez, J. C. Castro-Palacio, V. A. Kolombet, V. Panchelyuga, and G. Verdú, *"Fluctuations in measured radioactive decay rates inside a modified Faraday cage: Correlations with space weather*". (Accepted in Scientific Reports-Nature)

22. Miguel Enrique Iglesias Martínez, Pedro Fernández de Córdoba, Jose Alfonso Antonino-Daviu and J. Alberto Conejero, "*Detection of adjacent and non-adjacent bar breakages in induction motors via convolutional analysis of sound signals*", (Sent to Applied Science MDPI, under Revision).

23. Miguel Enrique Iglesias Martínez, Pedro Fernández de Córdoba, Jose Alfonso Antonino-Daviu and J. Alberto Conejero, "*Bispectrum Analysis of Stray Flux Signals for the Robust Detection of Winding Asymmetries in Wound Rotor Induction Motors*" (Accepted in ECCE 2020 IEEE Energy Conversion Congress and Exposition Conference, Detroit, Michigan , October 11-15, 2020).

24. M. E. Iglesias Martínez et al.:"*Flux Sensor Position Influence for Faults Detection. A Power Spectral Entropy Analysis: Case Study using the Asymmetries of Wound Rotor Induction Motor.*" (In the drafting phase to send to Energies, MDPI**)**

25. M. E. Iglesia Martínez, J. C. Castro-Palacio, P. Fernández de Córdoba, J. M. Isidro and E. Navarro Pardo *"Reaction time dynamics on the milisecond scale over consecutive visual stimuli"*. (In the drafting phase to send to Journal of the International Neuropsychological Society)

26. M. E. Iglesias Martínez et al.:*"Probable anomalies in radioactive decay rates and electronic filters time constant measurements inside a modified faraday cage"* **(In the drafting phase)**

27. M. E. Iglesias Martínez et al.:*"Correlations between the 226Ra decay rates inside a Multilayer Interleaving Structure, the Geomagnetic Activity and the Cosmic Radiation*". **(In the drafting phase)**